MODELLING AND ANALYSIS OF ENERGY METABOLISM IN POSTMORTEM MUSCLE

A Dissertation

presented to

the Faculty of the Graduate School

at the University of Missouri-Columbia

In Partial Fulfillment

of the Requirements for the Degree

Doctor of Philosophy

---

by

CHENGCHENG WANG

Dr. Jinglu Tan, Dissertation Advisor

December 2022

The undersigned, appointed by the dean of the Graduated School, have examined the dissertation entitled

MODELLING AND ANALYSIS OF ENERGY METABOLISM IN POSTMORTEM MUSCLE

presented by Chengcheng Wang,

a candidate for the degree of Doctor of Philosophy,

and hereby certify that, in their opinion, it is worthy of acceptance.

Professor Jinglu Tan

Professor Gang Yao

Professor Kiruba Krishnaswamy

Professor Satish Nair

ACKNOWLEDGEMENTS

I would like to say a special thank-you to my advisor, Dr. Jinglu Tan, who made this work possible. His support, guidance and encouragement have been invaluable throughout this research project. I thank him for his patience, for his constructive feedback on my work, and for training me to be a good researcher. I also thank him for providing me with information that helps me think about my future career. Without a good advisor and friend like him, I would not be able to complete my Ph.D. degree.

Special thanks are expressed to Dr. Gang Yao, Dr. Kiruba Krishnaswamy, and Dr. Satish Nair for their professional guidance and service on the program committee.

I would like to thank everyone in Dr. Tan's laboratory for their friendship, support and care. I would also like to thank the people of the Department of Biomedical, Biological and Chemical Engineering for their help with many aspects of my research.

Finally, I would like to extend my thanks to my family and friends for their love, support and encouragement.

TABLE OF CONTENTS

LIST OF FIGURES

LIST OF TABLES

MODELLING AND ANALYSIS OF ENERGY METABOLISM IN POSTMORTEM MUSCLE

Chengcheng Wang

Dr. Jinglu Tan, Dissertation Supervisor

ABSTRACT

Fresh-meat quality is largely determined by a number of biochemical reactions during the conversion of muscle to meat. To produce consistent high-quality meat, it is necessary to have an understanding of energy metabolism in postmortem muscle. Therefore, this research was conducted to model and analyze the energy metabolic process in postmortem muscle. The work included three main parts:

A kinetic model structure was developed to describe the major variations in energy metabolism and to gain further understanding of pH changes in postmortem muscle experimentally observed with an *in vitro* glycolytic system. Simulation and analysis of pH variations based on the model suggested that phosphofructokinase (PFK) activity has the strongest impact on the rate and extent of postmortem pH decline. Postmortem pH is also influenced by rates of ATP hydrolysis and glycolysis, and to a much lesser extent, pH buffering capacity. Other reactions, including those mediated by creatine kinase, adenylate kinase, and AMP deaminase, have minimal effects on postmortem pH decline.

The contributions of different pathways to ATP production and pH variations were analyzed by using a kinetic model based on data from beef *Longissimus lumborum* because the roles of energy pathways in postmortem muscles are still debated. Our results

indicated that ATP is produced primarily by creatine kinase- and myokinase-mediated reactions, and anaerobic glycolysis. Aerobic respiration lasts up to 9 hours postmortem but contributes less than 1% of the total ATP production. Similarly, pH decline in postmortem muscles is mainly due to ATP hydrolysis and glycolysis (-0.52 and -0.6 after 24 hours). Aerobic respiration, on the other hand, leads to a pH increase but the amount is negligible (0.0043 after 24 hours). Analysis of the effects of various factors on pH variations showed that electrical stimulation affects pH primarily through ATP hydrolysis and anaerobic glycolysis. The initial muscle oxygen saturation and phosphocreatine stores showed minor impacts on pH.

Since phosphofructokinase (PFK) plays a critical role in the regulation of glycolysis and a quantitative model for PFK activity is lacking, a new method by kinetic modeling was developed to estimate PFK activity and quantify the inhibitory effects of ATP and pH on PFK. In contrast to the conventional initial-velocity method, which gives a qualitative picture of the inhibition of PFK activity under varied conditions, the proposed model can separate the substrate effect from the inhibitor effect and thus quantify the inhibitor effect. The use of a kinetic model to evaluate enzyme activity and quantify the degree of inhibition can be extended to other enzymes as long as the underlying reaction mechanisms are known. Kinetic analyses of PFK based on the proposed model indicated that the affinity of the substrate binding to the catalytic sites is 4-fold of that to the inhibitory site. Increasing ATP concentration leads to a reduced overall reaction velocity as a result of increasing proportion of enzyme complexes with ATP bound to the inhibitory site.

CHAPTER 1

INTRODUCTION

The quality of meat mainly refers to its taste, color, and tenderness (Mortimer, van der Werf et al. 2014). Fresh meat quality is largely predicated on events occurring in muscle during its conversion to meat. While a number of factors affect meat quality, the most critical is pH, including the rate of pH decline and ultimate pH value (pH_u) in postmortem muscle (Scopes 1974). The rate and extent of pH decline have a significant influence on cooked beef tenderness (Lomiwes, Farouk et al. 2014). The pH-dependent degradation of desmin results in variations in meat water holding capacity, an essential factor influencing meat quality (Zeng, Li et al. 2017). Abnormal postmortem pH decline in pork leads to two major meat quality defects facing the meat industry - PSE (pale, soft and, exudative) meat and DFD (dark, firm, and dry) meat (Viljoen, de Kock et al. 2002) meat (Rathgeber, Boles et al. 1999; Page, Wulf et al. 2001; Viljoen, de Kock et al. 2002; Zhu, Ruusunen et al. 2013).

Hydrogen ion accumulation via glycolytic metabolism contributes to pH decline in postmortem muscle (England, Matarneh et al. 2018). Meat from different processing treatments such as the swift chilling (Hopkins, Holman et al. 2015) and electrical stimulation (England, Matarneh et al. 2018) tend to have different glycolytic metabolism levels, resulting in variations in pH decline rate and ultimate pH. For many years, the role of mitochondria has been neglected because the perceived lack of oxygen in postmortem muscle impedes mitochondrial function (Matarneh, Beline et al. 2018). However, oxygen

is retained well in muscle immediately after exsanguination and is gradually depleted rather than instantaneously exhausted during the postmortem period (England, Matarneh et al. 2018). Muscle oxygenation remains capable of supporting mitochondrial aerobic respiration (England, Matarneh et al. 2018). Moreover, mitochondria remain structurally intact and functional for several hours after slaughter (Ashmore, Doerr et al. 1971; Tang, Faustman et al. 2005). Several recent publications showed that the addition of mitochondria to an in vitro muscle glycolytic system could increase glycolytic flux (Scheffler, Matarneh et al. 2015; Matarneh, England et al. 2017; Matarneh, Beline et al. 2018). Other factors influencing postmortem energy metabolism, including the activity of PFK, one of the rate-limiting enzymes of glycolysis, and initial muscle glycogen content, are investigated in numerous studies (Warriss, Bevis et al. 1989; Henckel, Karlsson et al. 2002; Josell, Enfält et al. 2003; El Rammouz, Berri et al. 2004; England, Matarneh et al. 2014; England, Matarneh et al. 2015). The reaction kinetics of postmortem metabolism, however, remains an area of further studies.

Modelling is an effective way to synthesize data and reveal patterns or changes that may not be readily discoverable from laboratory experiments. Linear modelling (van de Ven, Pearce et al. 2013), random exponential modelling (van de Ven, Pearce et al. 2013), and spline-based random regression modelling (van de Ven, Pearce et al. 2014) have been applied to estimate the postmortem pH decline. However, these conventional regression models, linear or nonlinear, are not generalizable to yield a fundamental understanding of the processes involved in postmortem metabolism. A more efficacious and powerful approach is to model the reaction kinetics. A kinetic model based on the energy metabolism in sheep muscle was developed to describe postmortem pH decline

and metabolite concentrations under anaerobic conditions (Vetharaniam, Thomson et al. 2010). Ten substrates except glycogen were included in the model and an analysis of the main reactions was done to develop reaction rate expressions. After parameter optimization against NMR measurements of three muscles, the model was used to simulate the metabolic process till anoxia. The large number of heuristic relationships used made the model cumbersome and in-definitive for analysis. A simple kinetic model was reported to predict pH decline in postmortem glycolysis in beef under different chilling conditions (Kuffi, Lescouhier et al. 2018). This model focused on the effects of temperature on glucose conversion, and consequently pH, but did not explicitly account for other metabolites. There is, therefore, a need to develop models of appropriate complexity that capture the major kinetics for analysis of pH variations in postmortem muscle.

The overall goal of this dissertation research is to advance the understanding of muscle energy metabolism by modelling and analyzing the biochemical processes involved. This entails achievement of the following specific objectives:

1) Develop a kinetic model of energy metabolism and analyze pH variations based on an *in vitro* system of postmortem glycolytic conditions,

2) Augment the kinetic model of energy metabolism and analyze pH variations in real postmortem muscle, and

3) Model the dependence of phosphofructokinase activity on pH and ATP and analyze the influence of phosphofructokinase activity on pH variations in postmortem muscle.

CHAPTER 2

LITERATURE REVIEW

Fresh-meat quality is largely determined by a number of biochemical reactions during the conversion of muscle to meat (England, Matarneh et al. 2014; England, Matarneh et al. 2015; Scheffler, Matarneh et al. 2015; Matarneh, England et al. 2017; Kuffi, Lescouhier et al. 2018). In order to produce consistent high-quality meat, it is necessary to have an understanding of energy metabolism in postmortem muscle. This should begin with the understanding of how energy is managed in living muscles. Moreover, factors influencing energy metabolism in muscle are of interest.

2.1 Skeletal Muscle

2.1.1 *Muscle structure and contraction*

A skeletal muscle comprises hundreds to thousands of bundled muscle fibers (Delbono, O'Rourke et al. 1995; Gibbs and Barclay 1998; Chalovich 2002). Each muscle fiber is a tubular, multinucleated muscle cell with distinct regions known as sarcomeres. Sarcomeres are the fundamental contractile unit of skeletal muscles (DiCarlo, Sipe et al. 1998; Stokes and Gardner-Morse 2002). Each sarcomere is formed from actin filaments, myosin filaments, and associated proteins troponin and tropomyosin.

At rest, tropomyosin proteins cover the myosin-binding sites on actin, preventing the binding of actin to myosin and thus preventing muscle contraction (Gomes, Potter et

al. 2002). When muscle cells contract, calcium ions released from the sarcoplasmic reticulum to cytoplasm bind with troponin molecules, inducing a conformational change of tropomyosin that results in the exposure of cross-bridge binding sites on the actin for the myosin heads (Luo, Davis et al. 2003). The binding process requires hydrolysis of myosin-associated ATP to provide energy for the actin and myosin filaments to slide past each other. The movement of actin and myosin filaments shortens the sarcomere length and thus initiates muscle contraction. Muscle contraction ends when calcium ions are pumped back into the sarcoplasmic reticulum by the sarcoplasmic reticulum Ca^{2+}-ATPase (SERCA).

2.1.2 *Energy metabolism in skeletal muscle*

Muscle contraction requires energy, which is provided by the conversion of ATP to ADP and inorganic phosphate. ATP reserves in skeletal muscles are hydrolyzed immediately to provide energy for muscle contraction (Luo, Davis et al. 2003). However, the pool is limited and will be exhausted after a few muscle twitches without replacement. ATP must be regenerated to replenish the ATP pool (Hancock, Janssen et al. 2005). The immediate means of producing ATP is the conversion of ADP and phosphocreatine to ATP and creatine (Hancock, Janssen et al. 2005). Phosphocreatine, also known as creatine phosphate, a high energy-storing molecule in muscle cells, donates its high-energy phosphate group to ADP to form ATP and creatine. The phosphocreatine reserves in muscle cells can provide enough ATP to maintain muscle contraction for up to 15 seconds. It is reported that the existing ATP and phosphocreatine in muscles can provide energy for approximately 30 seconds (Hancock, Janssen et al.

2005). After 30 seconds, anaerobic and aerobic respiration are needed for ATP generation.

Skeletal muscle fibers are divided into two types: red and white muscle fibers. Red muscle fibers are also known as slow-twitched muscle fibers, containing high levels of myoglobin, mitochondria, and blood supply (Chal, Oginuma et al. 2015). The intrinsic structure characteristics of the red muscle fibers predetermine them to specialize in aerobic respiration. Conversely, white muscle fibers are alternatively known as fast muscle fibers and are characterized by a low content of myoglobin, mitochondria, and an inadequate vascular supply compared to red muscle fibers, enabling them to have a good performance on anaerobic respiration. The majority of the skeletal muscles are a combination of both fiber types (Zammit, Partridge et al. 2006; Rios and Marcelle 2009; Birbrair, Zhang et al. 2013). Therefore, anaerobic and aerobic respiration can both take place in a muscle. The alternated operation of the anaerobic and aerobic respiration depends on the oxygen level, which is affected by the length and intensity of muscle contraction.

At rest or under low work intensity, a muscle exhibits a relatively low ATP turnover rate, below the maximum oxygen transportation rate (Hochachka and McClelland 1997). In this case, aerobic respiration is used to generate ATP for cellular homeostasis maintenance. When oxygen is sufficient, pyruvate generated by glycolysis is transported into mitochondria and converted into additional ATP for muscle contraction via the tricarboxylic acid (TCA) cycle. The TCA cycle is also known as the citric acid cycle or the Krebs cycle, taking place in mitochondria, the 'powerhouse' of the cell. In mitochondria, pyruvate is first converted to acetyl-CoA by pyruvate dehydrogenase,

which subsequently proceeds through the TCA cycle. Eight enzymes are responsible for the reactions of the TCA cycle, converting one acetyl-CoA molecule to two carbon dioxide molecules with the concomitant production of three NADH, one $FADH_2$, and one GTP (or ATP) molecules. The NADH and $FADH_2$ molecules enter the electron-transport chain and are oxidized by oxygen with the concomitant formation of 11 ATP molecules. Consequently, through aerobic respiration, one molecule of glycogen can generate 36 molecules of ATP (Conley, Kemper et al. 2001).

When a muscle transitions from rest or low work intensity to high work intensity, the ATP turnover rate exceeds the oxygen transportation rate (Hochachka and McClelland 1997). Therefore, the generation of ATP from aerobic respiration is not capable of supporting muscle contraction, which requires the muscle to generate ATP in the absence of oxygen quickly. A crucial pathway is through anaerobic respiration, which is a sequence of ten reactions that extract energy from glucose 6-phosphate by splitting six-carbon molecules into three-carbon molecules of pyruvate. Each reaction through the pathway is catalyzed by its own enzyme. During intensive exercise or under low oxygen supply conditions, pyruvate is subsequently converted into lactate in the cytosol of a cell (Cheetham, Boobis et al. 1986). The net products of anaerobic respiration are three molecules of ATP (4 ATP produced and 1 ATP consumed) and two molecules of lactate and hydrogen ions. The accumulation of hydrogen ions causes the pH of the muscle to fall, leading to muscle acidification and muscle fatigue. Lactate generated from the pathway is transported to the liver, where it is converted back to glucose by gluconeogenesis. The glucose is subsequently released from the liver into the bloodstream and carried back to the muscle, indicating the completion of one Cori cycle.

2.2 Conversion of Muscle to Meat

2.2.1 *Biochemical reactions occurring postmortem*

In a living animal, blood circulation is responsible for providing oxygen to a muscle and removing waste products from the muscle. After slaughter, the muscle gradually loses oxygen. Although the oxygen in the muscle could maintain a certain degree of aerobic respiration, the lack of oxygen supply because of the cessation of blood circulation results in the termination of ATP production from aerobic respiration. In addition, the stored muscle ATP is limited, which could be rapidly consumed within seconds without replacement (Hancock 2005; Berg 2002). However, ATP is still continually required to maintain cellular membrane potential and other cellular functions, including muscle contraction, cell signaling, and macromolecule biosynthesis (St-Pierre, Brand et al. 2000; Pösö and Puolanne 2005). Thus, ATP must be generated through other biochemical pathways.

There are mainly five pathways for ATP biosynthesis in a postmortem muscle:

1) *Phosphorylation of ADP with phosphocreatine by creatine kinase*

The most immediate means of regenerating ATP in a muscle is the phosphorylation of ADP with phosphocreatine by creatine kinase. The high energy-carrying molecule, phosphocreatine, is ready to transfer its high-energy phosphate group to ADP to form ATP (phosphocreatine + ADP + H^+ ↔ creatine + ATP). The creatine kinase reaction is reversible under resting conditions. However, in a postmortem muscle, this reaction is dominated by the forward direction causing phosphocreatine to decline and eventually disappear. Although the stored phosphocreatine content (24-30 μmol g^{-1}) is higher than ATP (5-8 μmol g^{-1}) in muscles, the ATP produced through creatine kinase

reaction lasts brief periods, leading to a decreased ATP level. The combination of decreased ATP content and high energy demand in postmortem muscles triggers anaerobic respiration, which comprises glycogenolysis and anaerobic respiration.

2) *Glycogenolysis and anaerobic respiration*

As a storage form of glucose, glycogen makes up 1-2% of the muscle mass in skeletal muscles (Arkinstall, Bruce et al. 2004). In muscles, the need for ATP leads to the breakdown of glycogen to glucose-6-phosphate for entry glycolysis. The conversion of glycogen to glucose-6-phosphate involves three biochemical reactions catalyzed by three enzymes: glycogen phosphorylase, glycogen debranching enzyme, and phosphoglucomutase.

Glycogen phosphorylase catalyzes the controlling step of the glycogen degradation pathway. Glycogen phosphorylase cleaves the α-1,4 bond of glycogen by substituting an inorganic phosphate group, yielding glucose 1-phosphate (Glycogen + Pi ↔ Glucose-1-phosphate + Glycogen). This enzyme is only responsible for the release of glycosyl at least five units away from branch points. Once phosphorylase reaches the fourth glycosyl from the branch points, the glycogen debranching enzyme shifts glycogen's branches to the main chain, allowing the completion of glycogen phosphorylase reaction. Glycogen debranching enzyme also catalyzes the cleavage of α-1,6 linked glycosyl group to release glucose molecules. Glucose and glucose-1-phosphate are subsequently converted to glucose-6-phosphate, an immediate source for glycolysis, by hexokinase and phosphoglucomutase, respectively (Glucose + ATP →Glucose-6-phosphate; Glucose-1-phosphate → Glucose-6-phosphate). One ATP molecule is

consumed during the conversion of glucose to glucose-6-phosphate. Once generated, clucose-6-phosphate proceeds along the glycolysis pathway, where ATP is generated and lactate accumulated.

Glycolysis is the first stage of both aerobic and anaerobic respiration. Glycolysis is a sequence of ten reactions that extract energy from glucose 6-phosphate by splitting six-carbon molecules into three-carbon molecules of pyruvate. Each reaction through the pathway is catalyzed by its own enzyme. Under anaerobic respiration, pyruvate is further converted into lactate in the cytosol. The metabolites and rate-limiting enzymes in anaerobic respiration are shown in Figure 2.1.

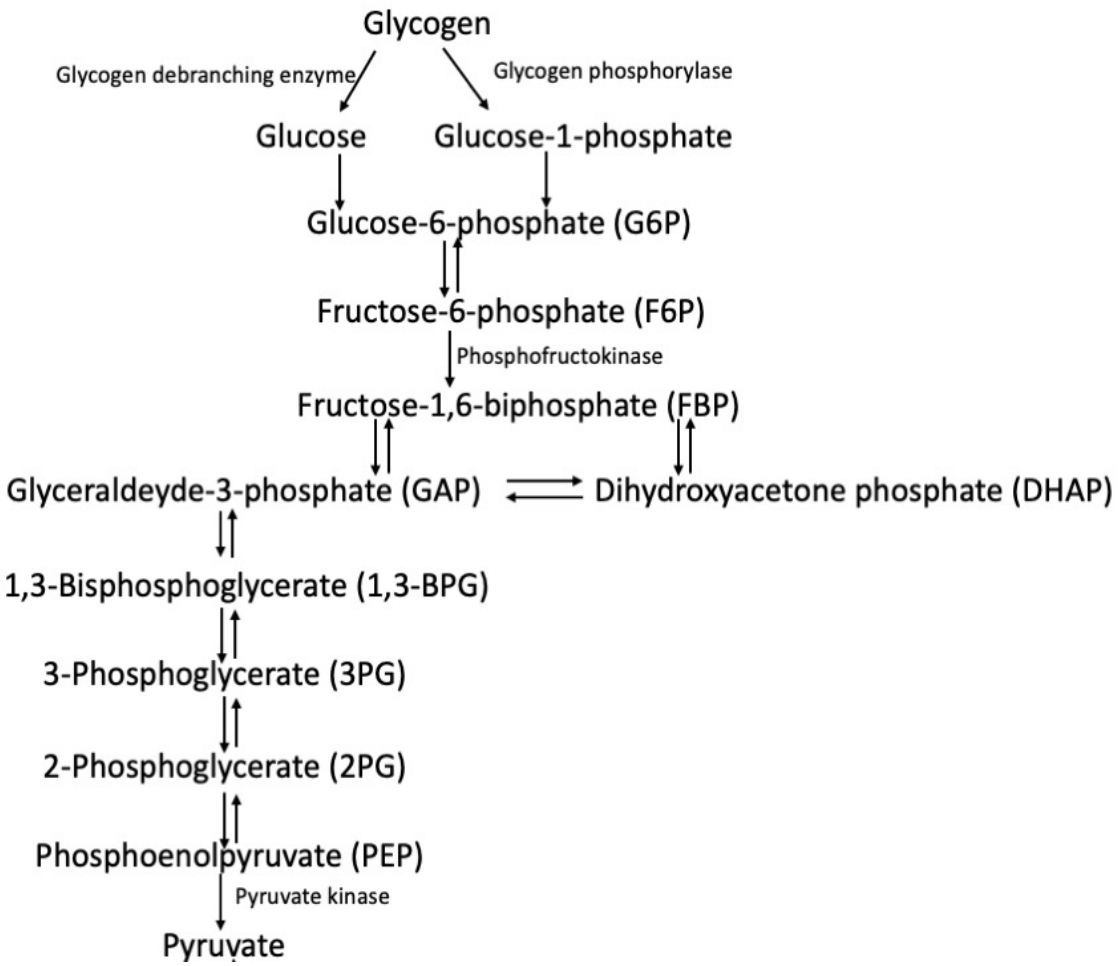

Figure 2.1 - The anaerobic respiration. Three rate-limiting enzymes responsible for the irreversible conversion of metabolites, glycogen phosphorylase, phosphofructokinase, and pyruvate kinase, are shown in the figure.

3) *Aerobic respiration*

Aerobic respiration in postmortem muscles has been neglected for many years based on the general belief that animals lose the ability to transport oxygen to muscles and thus oxygen is depleted immediately following exsanguination. However, several recent publications showed that muscles retain oxygen after stunning and exsanguination and its depletion is a gradual rather than instantaneous process in a postmortem muscle

(England et al., 2018; Ramos et al., 2020). Muscle oxygenation is capable of supporting some levels of mitochondrial aerobic respiration. Even a low level of aerobic respiration can significantly influence postmortem energy metabolism as a result of its high efficiency in generating ATP. One glucose molecule can be oxidized into 38 molecules of ATP via aerobic respiration, much more efficient than anaerobic respiration, where 3 molecules of ATP are generated. Moreover, mitochondria remain structurally intact and are capable of aerobic respiration at the early postmortem stage (Ashmore et al., 1971; Matarneh et al., 2018; Tang et al., 2005). As a result, some researchers believe mitochondrial aerobic respiration contributes little to ATP production because of the limited oxygen in postmortem muscles, while others argue that the role of aerobic respiration should not be underestimated since aerobic respiration is more efficient for ATP production than glycolysis (England et al., 2018).

4) *Adenylate kinase reaction*

Under non-steady-state circumstances, such as the case of a postmortem muscle, large amounts of ATP are needed to maintain cellular homeostasis. However, ATP generated from glycolysis is limited, and thus other pathways are necessary to provide ATP. Moreover, increased ADP concentration from continual ATP hydrolysis makes it available to generate ATP and AMP by adenylate kinase (ADP + ADP ↔ ATP + AMP). Once AMP is generated, it is converted to monophosphate (IMP) by AMP deaminase ($AMP + H^+ \leftrightarrow IMP + NH_4^+$).

In conclusion, the energy metabolism in postmortem muscles is summarized as follows:

ATP utilization:

i. ATP hydrolysis catalyzed by ATPase:

$$ATP^{4-} + H_2O \rightarrow ADP^{3-} + \delta HPO_4^{2-} + (1-\delta)H_2PO_4^- + \delta H^+ \quad (1)$$

ATP synthesis:

ii. Creatine kinase pathway for ATP synthesis:

$$CrP^{2-} + ADP^{3-} + H^+ \leftrightarrows Cr + ATP^{4-} \quad (2)$$

iii. Anaerobic glycolysis:

$$ADP^{3-} + \frac{1}{3}G + \delta HPO_4^{2-} + (1-\delta)H_2PO_4^- + \delta H^+ \rightarrow ATP^{4-} + H_2O + \frac{2}{3}La^- + \frac{2}{3}H^+ \quad (3)$$

iv. Aerobic respiration:

$$\frac{1}{38}G + \frac{6}{38}O_2 + ADP^{3-} + \delta HPO_4^{2-} + (1-\delta)H_2PO_4^- + \delta H^+ \rightarrow ATP^{4-} + \frac{6}{38}CO_2 + \frac{44}{38}H_2O \quad (4)$$

v. Interconversion of adenosine phosphates by adenylate kinase (or myokinase):

$$2ADP^{3-} \leftrightarrows ATP^{4-} + AMP^{2-} \quad (5)$$

where

$$\delta = \frac{10^{-\mathrm{pKa}}}{10^{-\mathrm{pKa}} + [H^+]} \quad (6)$$

is the fraction of free phosphate (P_i) existing as HPO_4^{2-} (P_i^{2-}) in equilibrium with $H_2PO_4^-$ (P_i^-) with pKa = 6.70 (Kushmerick, 1997), *Cr* is creatine, *G* is glycogen, *La* is lactate, and the other symbols are as commonly used in the literature.

2.2.2 *Factors influencing postmortem energy metabolism*

2.2.2.1 *Muscle glycogen reserves at slaughter*

Muscle glycogen, as the primary source of ATP generation, plays a critical role in determining the rate and extent of postmortem metabolism and thus the pH decline rate and ultimate pH. The relationship between glycogen level and pH has been widely

discussed. Lundstrom et al. (1996) reported that an abnormally high glycogen concentration results in a relatively lower ultimate pH in hams (Lundström, Andersson et al. 1996). High glycogen concentration was also found closely related to "acid meat" characterized by pale color, soft texture, and low water holding capacity. Warriss et al. (1989) reported that pigs with less muscle glycogen content tend to have a higher ultimate pH. They also showed a linear relationship between muscle glycogen level and ultimate pH by directly plotting muscle glycogen concentrations at slaughter with respect to ultimate pH (Warriss, Bevis et al. 1989). Later, Henckel et al. (2002) found that the negative linear relationship between glycogen level at slaughter and ultimate pH only existed in muscles with glycogen concentration below 53 mmol/kg (Henckel, Karlsson et al. 2002).

In consideration of the crucial role of glycogen level in ultimate pH, many studies investigated the factors influencing muscle glycogen content in an attempt to achieve an optimal ultimate pH. Factors affecting glycogen level could have an influence on ultimate pH.

Muscle glycogen level is affected by individual animals, muscle fiber types, and the preslaughter handling process. Monin et al. (1981) and Immonen et al. (2000) showed that muscle glycogen concentration varies broadly, ranging from 75 to 120 μmol/g in healthy cattle and sheep (Monin, Sellier et al. 1981; Immonen, Kauffman et al. 2000). Monin et al. (1981) observed that glycogen concentration in cattle is higher in muscles high in type IIa fibers (90-105 μmol/g) than in muscles high in type I or IIb fibers (70-80 μmol/g) (Monin, Sellier et al. 1981). Monin et al. (1987) reported that fast-white muscles contain more glycogen than slow-red ones in pigs (Monin, Mejenes-Quijano et al. 1987).

Later, Pethick (1999) and Gardner (2001) reported that bovine muscles with a high proportion of type IIa fibers had higher glycogen content than muscles predominantly comprising type IIb fibers (Pethick, Cummins et al. 1999; Gardner 2001). Moreover, pre-slaughter handling processes such as fasting and sudden environment change would also cause variations in glycogen loss during slaughtering and give rise to different glycogen levels. One of the prevalent meat defects, known as DFD meat, results from the lack of glycogen because of chronic stress in animals (Viljoen, de Kock et al. 2002).

2.2.2.2 *Postmortem metabolism-catalyzing enzymes*

2.2.2.2.1 ATPase

There are five types of ATPase in muscle cells: myofibrillar ATPase, sarcoplasmic reticulum $Ca2^{+}$-ATPase, plasmalemma Na^{+}/K^{+}-ATPase, plasmalemma $Ca2^{+}$-ATPase, mitochondrial F_1-ATPase (England, Matarneh et al. 2018; Matarneh, Beline et al. 2018). The rate of glycolysis is determined by the ATP hydrolysis rate catalyzed by ATPase (Scopes 1974). The myofibrillar protein amounts account for 25% of the muscle proteins, so myofibrillar ATPase is responsible for most ATP hydrolysis (Hamm,1977). However, myofibrillar ATPase is sensitive to pH and is inactivated by a rapid pH decline during postmortem metabolism. As the pH declines from 6.5 to 5.5, myofibrillar ATPase gradually decreases activity until it is completely inactivated (Scopes 1974).

Mitochondrial F_0F_1 ATP synthase is composed of a membrane-embedded F_0 domain and a matrix-soluble F_1 domain. During aerobic respiration, F_0F_1 ATP synthase catalyzes the phosphorylation of ADP to produce ATP driven by the proton gradient

generated by the electron transport chain (Matarneh, Beline et al. 2018). Under hypoxia or anoxia circumstances, the F_1 domain dissociates from the F_0 domain and acts as F_1-ATPase, which consumes ATP to maintain the mitochondrial inner membrane proton gradient (Foster and Fillingame 1979; Gibson 1983; Dubinsky 1987). This process has been termed "cellular treason" or "mitochondrial treason" (Scott and Nicholls 1980; St-Pierre, Brand et al. 2000; Lehmann, Segal et al. 2008).

Mitochondrial F_1-ATPase is less sensitive to pH and can still function at low pH. Mitochondrial F_1-ATPase retains 50% of its maximal activity when the pH declines to 5 (Scopes 1974). Several recent publications showed that the addition of mitochondria to an *in vitro* muscle glycolytic system could increase glycolytic flux (Scheffler, Matarneh et al. 2015; Matarneh, England et al. 2017; Matarneh, Beline et al. 2018). The authors argued that it is the ATPase in the mitochondria that elevates the glycolytic rate. The addition of mitochondria is accompanied by the addition of ATPase, which leads to an increased ATP hydrolysis rate. The enhanced ATP hydrolysis results in accelerated pH decline and lower ultimate pH. It is reported that beef typically has a lower ultimate pH than pork as a result of higher amounts of mitochondria in cattle muscles (England, Matarneh et al. 2018; Matarneh, Beline et al. 2018).

2.2.2.2.2 Glycolytic enzymes

Glycogenolysis, along with glycolysis, plays a vital role in carbohydrate metabolism and is the principal means of glycogen utilization and ATP generation in postmortem muscles. Degradation of glycogen via the glycolytic pathway involves ten reactions catalyzed by ten enzymes (Vetharaniam, Thomson et al. 2010). Among these

ten enzymatic reactions, three of them are irreversible: glycogen to glucose-1-phosphate, fructose-6-phosphate to fructose-1,6-bisphosphate, and phosphoenolpyruvate to pyruvate. These three reactions are catalyzed by glycogen phosphorylase (GP), phosphofructokinase (PFK), and pyruvate kinase, respectively (Hamm, 1977).

1) *Glycogen phosphorylase* (*GP*)

Glycogen phosphorylase (GP), one of the rate-limiting enzymes in anaerobic respiration, is responsible for the irreversible conversion of glycogen to glucose-1-phosphate. Glycogen phosphorylase exists in two inter-convertible forms: the active, phosphorylated form (GPa) and the less active, non-phosphorylated form (GPb) (Stanley and Connett 1991). The inter-conversion between these two forms is governed by phosphorylase kinase, with the latter regulated by calcium, AMP and cAMP (Hargreaves and Richter 1988). When a muscle contracts, calcium is released from the myofibrillar reticulum and activates phosphorylase kinase, causing the conversion of GPb to GPa and activation of glycogenolysis (Hargreaves and Richter 1988). In conditions of stress, epinephrine is secreted by the adrenal glands, resulting in an adrenaline-mediated increase in cAMP and subsequent activation of cAMP-dependent protein kinase. cAMP-dependent protein kinase is responsible for the activation of phosphorylase kinase, subsequent conversion of GPb to GPa (Meinke and Edstrom 1991), and accelerated glycogenolytic rate. Connett and Sahlin (1996) reported that GP is also allosterically activated by the presence of IMP and AMP in times of great energy demand, while inhibited by ATP, ADP, and glucose-6-phosphate (Connett and Sahlin 1996).

Phosphate availability, moreover, is critical for the phosphorylation of glycogen to glucose-1-phosphate. Chasiotis (1988) argued that the low glycogenolytic rate in a normal resting muscle is because of low inorganic phosphate concentration. The researcher further observed that as the phosphate level increases during muscle contraction, the inhibition effect of phosphate disappears and the glycogenolytic rate increases (Chasiotis 1988). Glycogen phosphorylase is also affected by muscle glycogen content. When glycogen concentration is high, GP is more active, resulting in an accelerated glycogenolytic rate (Vandenberghe, Richter et al. 1999; Shearer, Marchand et al. 2001).

2) *Phosphofructokinase* (*PFK*)

Phosphofructokinase (PFK, ATP:D-fructose-6-phosphate-1-phosphotransferase, EC 2.7.1.11), the first rate-limiting enzyme of glycolysis, catalyzes the irreversible conversion of fructose-6-phosphate (F6P) and ATP to fructose-1,6-biphosphate (F-1,6-P) and ADP (F6P + ATP ↔ F-1,6-P + ADP) (England et al., 2014; Matarneh et al., 2018). Glycolytic flux is tightly regulated by changing the catalytic activity and the behavior of PFK (Sola-Penna et al., 2010; Tanner et al., 2018). Therefore, PFK is often considered the essential control point of glycolysis and responsible for the cessation of postmortem muscle metabolism.

PFK is a tetrameric structural protein and can shift to a less active dimeric form during postmortem metabolism (England, Matarneh et al. 2014). The primary process of postmortem energy metabolism is the depletion of adenosine triphosphate (ATP) accompanied by the accumulation of hydrogen ions (H^+) (Hamm 1977). Decreased pH

from hydrogen ion accumulation leads to decreased PFK activity during postmortem metabolism (England, Matarneh et al. 2015). England (2014) investigated all the enzymes involved in the glycogenolysis and glycolysis pathway and found that all enzymes other than PFK are active at pH≤5.5. The researcher further showed that the termination of glycolysis is due to the inactivation of PFK. England (2015) showed that PFK isolated from beef retains 50% of its maximal activity when pH declines to 5.35. (England, Matarneh et al. 2015). Hamm (1977) showed that PFK from porcine muscle is inactivated at pH≤5.5 (Hamm, 1977). The variations in dependence of PFK activity on pH indicate that other factors might play a role in regulating PFK activity. Indeed, PFK is also allosterically activated by the presence of AMP, ADP, fructose 1,6-phosphate, phosphate and potassium, while inhibited by ATP and citrate (Ui, 1966; Bock, Frieden, 1976; Dobson, Yamamoto et al. 1986). PFK is one of the enzymes that undergo substrate inhibition (Reed et al., 2010; Schöneberg et al., 2013; Sharma, 2011a, 2011b; Webb et al., 2015). Substrate inhibition of PFK ensures that resources are not devoted to producing ATP when it is present in abundance (Reed et al., 2010).

The activators and inhibitors of PFK in most cases do not work independently, instead they act synergistically to affect the activity of PFK. It is known that ATP and H^+ have positive interactions in or additive effects on inhibiting PFK activity (Ui, 1966; Bock, Frieden, 1976; Dobson, Yamamoto et al. 1986). This is in agreement with previous work that pH-induced inhibition of muscle PFK is related to ATP levels and the optimal pH for PFK is shifted to the alkaline side at elevated ATP concentrations (Ui 1966; Bock, Frieden, 1976; Dobson, Yamamoto et al. 1986).

3) *Pyruvate kinase*

Pyruvate kinase (PK), one of the more distal enzymes of glycolysis, catalyzes the irreversible conversion of phosphoenolpyruvate and ADP to pyruvate and ATP. PK exists in at least three isoforms, and the conversion between isoforms is regulated by the phosphorylation of the enzyme (Schwägele, Haschke et al. 1996; Schwägele, Haschke et al. 1996). The researchers also demonstrated that PK from PSE (pale, soft, and exudative) pork exhibits a higher activity at lower pH. Allison et al. (2003) observed no correlation between the activity of PK and pH in postmortem pork muscle (Allison, Bates et al. 2003). Scheffler and Gerrard (2007) argued that enhanced PK activity is not responsible for accelerated postmortem metabolism in pork.

4) *Lactate dehydrogenase* (*LDH*)

Lactate dehydrogenase (LDH) catalyzes the conversion of pyruvate and NADH to lactate and NAD^+, which is the last step of anaerobic respiration. For a long time, lactate formation is considered the cause of pH decline and lactic acid is thus widely used as an indicator of postmortem metabolism and muscle pH. Although early studies indicated that a negative linear relationship exists between lactate level and muscle pH (Bendall, 1973; Sulaiman 2015), they did not establish a direct cause-and-effect relationship. Conversely, one hydrogen ion is consumed during the conversion of pyruvate to lactate, indicating that lactate formation is actually a buffering reaction that attenuates muscle acidity. Robergs et al. (2004) showed that glycolysis is prolonged by decreased hydrogen ion accumulation as a result of lactate formation (Robergs, Ghiasvand et al. 2004). Furthermore, the dissociation constant of lactate is 3.86, meaning that lactate always

exists as a salt rather than acid at the pH's observed in postmortem muscles. In conclusion, lactate formation is not responsible for postmortem pH decline and muscle acidity.

2.2.2.2.3 AMP deaminase

Adenosine triphosphate (ATP) is the energy source for muscle contraction. During postmortem metabolism, ATP is hydrolyzed to adenosine diphosphate (ADP), and ADP is subsequently converted to AMP and ATP by adenylate kinase (EC 2.7.4.3), followed by inosine monophosphate (IMP) formation catalyzed by AMP deaminase (EC 3.5.4.6) (Goodman and Lowenstein 1977).

The complete transformation of AMP to IMP by AMP deaminase coincides with the completion of glycolysis because IMP is the end product and is unable to contribute to ATP generation (Hamm 1977; Bendall 1973; Dalrymple 1975; Greaser 2001). Muscles with higher AMP deaminase activity tend to have elevated ultimate pH in pigs and chickens (EI Rammouz 2004; Van Laack 2001). Using his classical reconstituted muscle glycolytic system, Scopes (1974b) observed that glycolysis terminates earlier in the *in vitro* system with higher AMP deaminase concentration. Later, researchers reported that low AMP deaminase activity was found in abnormal acidic pork meat (England, Matarneh et al. 2015). Lambs under fast chilling treatment exhibited enhanced glycolysis, lower ultimate pH and decreased AMP deaminase activity early postmortem (Warner, Jacob et al. 2015). England et al. (2015) proposed that altered AMP deaminase activity may be partially responsible for extended postmortem glycolysis (England, Matarneh et al. 2015).

2.2.3 *Abnormal postmortem metabolism and meat quality defects*

Abnormal postmortem metabolism in pork leads to two major meat quality defects facing the meat industry - PSE (pale, soft and exudative) meat and DFD (dard, firm, and dry) meat (Viljoen, de Kock et al. 2002; Rathgeber, Boles et al. 1999; Page, Wulf et al. 2001; Viljoen, de Kock et al. 2002; Zhu, Ruusunen et al. 2013).

PSE meat has a pale color, soft texture, and low water-holding capacity, making it unattractive to consumers. The development of PSE meat is often associated with elevated glycolysis (Rathgeber, Boles et al. 1999; Zhu, Ruusunen et al. 2013), concomitant with increased hydrogen ion accumulation and heat production. The combination of low pH and high temperature leads to the denaturation of muscle proteins, causing a loss of their capability to bind water and thus water migration from cells to extracellular spaces. The higher level of water in extracellular space causes meat to appear exudative. The loss of meat pigments from denaturation of myoglobin and increased light reflectance of meat from high water levels in extracellular results in paler meat color. The soft texture of the meat is mainly because of the denaturation of myofibrillar structure proteins (Rathgeber, Boles et al. 1999; Zhu, Ruusunen et al. 2013).

On the contrary, DFD meat is characterized by a dark color, firm texture, and high water-holding capacity. The most common factor resulting in DFD meat is antemortem stress. It is reported that chronic stress prior to slaughter leads to the depletion of muscle-stored glycogen, making it less available for glycolysis postmortem. Consequently, the ultimate pH of DFD meat is higher than regular meat as a result of its abnormal glycolysis process. The high pH causes relatively low levels of denaturation of proteins and thus their high capability to bind water, resulting in fewer exudates in extracellular

spaces and thus a drier appearance of meat (Warriss, Bevis et al. 1989). Shrinkage of the myofilament lattice causes the muscle to absorb light and thus appear darker.

Extreme toughness because of cold shortening is another undesirable change in meat. Cold shortening occurs under the condition of rapid chilling of carcasses immediately after slaughter, when the muscle glycogen is still available as an energy source for muscle contraction in response to low temperature (<10^{o}C). The application of electrical stimulation (ES) can effectively reduce or even eliminate cold shortening by forcing extensive muscle contraction and using up energy reserves immediately after stunning before slaughtering or immediately after slaughtering. It is reported that cold-induced toughening is reduced by the application of electrical stimulation in beef (Sorinmade, Cross et al. 1982). Electrical stimulation accelerates postmortem metabolism, leading to a rapid pH decline and glycogen depletion (Hwang and Thompson 2001a; Hwang and Thompson 2001b). England et al. (2017) showed that electrical stimulation could also alter postmortem oxygenation and mitochondrial respiration in beef (England, Matarneh et al. 2015).

2.3 Modelling

Modelling is considered an effective way to synthesize data and reveal patterns or changes that may not be readily discoverable from laboratory experiments. Therefore, extensive work has been done to develop various model structures in an attempt to reflect postmortem muscle metabolism. Bruce et al. (2011) developed an exponential model to describe the pH decline in bovine muscle postmortem (Bruce, Scott et al. 2001).

McGeehin et al. (2001) utilized a regression model to analyze the factors influencing the pH decline in lamb after slaughter (McGeehin, Sheridan et al. 2001). Linear modelling (van de Ven, Pearce et al. 2013), random exponential modelling (van de Ven, Pearce et al. 2013), and spline-based random regression modelling (van de Ven, Pearce et al. 2014) have also been applied to estimate the postmortem pH decline. However, these conventional regression models, linear or nonlinear, are not generalizable to yield a fundamental understanding of the processes involved in postmortem metabolism.

A more efficacious and powerful approach is to model the reaction kinetics. A kinetic model based on the energy metabolism in sheep muscle was developed to describe postmortem pH decline and metabolite concentrations under anaerobic conditions (Vetharaniam, Thomson et al. 2010). Ten substrates except glycogen were included in the model and an analysis of the main reactions was done to develop reaction rate expressions. After parameter optimization against NMR measurements of three muscles, the model was used to simulate the metabolic process till anoxia. A simple kinetic model was reported to predict pH decline in postmortem glycolysis in beef under different chilling conditions (Kuffi, Lescouhier et al. 2018). This model focused on the effects of temperature on glucose conversion, and consequently pH, but did not explicitly account for other metabolites.

CHAPTER 3

MODELLING OF ENERGY METABOLISM AND ANALYSIS OF pH VARIATIONS IN POSTMORTEM MUSCLE

Abstract

A kinetic model structure was developed to describe the major variations in energy metabolism and to gain further understanding of pH changes in postmortem muscle experimentally observed with an *in vitro* glycolytic system. Comparison with experiments showed that the model could describe the kinetics of major metabolites and pH under varied conditions. Optimized model parameters definitively and consistently showed the observed effects of mitochondria, indicating a desirable level of model complexity. Simulation and analysis of pH variations based on the model suggested that phosphofructokinase activity has the strongest impact on the rate and extent of postmortem pH decline. Postmortem pH is also influenced by rates of ATP hydrolysis and glycolysis, and to a much lesser extent, pH buffering capacity. Other reactions, including those mediated by creatine kinase, adenylate kinase, and AMP deaminase, have minimal effects on postmortem pH decline.

3.1 Introduction

Fresh-meat quality is largely determined by a number of biochemical reactions during the conversion of muscle to meat (England, Matarneh et al. 2014; England, Matarneh et al. 2015; Scheffler, Matarneh et al. 2015; Matarneh, England et al. 2017;

Kuffi, Lescouhier et al. 2018). In order to produce consistent high-quality meat, it is necessary to have an understanding of energy metabolism in postmortem muscle. The primary process of postmortem energy metabolism is the depletion of adenosine triphosphate (ATP) accompanied by the accumulation of hydrogen ions (H^+) (Hamm 1977). Numerous studies have investigated the critical factors that significantly influence this process. Initial muscle glycogen content; the activity of phosphofructokinase (EC 2.7.1.11; PFK), one of the rate-limiting enzymes in glycolysis; and the activity of adenosine monophosphate (AMP) deaminase (EC 3.5.4.6), which converts AMP to inosine monophosphate (IMP) are major factors affecting the energy metabolism in postmortem muscle (Warriss, Bevis et al. 1989; Henckel, Karlsson et al. 2002; Josell, Enfält et al. 2003; El Rammouz, Berri et al. 2004; England, Matarneh et al. 2014; England, Matarneh et al. 2015). For many years, the role of mitochondria has been neglected because of the perceived lack of oxygen in postmortem muscle. Mitochondria, nonetheless, remain structurally intact and functional for several hours after slaughter (Ashmore, Doerr et al. 1971; Tang, Faustman et al. 2005). Several recent publications showed that addition of mitochondria to an *in vitro* muscle glycolytic system could increase glycolytic flux (Scheffler, Matarneh et al. 2015; Matarneh, England et al. 2017; Matarneh, Beline et al. 2018). The reaction kinetics of postmortem metabolism, however, remains an area of further studies.

Modelling is an effective way to synthesize data and reveal patterns or changes that may not be readily discoverable from laboratory experiments. Linear modelling (van de Ven, Pearce et al. 2013), random exponential modelling (van de Ven, Pearce et al. 2013), and spline-based random regression modelling (van de Ven, Pearce et al. 2014)

have been applied to estimate the postmortem pH decline. However, these conventional regression models, linear or nonlinear, are not generalizable to yield a fundamental understanding of the processes involved in postmortem metabolism. A more efficacious and powerful approach is to model the reaction kinetics. A kinetic model based on the energy metabolism in sheep muscle was developed to describe postmortem pH decline and metabolite concentrations under anaerobic conditions (Vetharaniam, Thomson et al. 2010). Ten substrates except glycogen were included in the model and an analysis of the main reactions was done to develop reaction rate expressions. After parameter optimization against NMR measurements of three muscles, the model was used to simulate the metabolic process till anoxia. A simple kinetic model was reported to predict pH decline in postmortem glycolysis in beef under different chilling conditions (Kuffi, Lescouhier et al. 2018). This model focused on the effects of temperature on glucose conversion, and consequently pH, but did not explicitly account for other metabolites.

In this research, a kinetic model structure was developed to gain further understanding of the variations in metabolites and pH in postmortem muscle experimentally observed in previous research (Scheffler, Matarneh et al. 2015; Matarneh, England et al. 2017; Matarneh, Beline et al. 2018) based on an *in vitro* glycolytic system (Scopes, 1973; Scopes, 1974; Matarneh, Beline et al. 2018). After parameter optimization and validation against experimental observations, the model was used to provide insights into the factors that affect pH behavior in the postmortem process.

3.2 Development of a Kinetic Model Structure for Postmortem Energy Metabolism

3.2.1 *Biochemical reactions in postmortem muscle*

The initial pool of ATP in skeletal muscle is limited and would be rapidly consumed within seconds without replacement (Hancock, Janssen et al. 2005). Postmortem muscle attempts to maintain cellular ATP homeostasis through a series of biochemical reactions (Scheffler and Gerrard 2007). In the pre-rigor period, ATP is continuously hydrolyzed to provide energy for muscle contractions, membrane potential maintenance, and calcium preservation within the sarcoplasmic reticulum (St-Pierre, Brand et al. 2000; Pösö and Puolanne 2005). Thus, ATP must be re-generated to replenish the ATP pool.

There are mainly three pathways for ATP biosynthesis in postmortem muscle: 1) phosphorylation of ADP with phosphocreatine (CrP) by creatine (Cr) kinase, 2) glycolysis via glycogen (G) conversion, and 3) generation of ATP and AMP from ADP by adenylate kinase (EC 2.7.4.3). Once generated, AMP is further irreversibly converted into IMP by AMP deaminase (EC 3.5.4.6) (Lowenstein 1972). The major reactions involved in postmortem energy metabolism can be represented as follows:

i. ATP hydrolysis catalyzed by ATPase:

$$ATP^{4-} + H_2O \rightarrow ADP^{3-} + \delta HPO_4^{2-} + (1-\delta)H_2PO_4^- + \delta H^+ \quad (1)$$

ii. Creatine kinase pathway for ATP synthesis:

$$CrP^{2-} + ADP^{3-} + H^+ \leftrightarrows Cr + ATP^{4-} \quad (2)$$

iii. Glycolysis:

$$ADP^{3-} + \frac{1}{3}G + \delta HPO_4^{2-} + (1-\delta)H_2PO_4^- + \delta H^+ \rightarrow ATP^{4-} + H_2O + \frac{2}{3}La^- + \frac{2}{3}H^+ \quad (3)$$

iv. Interconversion of adenosine phosphates by adenylate kinase:

$$2ADP^{3-} \leftrightarrows ATP^{4-} + AMP^{2-} \quad (4)$$

v. AMP deamination by deaminase:

$$AMP^{2-} + H^{+} \rightarrow IMP^{2-} + NH_4{}^{+} \quad (5)$$

where

$$\delta = \frac{10^{-\mathrm{pKa}}}{10^{-\mathrm{pKa}} + [H^{+}]} \quad (6)$$

is the fraction of free phosphate existing as HPO_4^{2-} in equilibrium with $H_2PO_4^{-}$ with pKa = 6.70 (Kushmerick 1997), CrP^{2-} is creatine phosphate, Cr is creatine, G is glycogen, La^{-} is lactate, ATP^{4-} is adenosine triphosphate, ADP^{3-} is adenosine diphosphate, AMP^{2-} is adenosine monophosphate, and IMP^{2-} is inosine monophosphate.

Reactions (1-2) and (4-5) are commonly known. Reaction (3) is an overall representation of the glycolytic pathway without explicit representation of the intermediates (Gevers 1977; Dennis, Gevers et al. 1991).

3.2.2 *Kinetic model structure*

A model for the postmortem muscle energy metabolism can be developed based on the enzymatic reactions (1-5). The reactions involve nine variables: concentrations of CrP^{2-}, Cr, Glycogen, ATP^{4-}, ADP^{3-}, AMP^{2-}, IMP^{2-}, H^{+} and phosphate (HPO_4^{2-} and $H_2PO_4^{-}$). Phosphate concentration can be omitted as a variable from the model based on the assumption that phosphate availability would not be a limiting factor of glycolysis in the *in vitro* glycolytic experiments described later. Cr concentration may be expressed in terms of CrP^{2-} concentration as the total of the two is a constant in a closed system without exchange of metabolites with the outside.

Reactions (1-5) can then be described by the following set of first-order differential equations expressed in terms of the reaction rates.

$$\frac{d[ATP]}{dt} = -r_1 + r_2 + r_3 + r_4 \quad (7)$$

$$\frac{d[ADP]}{dt} = r_1 - r_2 - r_3 - 2r_4 \quad (8)$$

$$\frac{dpH}{dt} = -\frac{1}{\beta}\left(\delta r_1 - r_2 + \left(\frac{2}{3} - \delta\right) r_3 - r_5\right) \quad (9)$$

$$\frac{d[G]}{dt} = -\frac{1}{3} r_3 \quad (10)$$

$$\frac{d[AMP]}{dt} = r_4 - r_5 \quad (11)$$

$$\frac{d[IMP]}{dt} = r_5 \quad (12)$$

$$\frac{d[CrP]}{dt} = -r_2 \quad (13)$$

where $[x]$ denotes the concentration of metabolite x; t is time; r_1-r_5 are the net forward reaction rates for Reactions (1-5), respectively; and β is pH buffering capacity.

Reaction rates r_1-r_5 can be represented in terms of substrate concentrations as follows if the enzymatic reactions in (1-5) behave in a Michaelis-Menten manner.

$$r_1 = \frac{k_1[ATP]^2}{(k_{m1}+[ATP])} \quad (14)$$

$$r_2 = r_{2f} - r_{2b} = \frac{k_2[CrP][ADP][H^+]}{k_{m2}+[CrP]+[ADP]+[H^+]} - \frac{k_3[ATP][Cr]}{k_{m3}+[ATP]+[Cr]} \quad (15)$$

$$r_3 = \left(\frac{k_4[G][ADP]}{(k_{m4}+[G]+[ADP])}\right)\left(\frac{1}{(1+([H^+]/k_h)^3)}\right) \quad (16)$$

$$r_4 = r_{4f} - r_{4b} = \frac{k_5[ADP]^2}{k_{m5}+[ADP]} - \frac{k_6[ATP][AMP]}{k_{m6}+[ATP]+[AMP]} \quad (17)$$

$$r_5 = \frac{k_7[AMP][H^+]}{(k_{m7}+[AMP]+[H^+])} \quad (18)$$

where r_{2f} and r_{4f} represent forward reaction rates, r_{2b} and r_{4b} denote backward reaction rates; k_1-k_7 are maximum rates of their associated reactions; k_{m1}-k_{m7} are Michaelis-Menten constants; and k_h is the H^+ concentration inhibiting one half of the PFK activity, which we will refer to as the half-inhibition H^+ concentration.

The second power of [ATP] in Eqn. (14) assumes that the rate of ATP hydrolysis is relatively insignificant for low ATP concentrations when compared with that at high ATP levels. The typical Michaelis-Menten representation assumes that enzymatic reverse reactions could be neglected (Paul and Gangopadhyay 2003). However, many enzymatic reactions are highly reversible and have significant backward reaction rates (Imperial and Centelles 2014). Here, the creatine kinase and the adenylate kinase reactions are both considered reversible (Rhoads and Lowenstein 1968; Stepanov, Mateo et al. 1997). Modification of the basic Michaelis-Menten equation to incorporate a backward reaction into r_2 and r_4 yields Eqns. (15) and (17), respectively.

The rate of glycolysis (r_3) is affected by the availability of phosphate and the activity of phosphofructokinase (PFK), the key regulatory enzyme in glycolysis. At the concentration used in the *in vitro* system, phosphate was not limiting and thus not explicitly represented in the glycogen phosphorylase reaction. Since PFK is highly sensitive to pH and is completely inactivated at a pH value close to 5.5 (England, Matarneh et al. 2014), the rate of glycolysis is influenced by pH, especially at low pH values. To model this behavior, the rate of glycolysis is written as a Michaelis-Menten term multiplied by a second, H^+-associated term in the form of the Hill equation as shown in Eqn. (16). The second term represents the strong dependence of PFK activity on H^+ with k_h being the half-inhibition hydrogen ion level. As hydrogen ion concentration ([H^+]) increases above k_h, the second term diminishes, leading to inactivation of PFK and thus termination of glycolysis.

Equations (6-18) form a kinetic model structure with adjustable parameters (the k-values) for the *in vitro* system used to analyze energy metabolism in postmortem muscle.

3.3 Model Validation

3.3.1 *Experimental data collection*

Details of the *in vitro* glycolytic system used and experiments conducted can be found in Matarneh et al. (2018). Briefly, all metabolites and cofactors required for glycolysis were included in the *in vitro* system. Powdered muscle was added as the source of glycolytic enzymes. Muscles used in the experiments were collected from six independent market-weight crossbred pigs (Yorkshire×Duroc, 100-125 kg, mixed sex). For each pig, the *longissimus lumborum* muscle was harvested, ground into fine powder, and then split into two groups: Control (the base *in vitro* system) and mitochondria treatment (with isolated mitochondria added to the *in vitro* system). Aliquots were removed at 0, 30, 120, 240, and 1440 minutes for metabolites (ATP, ADP, glycogen, AMP) and pH measurements. All experiments were conducted at 25°C.

3.3.2 *pH buffering capacity determination*

The rate of proton production (or consumption) in a system of biochemical reactions and pH change are related through pH buffering capacity β as shown below:

$$\beta = -\frac{d[H^+]_{total}}{d(pH)} = -\frac{d\left([H^+]+\sum\frac{[B][H^+]}{K_a+H^+}\right)}{d(pH)} \quad (19)$$

where $[B]$ denotes the concentration of buffering agent B and K_a is its dissociation constant.

Carnosine and acetate at concentrations of 0.025 mol/L and 0.01 mol/L, respectively, were used as buffering agents in the *in vitro* experiments. The buffering capacity was thus calculated as:

$$\beta = 2.303 \times 10^{-pH}\left(1 + \frac{10^{-pK_a^{carn}}[carn]}{\left(10^{-pK_a^{carn}} + 10^{-pH}\right)^2} + \frac{10^{-pK_a^{acet}}[acet]}{\left(10^{-pK_a^{acet}} + 10^{-pH}\right)^2}\right) \quad (20)$$

where the pKa values for carnosine and acetate are denoted as pK_a^{carn} and pK_a^{acet} and are 6.87 and 4.76, respectively.

A plot of the buffering capacity with respect to pH is shown in Figure 1. The plot indicates an approximately linear relationship between buffering capacity and pH over a broad range pH values. This linear relationship was also observed in postmortem muscles of pork and beef (Puolanne and Kivikari 2000; Matarneh, England et al. 2015). As a result, a linear function was used to represent the relationship between buffering capacity and pH as:

$$\beta = k_8[pH] - k_9 \quad (21)$$

where k_8 and k_9 are coefficients to be estimated as part of the model parameters as described below. It should be noted that this linear simplification overestimates the dependence of β on pH at low and high pH values where the curve flattens (Figure 3.1). Even with this overestimation, however, buffering capacity turns out to have only a minor influence on pH as will be shown later. This simplification, therefore, will not have a significant impact on the results obtained.

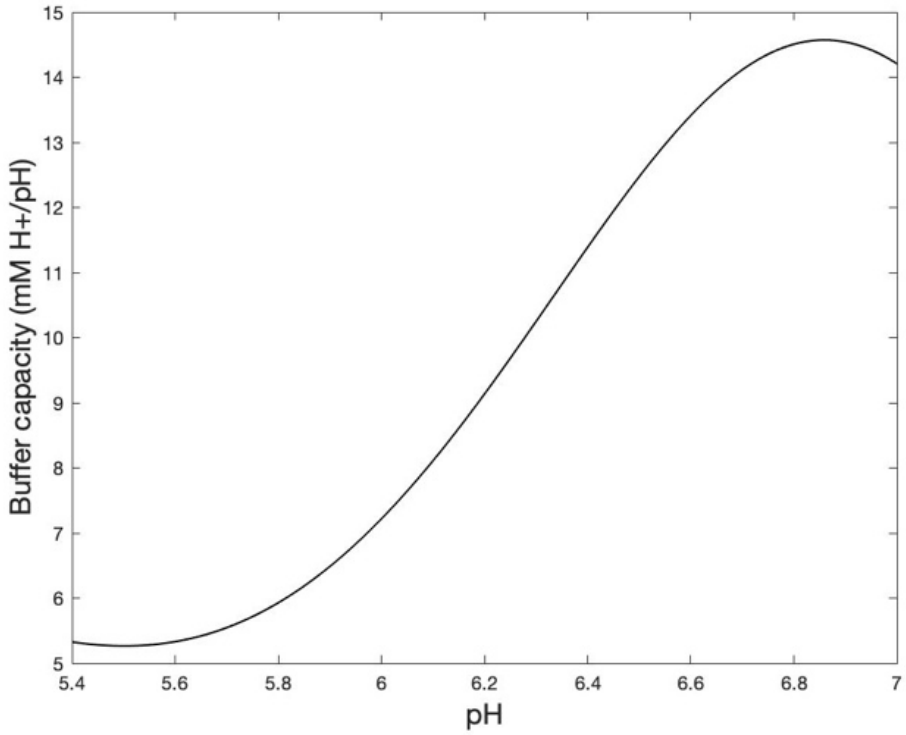

Figure 3.1 - Buffering capacity of the *in vitro* system with respect to pH

3.3.3 *Model structure validation and analysis*

The model parameters in Eqns. (7-18) and (21) were adjusted by using the Levenberg-Marquardt algorithm (Marquardt 1963) to achieve optimal model fit to the measured data. The least-squares optimization algorithm (Constantinides and Mostoufi 1999) was implemented in MATLAB (The MathWorks, Natick, MA, USA). During the optimization process, all model parameters were adjusted to give the optimal fit to observed data for the control group. For the mitochondria treatment group, model parameters k_{m1}-k_{m7} (m mol L^{-1}) determined for the control group were held unchanged (2.8206×10^{-24}, 5.100, 5.018, 3.357, 184.986, 4.830, 0.001, respectively) as these Michalis-Menten constants should not have changed by the addition of mitochondria,

while maximum reaction rates, k_1-k_7, coefficients of the buffering capacity expression, k_8 and k_9, and PFK half-inhibition H^+ concentration, k_h, were optimized since these parameters would be changed by the mitochondria treatment.

Comparisons between model predictions and experimental data are shown in Figure 3.2 and the optimized model parameter values are listed in Table 3.1.

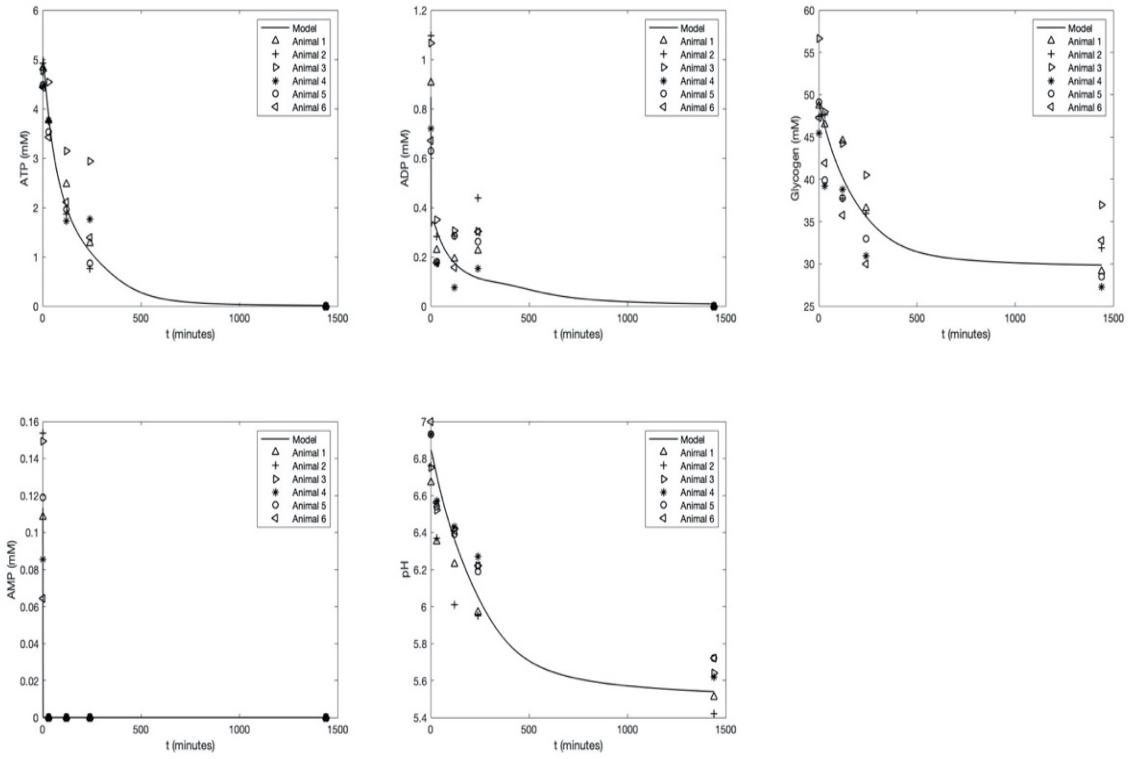

(a)

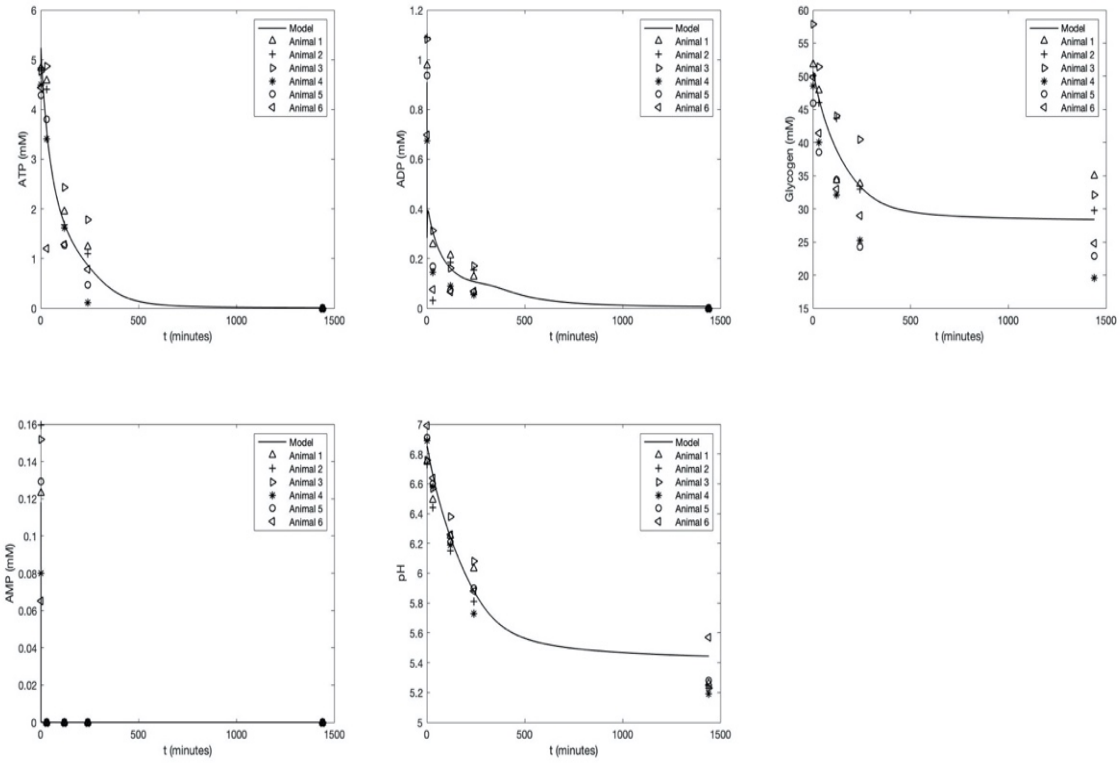

(b)

Figure 3.2 - Comparison between experimental observations and model predictions: (a) control group; (b) mitochondria group. Concentrations for ATP, ADP, glycogen, AMP and pH values were measured at 0, 30, 90, 240, 1440 min. Symbols represent experimental values while the solid lines represent the model predictions. Six separate datasets (indicated by different symbols) were measured from an *in vitro* system with powdered muscles collected from six different pigs. The model predictions were obtained with the parameter values listed in Table 3.1.

Table 3.1 Model parameter values used for model predications shown in Figures 2(a) and (b)

Parameter	Control Group	Mitochondria Group
k_1 (mmol L^{-1} min^{-1})	0.090	0.126
k_2 (mmol L^{-1} min^{-1})	12,590.583	380,000.978
k_3 (mmol L^{-1} min^{-1})	0.334	10.588
k_4 (mmol L^{-1} min^{-1})	1.009	1.356
k_5 (mmol L^{-1} min^{-1})	75.354	83.528
k_6 (mmol L^{-1} min^{-1})	3.772	3.803
k_7 (mmol L^{-1} min^{-1})	2,800.113	3,521.806
k_8 (mmol L^{-1} pH^{-2})	17.554	17.930
k_9 (mmol L^{-1} pH^{-1})	81.510	81.181
k_h (mmol L^{-1})	0.0016	0.0019

The relative standard error of prediction (RSEP) for metabolites (ATP, ADP, glycogen, AMP) and pH of the control and mitochondria groups was calculated as:

$$RSEP = \frac{1}{n}\sqrt{\frac{\sum_{i=1}^{N}(x_i^* - x_i)^2}{\sum_{i=1}^{N}(x_i^*)^2}} \quad (22)$$

where x_i^* and x_i are the i^{th} measured and predicted data points, respectively; N is the number of data points in an experimental run; and n is the number of runs. The degree of agreement between model predictions and experiments was also assessed in terms of R^2 values. The average relative errors and R^2 values for the control and mitochondria groups (Figures 3.2(a) and 3.2(b)) are listed in Table 3.2. It is obvious that the model structure could represent the kinetic variations in the major metabolites (ATP, ADP, Glycogen,

AMP) and pH with small relative errors for both groups of experiments, indicating the capability of the model structure.

Table 3.2 Relative standard errors of prediction and R^2 values for Figures 3.2(a) and (b)

	Control Group		Mitochondria Group	
	RSEP (%)	R^2	RSEP (%)	R^2
ATP	2.61	0.93	3.71	0.88
ADP	5.14	0.80	4.56	0.88
Glycogen	1.56	0.74	2.21	0.72
AMP	4.53	0.91	4.71	0.90
pH	0.47	0.83	0.36	0.94

In consideration of variations among individual animals, the model structure was further validated against measured data for each animal in the control or mitochondria group to test its capability to represent animal-to-animal variations. Model predictions and experimental data for an example animal are shown in Figure 3.3. The average R^2 values for ATP, ADP, glycogen, AMP and pH are, respectively, 0.97 ± 0.03, 0.87 ± 0.08, 0.85 ± 0.09, 0.99 ± 0.00 and 0.89 ± 0.06 for the control group and 0.94 ± 0.08, 0.97 ± 0.02, 0.94 ± 0.06, 0.99 ± 0.00 and 0.97 ± 0.03 for the mitochondria group. The optimized model parameters are represented as mean ± standard deviation in Table 3.3. It should be noted that the mean parameter values are similar to but not equal to those obtained from using all the animals in each group simultaneously (Table 3.1) since the two computational operations are not mathematically equivalent. The individually determined parameter values, nonetheless, reflect animal-to-animal variations. One-way analysis of

variance (ANOVA) was then used to determine if there were significant differences ($P < 0.05$) in the model parameters between the two groups.

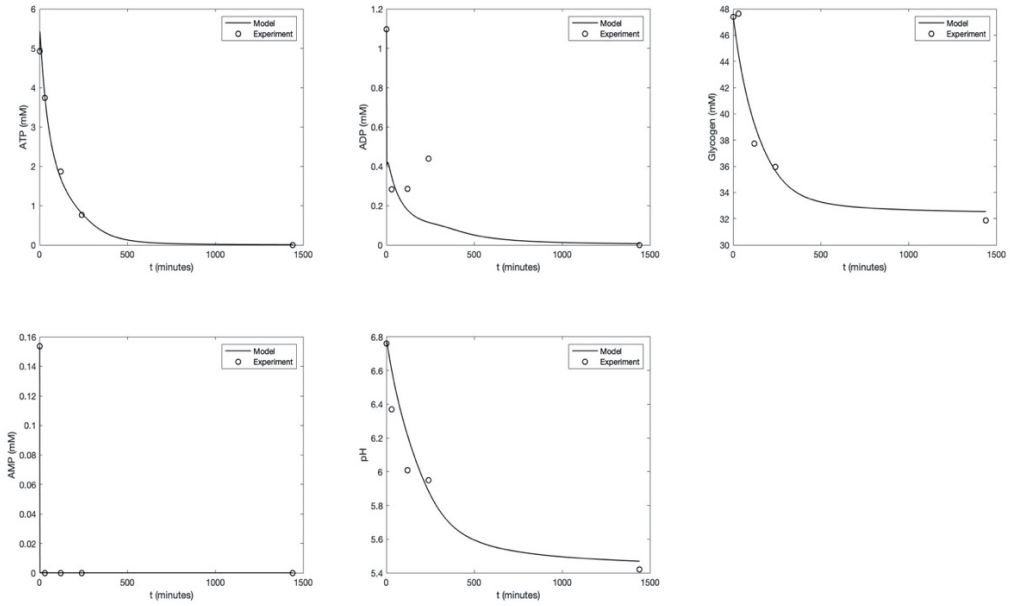

(a)

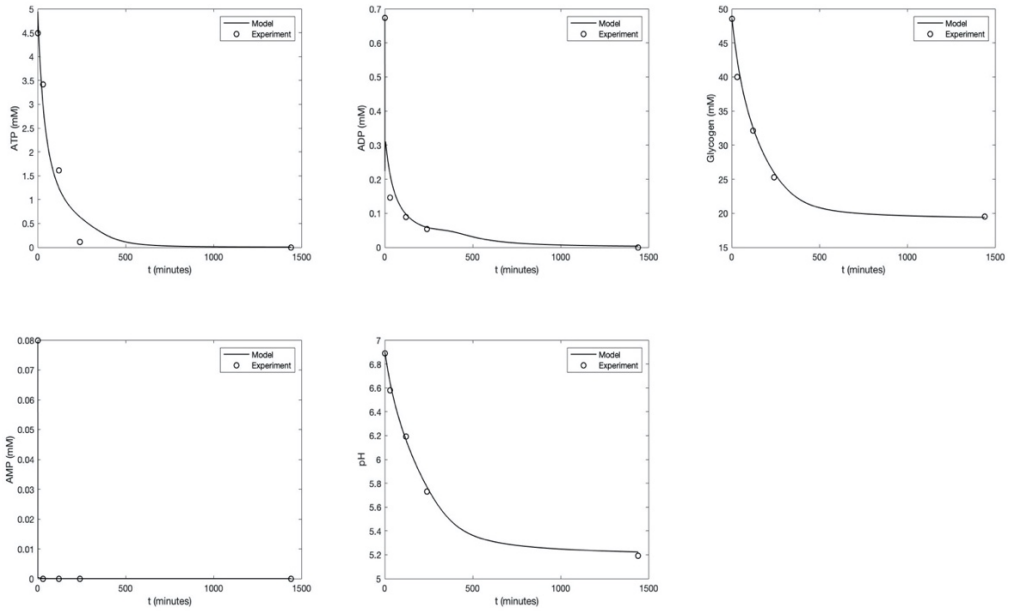

(b)

Figure 3.3 - Example plots comparing model predictions against experimental measurements for a single animal: (a) control, (b) mitochondria. Concentrations for ATP, ADP, glycogen, AMP and pH values were measured at 0, 30, 90, 240, 1440 min.

Table 3.3 Model parameter values obtained from individual animals

Parameter	Control	Mitochondria	P-value
k_1 (mmol L^{-1} min^{-1})	0.0838 ± 0.0002	0.146 ± 0.003	0.0224
k_2 (mmol L^{-1} min^{-1})	12590 ± 0	380000 ± 4.065×10^{-21}	7.844×10^{-158}
k_3 (mmol L^{-1} min^{-1})	0.322 ± 0.028	10.584 ± 1.484×10^{-5}	4.264×10^{-18}
k_4 (mmol L^{-1} min^{-1})	0.979 ± 0.020	2.165 ± 0.216	0.000137
k_5 (mmol L^{-1} min^{-1})	75.327 ± 0.323	183.832 ± 0.448	3.821×10^{-21}
k_6 (mmol L^{-1} min^{-1})	3.367 ± 0.624	4.209 ± 0.150	0.0410
k_7 (mmol L^{-1} min^{-1})	2800.113 ± 0	3321.806 ± 3.467×10^{-8}	1.061×10^{-64}
k_8 (mmol L^{-1} pH^{-2})	17.565 ± 0.549	18.003 ± 0.342	0.282
k_9 (mmol L^{-1} pH^{-1})	81.017 ± 0.674	80.677 ± 0.715	0.496
k_h (mmol L^{-1})	0.00166 ± 4.229×10^{-8}	0.00262 ± 3.346×10^{-7}	0.00336

As shown in Table 3.3, the values of parameters k_1-k_7 of the mitochondria group were significantly higher than those of the control group ($P < 0.05$), indicating that ATP hydrolysis; glycolysis; creatine kinase-, adenylate kinase-, and AMP deaminase-mediated reactions were all elevated by the addition of mitochondria. This suggests that mitochondria positively regulate postmortem energy metabolism, which is consistent with previous studies (Matarneh, England et al. 2017; Matarneh, Yen et al. 2018).

k_8 and k_9 describe the dependence of buffering capacity on pH. No significant difference between the mitochondria group and the control group was observed ($P > 0.05$) in these two parameters. This is expected since the addition of isolated mitochondria should not change the pH buffering capacity behavior.

k_h is the H^+ concentration for half-inhibition of PFK activity and it was significantly higher ($P < 0.01$) for the mitochondria group (0.00262 mmol/L) than for the control group (0.00166 mmol/L). The difference can be explained by the difference in ATP level in the two groups. It is known that ATP and H^+ have positive interactions in or additive effects on inhibiting PFK activity (Ui, 1966; Bock, Frieden, 1976; Dobson, Yamamoto et al. 1986). Addition of mitochondria enhanced ATP hydrolysis (as shown by the greater k_1 value for the mitochondria group in Tables 3.1 and 3.3) and thus decreased the ATP level in the mitochondria group, which is discernable by comparing the plots in Figures 3.2 and 3.3. The lower ATP level would lead to a higher half-inhibition H^+ concentration for PFK in the mitochondria group as correctly shown by the greater estimated k_h value. This higher H^+ concentration for half-inhibition of PFK activity would result in a lower ultimate pH for the mitochondria group, which is clearly observable from Figures 3.2 and 3.3. This is in agreement with previous work that pH-induced inhibition of muscle PFK is related to ATP levels and the optimal pH for PFK is shifted to the alkaline side at elevated ATP concentrations (Ui 1966; Bock, Frieden, 1976; Dobson, Yamamoto et al. 1986).

Experimental validation of the model structure indicated a good balance in model complexity between flexibility and definitiveness. The model showed sufficient flexibility to describe variations in metabolites and pH for individual or grouped animals of different treatments, and yet this flexibility did not come from excessive complexity which would sacrifice definitiveness of the estimated model parameters. It is noteworthy that the estimated parameter values consistently reflected what is known or can be expected. This included the unchanged Michaelis-Menten constants between treatment

groups, the significant impact of mitochondria on the maximum reaction rates, the lack of influence of mitochondria on pH buffering capacity, and most interestingly, the correct reflection of the changes in the half-inhibition H^+ concentration for PFK. This indicates that the proposed model structure captures the most important kinetics of energy metabolism without being overly complex.

3.4 Simulation and Analysis of pH Variations

The rate and extent of pH fall significantly influences meat quality. Abnormal postmortem pH decline in pork leads to two major meat quality defects facing the meat industry - PSE (pale, soft and exudative) meat and DFD (Viljoen, de Kock et al. 2002) meat (Rathgeber, Boles et al. 1999; Page, Wulf et al. 2001; Viljoen, de Kock et al. 2002; Zhu, Ruusunen et al. 2013). It is therefore important to know which factor(s) contribute(s) to pH changes postmortem. To investigate this, simulations were performed. A small change was introduced to each parameter from its optimized value while keeping the other parameters unchanged, and the ratio of the pH change over the parameter change was computed as partial derivative $\frac{\partial pH}{\partial k_i}$ (i = 1-9 or h) and used as an indicator of direct parameter influence on pH or relative sensitivity. The partial derivative profiles over time are shown in Figure 3.4.

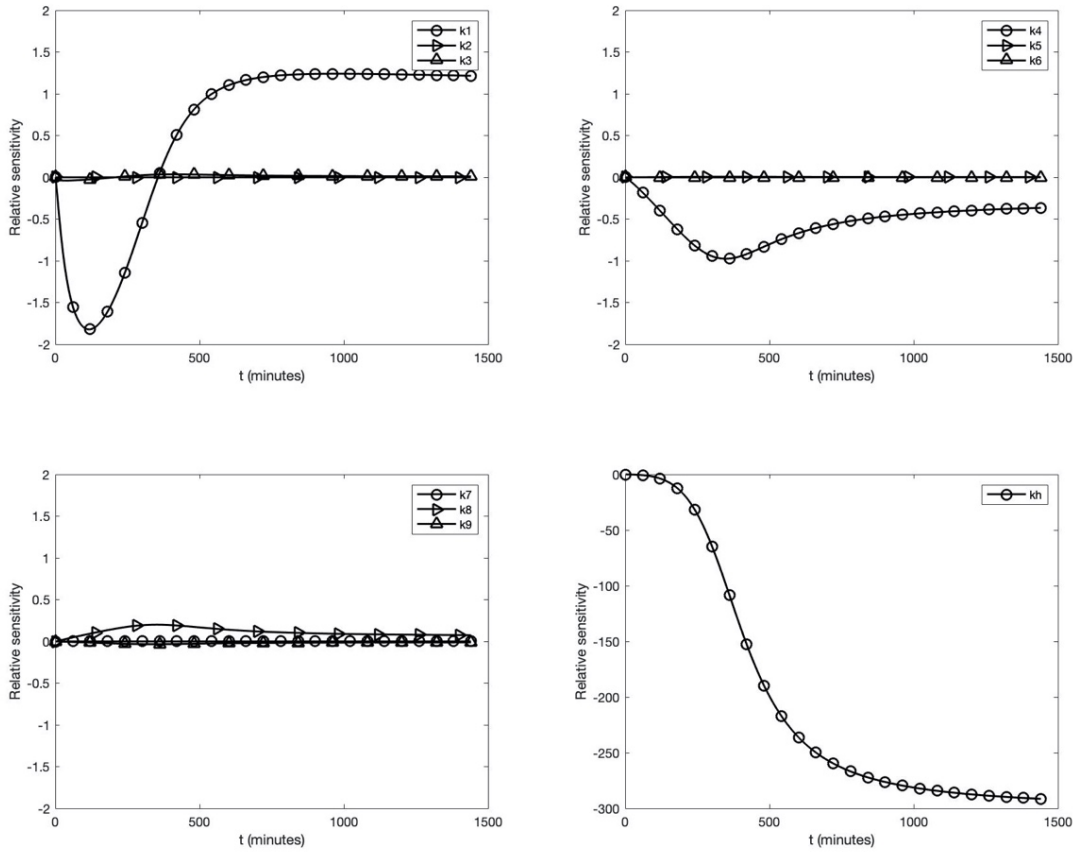

Figure 3.4 - Partial derivatives of pH with respect to model parameters (or relative parameter sensitivities) indicating the direct influences of parameters on pH in postmortem muscle.

As shown in Figure 3.4, pH is strongly influenced by k_1, k_4, and k_h, which represent the maximum rates of ATP hydrolysis and glycolysis, and the half-inhibition H^+ concentration for PFK, respectively. k_8, which is associated with buffering capacity, shows only a minor effect on pH. All the other parameters show negligible influence on pH.

ATP hydrolysis has a strong impact on pH as shown by the k_1 curve in the upper-left panel of Figure 3.4. It is interesting to note the sign change of the derivative $(\frac{\partial pH}{\partial k_1})$ from negative to positive as time progresses. In the initial stage, an increase in the rate of

ATP hydrolysis will accelerate the initial pH decline, while at a later stage (after approximately 250 min postmortem), increasing ATP hydrolysis will slow down the pH decline, thereby leading to a higher ultimate pH. This is consistent with early research that the rate of pH decline is driven by the rate of postmortem ATP hydrolysis (Scopes 1974; Bowker, Botrel et al. 2004).

It can be observed from the upper-right panel of Figure 3.4 that elevated glycolysis rate (k_4) will accelerate the rate of pH decline. The influence is predominantly in the initial stages. As time progresses, the impact will diminish but still result in a decline in the ultimate pH, which is consistent with previous research (Matarneh, England et al. 2017; Matarneh, Beline et al. 2018).

Buffering capacity has a relatively minor effect on pH as shown by the k_8 curve in Figure 3.4 (bottom-left panel). The graph shows that increasing buffering capacity will slow down the rate of pH decline and lead to a slightly higher ultimate pH. This is consistent with the previous study that lower buffering capacity was responsible for lower ultimate pH in the AMPK$\gamma 3^{R200Q}$ mutant pigs compared to wild-type pigs (Matarneh, England et al. 2015). Indeed, differences in buffering capacity contribute to variations in the ultimate pH in postmortem muscle, though the influence is relatively small compared to ATP hydrolysis, glycolysis and half-inhibition H^+ concentration for PFK.

The half-inhibition H^+ concentration for PFK (k_h) shows a strong influence on pH as shown in the lower-right panel of Figure 3.4. An increase in k_h will markedly accelerate the pH decline after approximately 400 min postmortem and result in a reduced ultimate pH because an elevated H^+ concentration is required to inactivate PFK and terminate glycolysis.

The influences represented by the partial derivatives as discussed above are partial effects in that each derivative indicates the direct effect of changes in one parameter alone without considering any potential accompanying changes in other parameters or indirect effects. Changes in one parameter, however, often occur with simultaneous variations in other parameters. As discussed in the previous section and shown in Tables 3.1 and 3.3, for example, the change in k_1 resulting from mitochondria addition is accompanied by significant changes in k_2-k_7 and k_h. Evaluation of the total influence of a treatment on a metabolite or pH entails the computation of a total derivative.

To evaluate the total effect of mitochondria addition on pH decline, the total derivative was calculated as $\frac{\partial pH}{\partial k_1} + \sum_{i=2}^{N} \frac{\partial pH}{\partial k_i}\frac{\partial k_i}{\partial k_1}$, where N is the number of parameters. The first term ($\frac{\partial pH}{\partial k_1}$) represents the direct effect of ATP hydrolysis on pH resulting from the addition of mitochondria (or ATPase), and the second term ($\sum_{i=2}^{N} \frac{\partial pH}{\partial k_i}\frac{\partial k_i}{\partial k_1}$) denotes the simultaneous indirect effects of mitochondria addition on pH via other parameters. As is shown in Figure 3.4, the partial derivatives ($\frac{\partial pH}{\partial k_i}$) with respect to parameters k_2, k_3, k_5, k_6, k_7 and k_9 are small and could be neglected. Moreover, there were no changes parameters k_{m1}-k_{m7} and k_8 as these parameters should not be influenced by the addition of mitochondria; therefore, the partial derivative $\frac{\partial k_i}{\partial k_1}$ for these parameters (i = m1-m7, 8) are zero. Thus, the total influence of mitochondria on pH includes direct effect of ATP hydrolysis (k_1) and indirect effects via glycolysis (k_4) and the half-inhibition H^+ concentration for PFK (k_h), which is represented by the total derivative:

$$\frac{dpH}{dk_1} = \frac{\partial pH}{\partial k_1} + \frac{\partial pH}{\partial k_4}\frac{\partial k_4}{\partial k_1} + \frac{\partial pH}{\partial k_h}\frac{\partial k_h}{\partial k_1} \quad (23)$$

If $\frac{\partial k_4}{\partial k_1}$ and $\frac{\partial k_h}{\partial k_1}$ associated with mitochondria addition did not change greatly over time, they may be estimated with the parameter increments (Δk_1, Δk_4 and Δk_h) in Table 3.1. The other partial derivatives in Eqn. (23) are shown in Figure 3.4. The total derivative may then be computed. The total effect of mitochondria on pH decline over time can then be estimated as $\frac{dpH}{dk_1}\Delta k_1$ as shown in Figure 3.5.

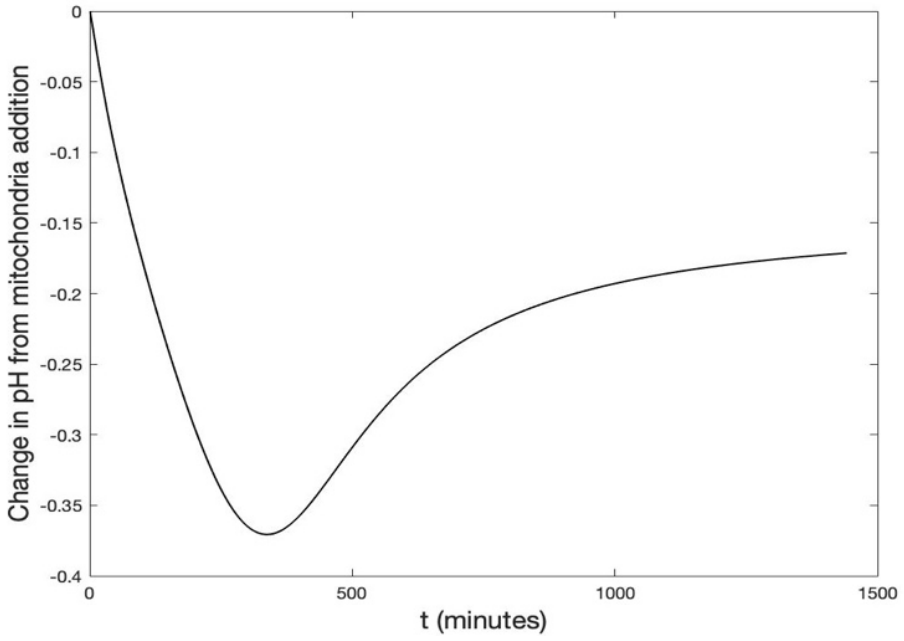

Figure 3.5 - Total effect of mitochondria addition on pH in the *in vitro* glycolytic system.

Figure 3.5 shows that addition of mitochondria will accelerate the pH decline and result in a lower ultimate pH. The curve indicates that the addition of mitochondria causes a net decrease of 0.17 in the ultimate pH, which is in nearly perfect agreement with the experimental measurements. It is interesting to observe that the resulting pH decline is more drastic in the early stage, reaching a maximum at around 300 min post addition of mitochondria, and then moderates later in the process. While Figure 3.5 shows the change in pH rather than the pH value itself, it points in the direction of the

working model for postmortem pH decline previously presented (Scheffler, Matarneh et al. 2015; Matarneh, England et al. 2017; Matarneh, Beline et al. 2018).

While the faster pH decline and lower final pH in the mitochondria group is the combined effect of enhanced ATP hydrolysis and glycolysis and higher half-inhibition H^+ concentration for PFK, evaluation of the three terms in Eqn. (23) shows that the change in the half-inhibition H^+ concentration is the most consequential part because of the strong effect of the k_h as shown in Figure 3.4. As discussed earlier, a lower ATP level resulting from enhanced ATP hydrolysis by mitochondrial ATPase would increase the half-inhibition H^+ concentration for PFK (Ui 1966; Bock and Frieden 1976; Dobson, Yamamoto et al. 1986). It can thus be inferred that when changes in ATPase lead to variations in ATP concentration, the subsequent changes in PFK activity will amplify the effect and predominantly determine the pH behavior and the ultimate pH.

3.5 Conclusions

The proposed kinetic model structure with optimized parameters closely described observed variations in metabolites and pH under varied conditions and the estimated parameter values consistently reflected what is known or can be expected, indicating a desirable level of model complexity. Simulation and analysis of pH variations based on the model provided insights into the rate and extent of pH decline in postmortem muscles. Postmortem pH is influenced by the rates of ATP hydrolysis and glycolysis, half-inhibition H^+ concentration for phosphofructokinase activity, and to a much lesser extent, pH buffering capacity. All other reactions have negligible effects and

phosphofructokinase activity has the strongest influence. Further experimental confirmation of these results is warranted.

Acknowledgement

This project was supported by the National Institute of Food and Agriculture, U.S. Department of Agriculture, under award number 2017-67017-26470.

CHAPTER 4

CONTRIBUTIONS OF ENERGY PATHWAYS TO ATP PRODUCTION AND pH VARIATIONS IN POSTMORTEM MUSCLES

Abstract

The roles of energy pathways in postmortem muscles are still debated. In this study, the contributions of different pathways to ATP production and pH variations were analyzed by using a kinetic model based on data from beef *longissimus lumborum*. Phosphocreatine represents over 92% of the initial ATP production but, after 24 hours, glycolysis, phosphocreatine, myokinase reaction, and aerobic respiration contribute, respectively, 89.44%, 5.26%, 4.44%, and 0.86% of the cumulative amount of ATP produced. ATP hydrolysis and glycolysis result in 0.52 and 0.6 units of pH decline, respectively, at 24 hours with ATP hydrolysis accounting for most of the early decline. Phosphocreatine, myokinase reaction, and aerobic respiration lead to, respectively, 0.08, 0.07, and 0.004 units of pH increase after 24 hours though phosphocreatine is depleted within the first 30 minutes. Furthermore, electrical stimulation affects pH primarily through ATP hydrolysis and glycolysis. The initial muscle oxygen saturation level and phosphocreatine content affect pH but the influences are small.

4.1 Introduction

Postmortem muscles attempt to maintain cellular energy homeostasis by preserving adenosine triphosphate (ATP) content at a normal level (Bowker et al., 2000; Scheffler & Gerrard, 2007; Vetharaniam et al., 2010). ATP, the energy currency in cells, is continuously hydrolyzed to fuel cellular functions such as ion channel regulation, signal transduction, and gene transcription (Wang et al., 2017; Wei et al., 2019). Because the stores of ATP in a skeletal muscle are limited and would be exhausted after a few muscle twitches without replacement, ATP-regenerating pathways are critical for maintaining ATP homeostasis. The immediate metabolic pathway for producing ATP is the degradation of phosphocreatine (PCr) (Hancock et al., 2005). Phosphocreatine or creatine phosphate is a high energy-storing molecule in muscle cells that donates its high-energy phosphate group to ADP to form ATP and creatine. However, ATP produced through creatine kinase-mediated reaction lasts for only a brief period and is subsequently followed by a decrease in ATP level. The combination of decreased ATP content and high energy demand in postmortem muscle triggers other metabolic pathways to synthesize ATP. Two pathways, anaerobic glycolysis and mitochondrial oxidative respiration, are the major mechanisms for ATP production. Under aerobic conditions, mitochondrial oxidative respiration is the dominant pathway. Under anaerobic conditions such as fast-moving or postmortem muscles, however, mitochondrial oxidative respiration is suppressed by the lack of oxygen while glycolysis becomes a significant contributor to ATP production.

Aerobic respiration in postmortem muscles has been neglected for many years based on the general belief that animals lose the ability to transport oxygen to muscles

and thus oxygen is depleted immediately following exsanguination. However, several recent publications showed that muscles retain oxygen after stunning and exsanguination and its depletion is a gradual rather than instantaneous process in a postmortem muscle (England et al., 2018; Ramos et al., 2020). Moreover, mitochondria remain structurally intact and are capable of aerobic respiration at the early postmortem stage (Ashmore et al., 1971; Matarneh et al., 2018; Tang et al., 2005). As a result, some researchers believe mitochondrial aerobic respiration contributes little to ATP production because of the limited oxygen in postmortem muscles, while others argue the role of aerobic respiration should not be underestimated since aerobic respiration is more efficient for ATP production than glycolysis (England et al., 2018). Thus, the relative contribution of the different ATP-generating pathways to postmortem ATP production remains to be quantitatively studied.

Another central product of postmortem metabolism is the accumulation of hydrogen ions (H^+). Hydrogen ion accumulation leads to pH decline in postmortem muscles (Matarneh et al., 2018; Scheffler et al., 2015; Scopes et al., 1974). The rate and extent of pH decline significantly influence meat quality attributes in terms of color, water-holding capacity (WHC) and tenderness (Savell et al., 2005; Thompson et al., 2006). It is reported that rapid postmortem pH decline is associated with the development of PSE (pale, soft and exudative) meat (Rathgeber et al., 1999; Zhu et al., 2013), while DFD (dark, firm and dry) and acidic products are defects related to limited and extended ultimate pH declines, respectively. Therefore, to produce meat with consistent quality, it is necessary to understand the factors that affect the rate and extent of postmortem pH decline.

In this study, the relative contributions of ATP-generating pathways to ATP production and pH variations in postmortem muscles were analyzed by using a kinetic model developed for postmortem energy metabolism based on the major biochemical reactions and data collected from beef *longissimus lumborum* muscles. The results shed quantitative light on the role of different ATP-generating pathways in postmortem muscles. Furthermore, the impacts of initial stores of muscle phosphocreatine, initial muscle oxygen saturation level and electrical stimulation on pH were analyzed based on the model to provide insights into the factors that influence pH behavior in postmortem muscles.

4.2 Model development

4.2.1 *Biochemical reactions in postmortem muscles*

Muscle energy metabolism involves a series of chemical reactions that maintain cellular energy homeostasis. The central outcome of muscular energy metabolism is the maintenance of cellular ATP. When a living animal is at rest or under low labor intensity, the ATP turnover rate is relatively slow and mitochondrial oxidative respiration is sufficient to maintain cellular ATP homeostasis (Hochachka and McClelland 1997; Conley et al., 2001). However, after slaughter, muscles lose the ability to obtain oxygen through the circulatory system. Oxygen retained in a postmortem muscle can only support limited levels of mitochondrial aerobic respiration. In this circumstance, anaerobic glycolysis, and creatine kinase- and adenylate kinase-catalyzed reactions

become major contributors to ATP production. The major reactions involved in postmortem energy metabolism are as follows:

i. ATP hydrolysis catalyzed by ATPase:

$$ATP^{4-} + H_2O \rightarrow ADP^{3-} + \delta HPO_4^{2-} + (1-\delta)H_2PO_4^- + \delta H^+ \quad (1)$$

ii. Creatine kinase pathway for ATP synthesis:

$$CrP^{2-} + ADP^{3-} + H^+ \leftrightarrows Cr + ATP^{4-} \quad (2)$$

iii. Anaerobic glycolysis:

$$ADP^{3-} + \frac{1}{3}G + \delta HPO_4^{2-} + (1-\delta)H_2PO_4^- + \delta H^+ \rightarrow ATP^{4-} + H_2O + \frac{2}{3}La^- + \frac{2}{3}H^+ \quad (3)$$

iv. Interconversion of adenosine phosphates by adenylate kinase (or myokinase):

$$2ADP^{3-} \leftrightarrows ATP^{4-} + AMP^{2-} \quad (4)$$

v. AMP deamination by deaminase:

$$AMP^{2-} + H^+ \rightarrow IMP^{2-} + NH_4^+ \quad (5)$$

vi. Aerobic respiration:

$$\frac{1}{38}G + \frac{6}{38}O_2 + ADP^{3-} + \delta HPO_4^{2-} + (1-\delta)H_2PO_4^- + \delta H^+ \rightarrow ATP^{4-} + \frac{6}{38}CO_2 + \frac{44}{38}H_2O \quad (6)$$

where

$$\delta = \frac{10^{-\mathrm{pKa}}}{10^{-\mathrm{pKa}} + [H^+]} \quad (7)$$

is the fraction of free phosphate (P_i) existing as HPO_4^{2-} (P_i^{2-}) in equilibrium with $H_2PO_4^-$ (P_i^-) with pKa = 6.70 (Kushmerick, 1997), *Cr* is creatine, *G* is glycogen, *La* is lactate, and the other symbols are as commonly used in the literature.

4.2.2 *Kinetic model structure*

Based on reactions a-f (Eqns. 1-6), the concentrations of the major substrates including ATP^{4-}, ADP^{3-}, AMP^{2-}, IMP^{2-}, glycogen (G), lactate (La), creatine phosphate (CrP^{2-}); pH; and percent muscle oxygen saturation (O_m) can be described by,

$$\frac{d[ATP]}{dt} = -r_1 + r_2 + r_3 + r_4 + r_6 \tag{8}$$

$$\frac{d[ADP]}{dt} = r_1 - r_2 - r_3 - 2r_4 - r_6 \tag{9}$$

$$\frac{dpH}{dt} = -\frac{1}{\beta}\left(\delta r_1 - r_2 + \left(\frac{2}{3} - \delta\right) r_3 - r_5 - \delta r_6\right) \tag{10}$$

$$\frac{d[G]}{dt} = -\frac{1}{3} r_3 - \frac{1}{38} r_6 \tag{11}$$

$$\frac{d[AMP]}{dt} = r_4 - r_5 \tag{12}$$

$$\frac{d[IMP]}{dt} = r_5 \tag{13}$$

$$\frac{d[La]}{dt} = \frac{2}{3} r_3 \tag{14}$$

$$\frac{d[O_m]}{dt} = \frac{-6}{38} \frac{1}{4[Mb]} r_6 \tag{15}$$

$$\frac{d[CrP]}{dt} = -r_2 \tag{16}$$

where r_1-r_6 are the net forward reaction rates corresponding to reactions a-f (Eqns. 1-6), respectively; t is time; Mb is myoglobin; and [x] denotes the concentration of metabolite x. The reaction rates (r_1-r_6) may be represented in terms of the major substrate concentrations and undetermined model parameters (k_1-k_{10}, k_{m1}-k_{m8}) in simplified Michaelis-Menten forms as:

$$r_1 = \frac{k_1[ATP]^2}{(k_{m1}+[ATP])} \tag{17}$$

$$r_2 = \frac{k_2[CrP][ADP][H^+]}{k_{m2}+[CrP]+[ADP]+[H^+]} - \frac{k_3[ATP][Cr]}{k_{m3}+[ATP]+[Cr]} \tag{18}$$

$$r_3 = \left(\frac{k_4[G][ADP][Pi]}{(k_{m4}+[G]+[ADP])}\right)\left(\frac{1}{(1+([H^+]/k_h)^3)}\right) \tag{19}$$

$$r_4 = \frac{k_5([ADP]-[ADP]_r)^2}{k_{m5}+[ADP]} - \frac{k_6[ATP][AMP]}{k_{m6}+[ATP]+[AMP]} \quad (20)$$

$$r_5 = \frac{k_7([AMP]-[AMP]_r)[H^+]}{(k_{m7}+[AMP]+[H^+])} \quad (21)$$

$$r_6 = \frac{k_8[G][O_2][ADP][Pi]}{(k_{m8}+[G]+[O_2]+[ADP]+[Pi])} \quad (22)$$

where

$$\beta = k_9[pH] - k_{10} \quad (23)$$

is an approximate relationship between pH buffering capacity and pH (Wang et al., 2021), k_1-k_8 are reaction rates, k_{m1}-k_{m8} are Michaelis constants, k_h is the H^+ concentration inhibiting 7/8 of the phosphofructokinase (PFK) activity, $[ADP]_r$ and $[AMP]_r$ are residual ADP and AMP concentrations which averaged at 0.35 mmol L^{-1} and 0.21 mmol L^{-1}, respectively, based on laboratory measurements (England et al., 2018). More details of the method used for model development can be found in Wang et al. (2021).

4.3 Model validation

4.3.1 *Experimental data collection*

The entire *longissimus lumborum* was excised from one side of eight market-weight cattle (550-700 kg) and then split in half perpendicular to the longitudinal axis of the muscle. To eliminate temperature effects, each half of the *longissimus lumborum* was placed on a Styrofoam tray at 25 °C for 120 min postmortem and then kept at 4 °C till completion of all measurements. One half of the *longissimus lumborum* was directly measured for muscle oxygenation and then sampled as the control group at 0, 60, 240, and 1440 min postmortem for pH and metabolites (ATP, ADP, AMP, IMP, glycogen, and lactate) measurements. The other half was electrically stimulated with a Jarvis Model

BV80 stimulator (Jarvis, Middletown, CT) at 21 V, 0.25 A, and 60 Hz for 90 s as a treatment group and then measured for muscle oxygenation and sampled for pH and metabolites measurements at 0, 60, 240, and 1440 min. A Moxy muscle oxygen monitor (Fortiori Design LLC, Hutchinson, MN) was used to measure muscle oxygenation. The monitor was pressed against an exposed muscle until the reading stabilized. Electrical stimulation is known to expedite postmortem reactions and the treatment group was used in this work to alter the initial conditions of the muscle samples and thus to add data variations beyond the control group for more rigorous testing of the model. More details of the experiments conducted can be found in England et al. (2018).

4.3.2 *Model validation and analysis*

The model parameters in Eqns. (8-23) were adjusted by using the Levenberg-Marquardt algorithm (Marquardt, 1963) to achieve optimal fit to the measurements. All model parameters were adjusted during the optimization process to give the optimal fit to experimental observations for the control group. For the electrical stimulation group, model parameters k_{m1}-k_{m8} (mmol L^{-1}) determined for the control group were used and held unchanged (8.600, 5.100, 5.018, 3.357, 0.0002, 4.830, 0.010, 0.001, respectively) as these constants were not expected to change from electrical stimulation, while reaction rates, k_1-k_8; coefficients of the buffering capacity expression, k_9 and k_{10}; and PFK inhibition H^+ concentration, k_h were optimized since these parameters would be changed by electrical stimulation.

Comparisons between model predictions and experimental data are shown in Figure 4.1 and the optimized model parameter values are listed in Table 4.1. The relative standard

errors of prediction (RESP) were calculated to assess the degree of agreement between model predictions and experiments. The RESP for the control and electrical stimulation groups (Figure 4.1(a) and (b)) are listed in Table 4.2.

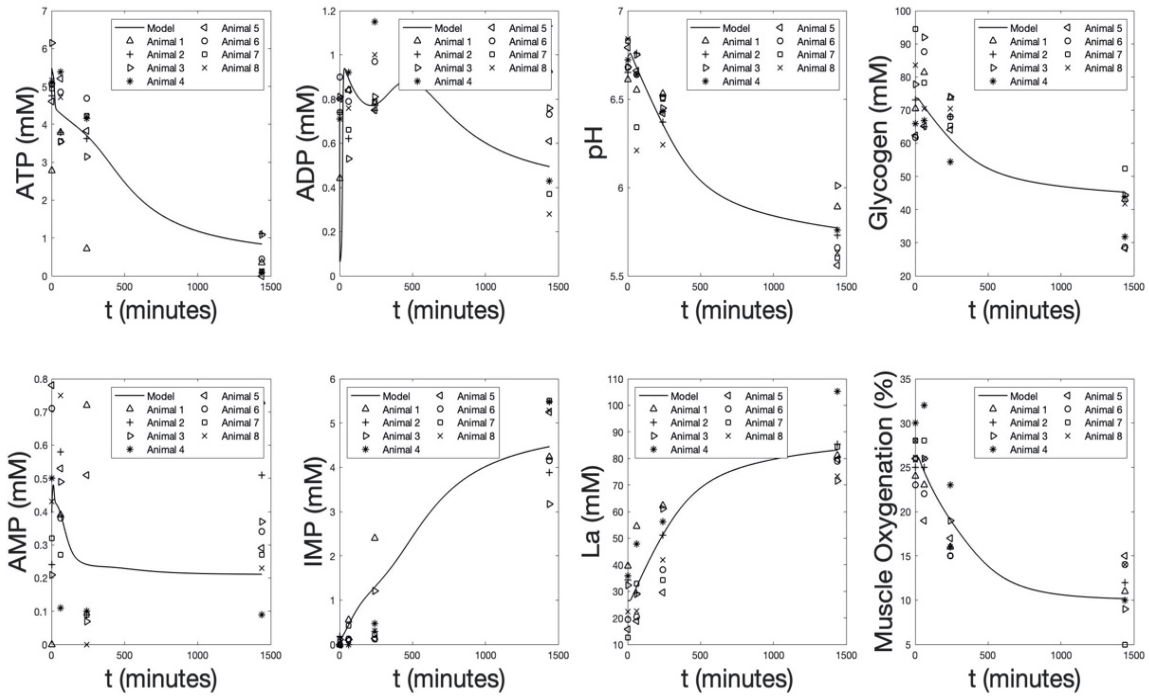

(a)

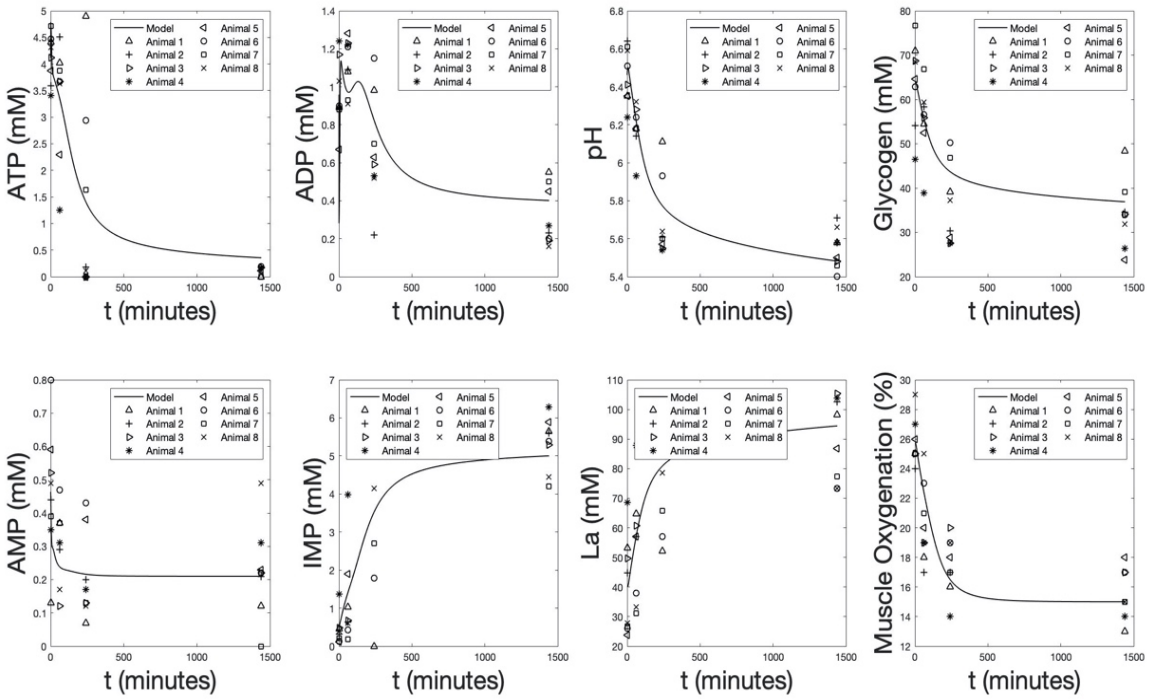

(b)

Figure 4.1 - Comparison between experimental observations and model predictions: (a) control group; (b) electrical stimulation group. Concentrations of ATP, ADP, glycogen, AMP, IMP, and La; pH and muscle oxygenation were measured at 0, 60, 240, 1440 min postmortem. Different symbols represent eight separate datasets measured from eight different cattle, while the solid lines represent the model predictions. The model predictions were obtained with the parameter values listed in Table 4.1.

Table 4.1 Model parameter values used for model predictions shown in Figures 4.1(a) and (b)

Parameter	Control Group	Electrical stimulation Group
k_1 (mmol L^{-1} min^{-1})	0.1355	0.4584
k_2 (mmol L^{-1} min^{-1})	50200.12	89047.3
k_3 (mmol L^{-1} min^{-1})	0.00003	0.726
k_4 (mmol L^{-1} min^{-1})	0.0411	0.1086
k_5 (mmol L^{-1} min^{-1})	0.0152	0.03
k_6 (mmol L^{-1} min^{-1})	0.00004	0.0016
k_7 (mmol L^{-1} min^{-1})	68.05	178.05
k_8 (mmol L^{-1} pH^{-1})	0.0035	0.0082
k_9 (mmol L^{-1} pH^{-2})	20.014	20.014
k_{10} (mmol L^{-1} pH^{-1})	70.57	70.57
k_h (mmol L^{-1})	0.000617	0.00083

Table 4.2 Relative standard errors (%) of prediction (RESP) for Figures 4.1(a) and (b)

Predicted variable	Control group	Electrical stimulation group
ATP	2.86	4.40
ADP	2.61	3.01
Glycogen	1.88	2.02
AMP	6.11	2.15
pH	0.29	0.32
IMP	3.47	4.43
Lactate	2.61	2.32
Muscle oxygenation	1.86	1.40

Figure 4.1 and the RESP values listed in Table 4.2 show that the model structure could represent the measured postmortem variations in metabolites, pH and muscle oxygenation for the control and the electrical stimulation groups with small relative errors. The parameter values listed in Table 4.1 show that electrical stimulation accelerates postmortem energy metabolism by increasing the rates of reactions for ATP hydrolysis, creatine kinase-catalyzed reaction, myokinase-catalyzed reaction, anaerobic glycolysis, and aerobic respiration, which is consistent with the previous studies (England et al., 2018; Hammelman et al., 2003; Hwang et al., 2003).

4.4 Contributions of ATP-generating pathways to ATP production and pH variations

4.4.1 *Contributions of ATP-generating pathways to ATP production*

Partitioning of ATP production among the energy-producing pathways is essential for cellular bioenergetics but cumbersome to measure experimentally in the laboratory (Mookerjee et al., 2017). Hence, the kinetic model with optimized parameters presented above was used to evaluate the contribution of each pathway to total ATP production. Cellular ATP is mainly maintained by creatine kinase- and myokinase-mediated reactions, anaerobic glycolysis, and aerobic respiration. The rate of ATP production by each pathway (r_2, r_4, r_3, and r_6) is plotted as a percentage of the total rate of ATP production ($r_2 + r_4 + r_3 + r_6$) over time in Figure 4.2(a). In addition, the cumulative amount of ATP produced by each pathway was computed by integrating the

corresponding reaction rate over time and is plotted as a fraction of the total ATP produced in Figure 4.2(b).

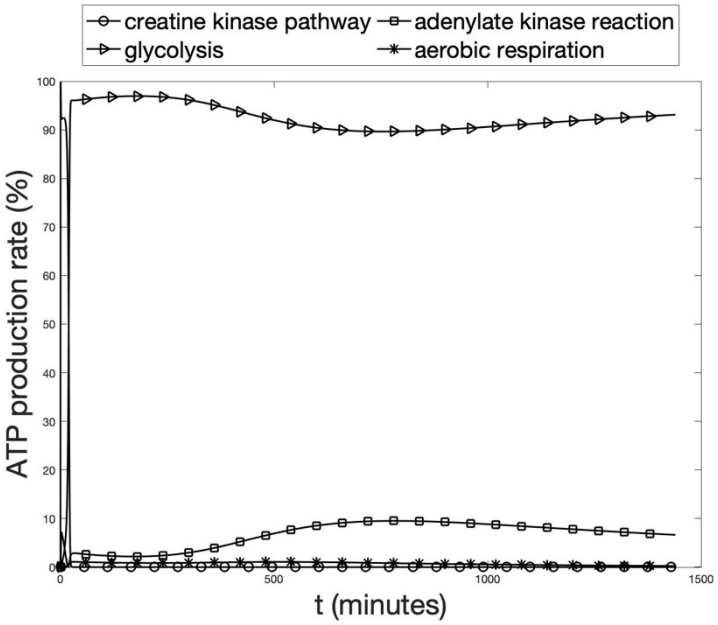

(a)

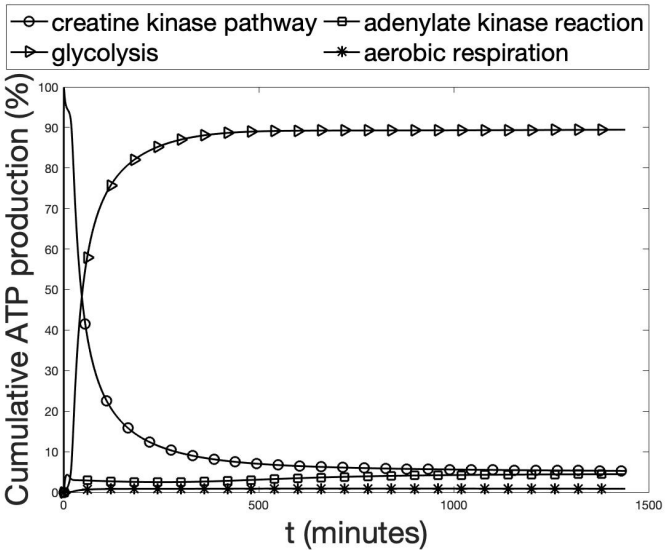

(b)

Figure 4.2 - Rate (a) and cumulative amount (b) of ATP production via each of four pathways (indicated by different symbols) as a percentage of the total over time.

As shown in Figure 4.2(a), initially, the creatine kinase pathway is the dominant one to generate ATP, accounting for about 92% of total rate of ATP production. However, the creatine kinase-mediated reaction can only last for a short time, as is commonly known. As the stored phosphocreatine is depleted, the creatine kinase reaction stops and no longer contributes to ATP production. Meanwhile, the rate of ATP production by anaerobic glycolysis increases immediately and dominates the remaining process. The contribution of the myokinase-mediated reaction to ATP production is very small (approximately 1%) at an early stage (0-240 min) and later increases to account for 8%-10% of ATP production rate. The proportion of ATP generated by aerobic respiration to total ATP production rate is very low (less than 1%) in the whole postmortem metabolism process. ATP produced by aerobic respiration stops around 9 hours postmortem, at which oxygen drops to a level near its minimum (as shown in Figure 4.1). It is worth noting that aerobic respiration is still active before 9 hours though its contribution to postmortem ATP production is insignificant.

Figure 4.2 (b) shows the proportion of cumulative ATP produced by each generating pathway to total ATP production. Before 47 min, ATP by the cumulative amount is mainly supplied by the creatine kinase pathway, while after 47 min, anaerobic glycolysis is the primary pathway. At 24 hours postmortem, the proportions of ATP produced by creatine kinase-, myokinase-mediated reactions, anaerobic glycolysis and aerobic respiration to the cumulative total amount of ATP produced are 5.26%, 4.44%, 89.44%, and 0.86%, respectively.

4.4.2 *Contributions of ATP-generating pathways to pH variations*

As mentioned earlier, hydrogen ions (H^+) are another major product of postmortem metabolism. The rate and extent of pH decline affect meat quality development. To produce meat with consistent quality, the factors contributing to pH decline are worthy of investigation.

Among the major reactions involved in postmortem metabolism, ATP hydrolysis, creatine kinase-mediated reaction, anaerobic glycolysis, deaminase-mediated reaction, and aerobic respiration contribute to pH changes by either consuming or producing H^+ (Eqn. 10). The contribution of each reaction to pH changes at a given time point was computed by integrating the corresponding term involving r_1, r_2, r_3, r_5, or r_6 in Eqn. 10 over time and is plotted in Figure 4.3.

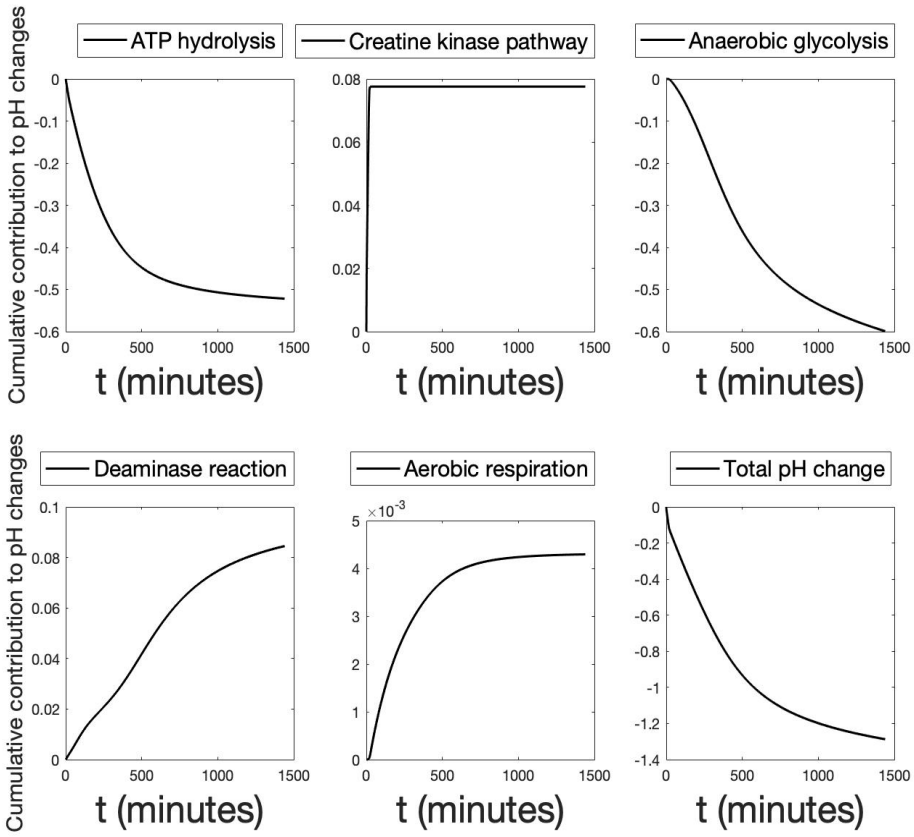

Figure 4.3 - Cumulative contribution to pH changes over time by ATP hydrolysis, creatine kinase-mediated reaction, anaerobic glycolysis, deaminase-mediated reaction, and aerobic respiration; and total pH decline over time.

As shown in Figure 4.3, ATP hydrolysis and glycolysis produce H^+ and thus result in pH decline by 0.52 and 0.6 units, respectively, after 24 hours; while creatine kinase-, deaminase-mediated reactions and aerobic respiration consume H^+ and thus lead to pH increases by 0.08, 0.07, and 0.004 units, respectively, after 24 hours. As a result, the total pH decreases by approximately 1.3 units after 24 hours.

ATP hydrolysis and anaerobic glycolysis are clearly the dominate contributors to pH changes postmortem. The initial pH decline is mainly due to ATP hydrolysis while

the contribution of glycolysis is delayed (compare the upper-left panel with the upper-right panel in Figure 4.3). This obviously results from the fact that glycolysis is low while creatine phosphate is the main source of ATP initially as discussed in Subsection 4.1. The creatine kinase-mediated reaction thus leads to a small but quick increase in pH early in the process (upper-middle panel in Figure 4.3), whereas the positive contribution from the deaminase-mediated reaction is relatively gradual (bottom-left panel in Figure 4.3). The effect of aerobic respiration on pH is relatively small, which is consistent with its minor role in ATP production.

4.5 Influences of initial muscle treatment and conditions on postmortem pH variations

4.5.1 *Effect of electrical stimulation on pH variations*

The application of electrical stimulation can effectively reduce or even eliminate cold shortening by forcing extensive muscle contraction and using up energy reserves immediately after stunning before slaughtering or immediately after slaughtering. It is reported that cold-induced toughening is reduced by the application of electrical stimulation in beef (Sorinmade et al., 1982). Electrical stimulation could accelerate postmortem metabolism and result in a rapid pH decline (Hwang and Thompson 2001).

The model was used to analyze the effect of electrical stimulation on postmortem energy metabolism and pH decline. A small change was introduced to each model parameter from its optimized value for the control group (Table 4.1) while keeping the other parameters unchanged, and the ratio of the pH change over the parameter change

was computed as a partial derivative $\frac{\partial pH}{\partial k_i}$ (i = 1-10, or h). The effect of electrical stimulation on pH via each parameter was computed as $\frac{\partial pH}{\partial k_i}\Delta k_i$ (i = 1-10, or h), where Δk_i is the parameter change from the control group caused by electrical stimulation (the difference between the two groups in Table 1). The total effect of electrical stimulation on pH decline over time was computed as $\sum \frac{\partial pH}{\partial k_i}\Delta k_i$ (i = 1-10, or h) and is shown in Figure 4.4. The proportion of the contribution of electrical stimulation on pH decline via each parameter over the total effect can then be estimated as $\frac{\partial pH}{\partial k_i}\Delta k_i / \sum \frac{\partial pH}{\partial k_i}\Delta k_i$ (i = 1-10, or h) and is shown in Figure 4.5.

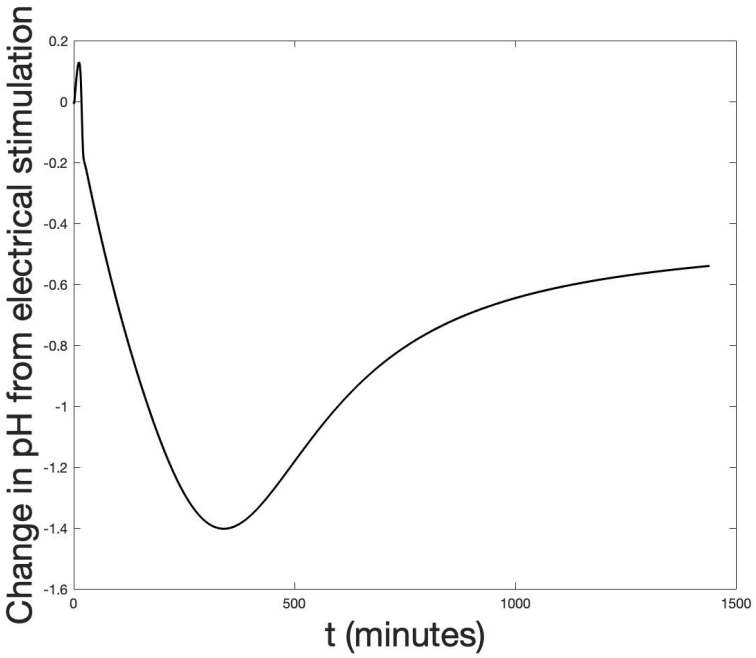

Figure 4.4 - Total effect of electrical stimulation on pH

It can be observed from Figure 4.4 that electrical stimulation slows down pH decline before approximately 15 min because of expedited ATP production from creatine phosphate; while after 15 min, electrical stimulation accelerates pH decline and results in

a net decrease of 0.5 in the ultimate pH. It is interesting to note that electrical stimulation leads to added pH decline at an accelerating pace before 6 hours postmortem and at a reducing pace after that.

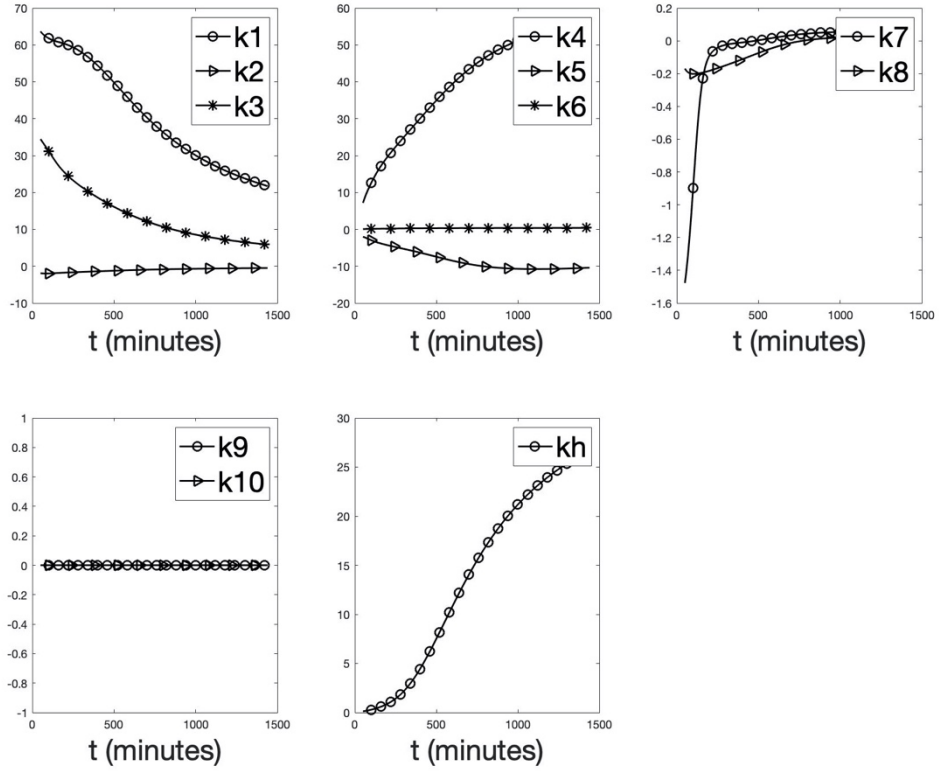

Figure 4.5 - Percent contribution of electrical stimulation to pH *decline* via different reactions as indicated by the associated model parameters (k_i, i = 1-10, or h). A positive percentage indicates a pH decrease while a negative percentage indicates a pH increase.

As is shown in Figure 4.5, the impact of electrical stimulation on pH decline is mainly through the combined effects of k_1, k_3, k_4, and k_h, which represent the rates of ATP hydrolysis (k_1), creatine kinase-catalyzed reaction (k_3), anaerobic glycolysis (k_4), and H^+ concentration inhibiting PFK activity (k_h), respectively. Among them, ATP hydrolysis and creatine kinase-catalyzed reaction account for approximately 62% and

35%, respectively, of the initial effect of electrical stimulation on pH decline and these percentages decline to 20% and 5%, respectively, after 24 hours. On the other hand, anaerobic glycolysis and PFK activity play an increasing role in pH decline from 5% and 0% initially to 55% and 28% at 24 hours, respectively. Electrical stimulation suppresses pH decline through the AMP deaminase reaction (k_7) and aerobic respiration (k_8) but the effect is very minor and primarily early in the process (Figure 4.5, upper-right panel). The effect of electrical stimulation on pH decline through buffering capacity (k_9, k_{10}) is negligible (Figure 4.5, bottom-left panel). As a result of the combined contributions from the processes associated with k_1, k_3, k_4, k_5, k_7, k_8, and k_h, the effect of electrical stimulation on pH decline exhibits a triphasic kinetic (Figure 4.4).

4.5.2 *Effect of initial muscle oxygen saturation level on pH variations*

The model uses the initial muscle oxygenation level (O_m, in % myoglobin oxygen saturation) as an input. The initial muscle oxygen is an initial process condition that can affect the postmortem metabolism, which generally depends on the conditions to which animals are exposed during the pre-slaughter periods (Xing et al., 2019).

For further analysis of the impact of aerobic respiration on postmortem metabolism, the effect of initial muscle oxygen saturation (%) on pH was investigated. Based on the parameter values estimated and the initial muscle oxygenation level measured for the control group, a small change was introduced to the initial muscle oxygen saturation. Simulations were run by using the estimated parameter values. The ratio of pH change over initial muscle oxygen change was computed as a partial

derivative $\frac{\partial pH}{\partial O_m}$ and used as an indicator of the influence of initial muscle oxygen on pH. The partial derivative profile over time is shown in Figure 4.6.

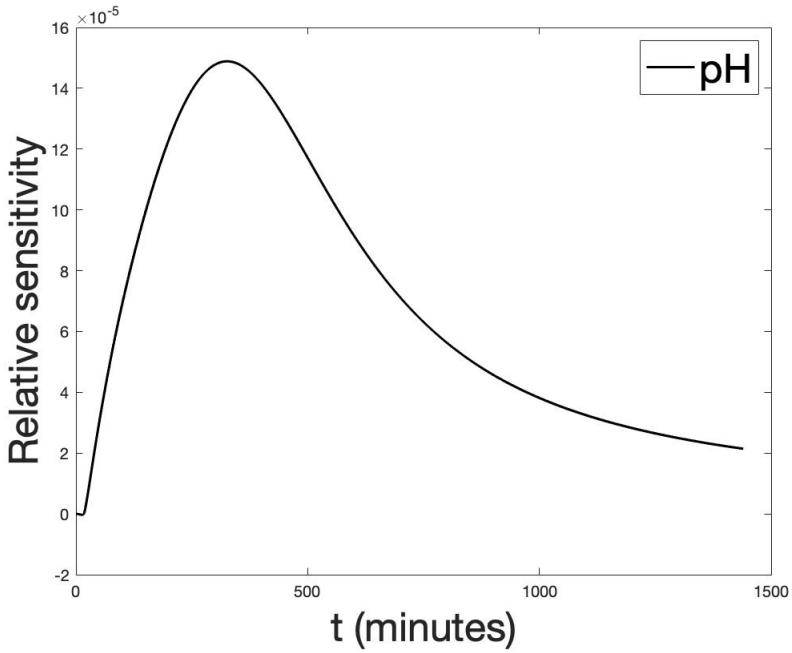

Figure 4.6 - Partial derivative of pH with respect to initial muscle oxygen saturation indicating the influence of initial muscle oxygen on pH in a postmortem muscle

As shown in Figure 4.6, initial muscle oxygen increases pH but the overall effect is relatively small, less than 15×10^{-5} pH unit per percent of oxygen saturation. During the first 6-7 hours postmortem, the impact increases over time. However, the influence starts to decrease thereafter possibly because of the depletion of accessible oxygen in the muscle. At a later stage, the impact is relatively insignificant but still results in an increase in the ultimate pH.

It is worth noting that the impact of initial muscle oxygen on pH represented by the partial derivatives is the direct effect without the indirect effects of potential

accompanying changes in k_h, the H^+ concentration inhibiting PFK activity, which has a strong impact on pH and is affected by ATP level. In consideration of the insignificant contribution of aerobic respiration to ATP production, the change in ATP from a change in initial muscle oxygen would be also small, resulting in a minor change in k_h. Therefore, the overall effect of initial muscle oxygen on pH is small.

4.5.3 *Effect of initial muscle phosphocreatine content on pH variations*

Regeneration of ATP is initiated by the degradation of phosphocreatine in postmortem muscles (Welsh and Lindinger 1993; Baker et al., 1994). The content of muscle phosphocreatine at slaughter greatly influences the rate of postmortem pH decline (Henckel et al., 2002). Pre-slaughter events such as transportation and handling lead to the variations in phosphocreatine stores among animals at slaughter (Henckel et al., 2002).

To better understand the effect of phosphocreatine on postmortem pH, simulations were run by using the estimated parameter values. The ratio of pH change over initial muscle phosphocreatine concentration change was computed as a partial derivative $\frac{\partial pH}{\partial C_rP}$ and used as an indicator of the influence of muscle phosphocreatine stores at slaughter on pH. The partial derivative profile over time is shown in Figure 4.7.

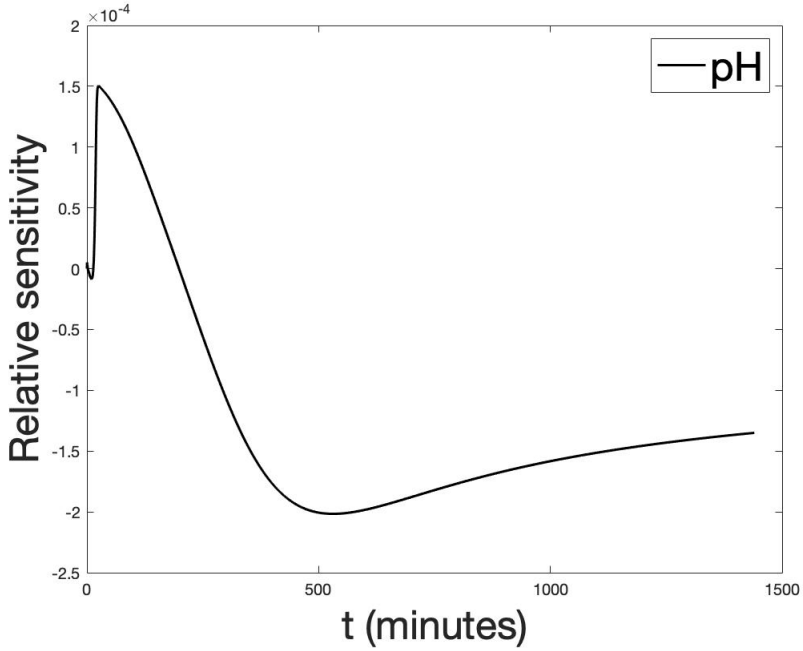

Figure 4.7 - Partial derivative of pH with respect to muscle phosphocreatine stores at slaughter indicating the influence of muscle phosphocreatine on pH in a postmortem muscle

It can be observed from Figure 4.7 that increased initial muscle phosphocreatine stores slow down pH decline before 200 min as can be expected from the dominate initial ATP production from phosphocreatine; while after 200 min, increased muscle phosphocreatine content accelerates pH decline and results in a decrease in the ultimate pH. However, the overall effect of phosphocreatine content on pH is relatively small, less than 2×10^{-4} pH unit per mmol L^{-1} of phosphocreatine.

4.6 Conclusions

A kinetic model was developed to describe variations in metabolites (ATP, ADP, AMP, IMP, glycogen, lactate, and muscle oxygenation) and pH in postmortem muscles and was validated with data measured from normal and electrically stimulated beef

samples. Analysis of ATP production and pH variations based on the model showed the relative contributions of different pathways. ATP is produced primarily by creatine kinase- and myokinase-mediated reactions, and anaerobic glycolysis. Aerobic respiration lasts up to 9 hours postmortem but contributes less than 1% of the total ATP production. Similarly, pH decline in postmortem muscles is mainly due to ATP hydrolysis and glycolysis (-0.52 and -0.6 after 24 hours). Aerobic respiration, on the other hand, leads to a pH increase but the amount is negligible (0.0043 after 24 hours). Analysis of the effects of various factors on pH variations showed that electrical stimulation affects pH primarily through ATP hydrolysis and anaerobic glycolysis. The initial muscle oxygen saturation and phosphocreatine stores showed minor impacts on pH.

Acknowledgement

This project was supported by the National Institute of Food and Agriculture, U.S. Department of Agriculture, under award number 2017-67017-26470.

CHAPTER 5

ANALYSIS OF PHOSPHOFRUCTOKINASE ACTIVITY AS AFFECTED BY pH AND ATP CONCENTRATION

Abstract

A kinetic model was developed to evaluate phosphofructokinase (PFK) activity and quantify the inhibitory effects of ATP and pH based on experiments conducted with porcine muscles. The kinetic modeling method was compared with the conventional initial-velocity method. Similar general trends of ATP and pH effects on PFK activity were shown by the two methods, but the initial-velocity method can only give a qualitative picture of PFK inhibition while the modeling method can quantify and model the degree of PFK inhibition. This is because the model can be used to separate the inhibitor effect from the substrate effect without inhibition. Analysis based on the model suggests that the affinity of ATP to the PFK catalytic site is much greater than that of the inhibitory site, but the velocity of product generation via the inhibited ATP-PFK-ATP complex is much slower than that of the uninhibited PFK-ATP complex, leading to increased proportion of the former and reduced overall reaction velocity when ATP concentration increases. The initial-velocity method is simple and useful for general observation of enzyme activity with substrate inhibition, while the modeling method has advantages in quantifying the inhibition effects and providing insights into the process.

5.1 Introduction

Phosphofructokinase (PFK, ATP:D-fructose-6-phosphate-1-phosphotransferase, EC 2.7.1.11), one of the rate-limiting enzymes of the glycolytic pathway, plays a critical role in the regulation of glycolysis by irreversibly converting fructose-6-phosphate (F6P) and adenosine triphosphate (ATP) to fructose-1,6-biphosphate (F-1,6-P) and adenosine diphosphate ADP (F6P + ATP $\rightarrow$ F-1,6-P + ADP) (England et al., 2014; Matarneh et al., 2018). Glycolytic flux is tightly regulated by changing the catalytic activity and the behavior of PFK (Sola-Penna et al., 2010; Tanner et al., 2018). Previous studies have shown that approximately 25% of the known enzymes are affected by substrate inhibition, which is characterized by reaction velocity curves that increase to a maximal peak, then drop as the substrate concentration increases (Hill and Robinson 1975; Kokkonen et al., 2021; Lin et al., 2001; Shou et al., 2000; Wu, 2011; Zhang et al., 1998). PFK is one of the enzymes that undergo substrate inhibition (Reed et al., 2010; Schöneberg et al., 2013; Sharma, 2011a, 2011b; Webb et al., 2015). Substrate inhibition of PFK ensures that resources are not devoted to producing ATP when it is present in abundance (Reed et al., 2010).

Enzyme activity is generally measured in terms of the rate of reaction catalyzed by an enzyme expressed in substrate consumed (or product generated) per unit time (Bisswanger, 2014). The conventional enzymatic assay involves measuring the initial reaction velocity at various substrate concentrations by coupling the reaction of interest with a chromogenic indicator reaction observable with a spectrophotometer (Eicher et al., 2012). The initial velocity is approximated with the slope of the initial linear portion of the reaction curve and the initial substrate concentration is taken as the concentration in

effect. PFK activity is often expressed in units of fructose 1,6-P (F-1,6-P) generated per minute, which corresponds to the oxidation of twice as many units of NADH observed optically. By using initial velocity as a measure of PFK activity, the kinetic and regulatory properties of PFK have been extensively studied. Ui (1966) reported that the inhibition of PFK by ATP is related to pH. Bosca et al. (1985) showed that the inhibition of PFK by ATP is the basis for the activation effect of fructose-2,6-P_2. Fructose-2,6-P_2 enhances PFK activity by releasing ATP from the regulatory site of PFK, hence reducing the inhibition effect of ATP (Bosca et al., 1985). Dobson et al. (1986) indicated that pH affects PFK by affecting the interaction of ATP with the regulatory site of PFK, hence modifying the inhibition effect of ATP. Since ATP acts as both a substrate that accelerates the reaction, and an inhibitor, which impedes reaction; the two effects cannot be easily separated in the conventional initial-velocity measurement.

Modeling the reactions occurring in an enzymatic assay is an alternative way to quantify enzyme activity and isolate the inhibitor effect from the substrate effect. Enzyme activities of pyruvate decarboxylase and alcohol dehydrogenase were estimated by using kinetic models that described the reactions catalyzed by these two enzymes based on Michalis-Menten and first-order kinetics (Boeckx et al., 2017). Using a kinetic model representing the underlying enzymatic reactions, the substrate inhibition of the reaction catalyzed by cytochrome P450 was found to depend on the concentration of the substrate occupying the inhibitory site (Lin et al., 2001). Furthermore, substrate inhibition of paramecium arginine kinase 3 (AK3) was analyzed by using kinetic reaction models and substrate binding to the catalytic site was found to promote substrate binding to the inhibitory site, hence resulting in stronger substrate inhibition (Yano and Suzuki 2018).

In spite of the extensive use of modeling in enzyme studies, surprisingly little has been done on the quantification of PFK activity and the degree of substrate inhibition by using a modeling method. Without a quantitative model for PFK activity, Wang et al. (2021, 2022) represented the binding of protons to PFK with the Hill equation to account for the pH effect on PFK activity, but the effect of ATP as an inhibitor was not included. Although much work has been dedicated to studying PFK activity, quantifying the inhibitory effects of ATP and pH on PFK requires further investigation. In this study, two methods were used to study the effects of ATP and pH on PFK activity, the conventional initial-velocity method and a new method of kinetic modeling. In the modeling method, a kinetic model was developed to describe the underlying enzymatic reactions, and PFK activity and inhibitory effects were quantitatively evaluated. In addition, an analysis based on the model was performed to provide insights into the mechanisms involved in the regulation of PFK activity.

5.2 Material and Methods

5.2.1 *Muscle samples*

Animal muscle was used as a source of PFK in its natural environment. Two market-weight pigs (100-125 kg) of similar genetics were harvested at the Utah State University Animal Harvest Facility following standard commercial practices and in accordance with the US Department of Agriculture inspection guidelines. Within 5 min postmortem, the *longissimus lumborum* (LL) muscle was excised from one side of each carcass, snap-frozen in liquid nitrogen, and stored at −80 °C until used for the PFK assay.

5.2.2 *PFK assay*

PFK assay was performed in a 96-well plate by following a modified procedure of England et al. (2014). Frozen LL muscle samples were pulverized under liquid nitrogen with a mortar and pestle, and aliquots (~ 0.1 g) were collected from each sample in 15-ml centrifuge tubes. Samples were homogenized at 1:20 (w/v) in an ice-cold buffer (100 mM K_2HPO_4, pH 7.4) with a Polytron homogenizer (PT 2500 E, Kinematica AG, Switzerland). Aliquots of the muscle homogenates were then added to a reaction solution containing 3.2 mM $MgSO_4$, 1 mM NADH, 3 mM fructose 6-phosphate, 2 U/ml triosephosphate isomerase, 1 U/ml glycerol-3-phosphate dehydrogenase, and 1 U/ml aldolase.

The buffer pH was adjusted to 5.3, 6.4, 6.5, 6.6, 6.7, 6.8, 6.9, 7, 7.1, 7.2, 7.3, 7.4, 7.5, 7.6, 7.7, 7.8, 7.9, 8, or 9. Depending on the pH tested, the reaction was buffered with either MES (120 mM, pH 5.3), PIPES (120 mM, pH 6.4-7), HEPES (120 mM, pH 7.1-8), or Tris-base (120 mM, pH 9). For each tested pH, different concentrations of ATP (0.3, 0.625, 1.25, 2.5, 3.75, or 5 mM) were added to initiate the reaction.

Immediately after the addition of ATP, 200-µl aliquots of the reaction mixture were transferred in duplicates to a 96-well microplate, where kinetic measurements were carried out with a spectrophotometer (Epoch 2, BioTek, Winooski, VT, USA). The absorbance resulting from NADH was measured at 340 nm every minute for 7 minutes at 25 °C and then converted to a concentration of NADH in mM by using a calibration curve.

5.2.3 *Conventional initial-velocity method*

The measured initial velocity of the PFK-catalyzed reaction was evaluated as a measure of PFK activity. It was computed as the slope of the initial linear portion of the measured NADH concentrations over time. Linearity was assessed visually and the first 2-5 measured values were used to compute the slope. The initial ATP concentration was taken as the concentration in effect.

5.2.4 *Kinetic modeling method*

5.2.4.1 *Enzymatic reactions in PFK assay*

The enzymatic reactions occurring in the PFK assay include a phosphate transformation reaction catalyzed by PFK coupled with an indicator reaction catalyzed by aldolase, triosephosphate isomerase, and glycerophosphate dehydrogenase; i.e.,

$$\text{F6P} + \text{ATP} \rightarrow \text{F-1,6-P} + \text{ADP} \quad (1)$$

$$\text{F-1,6-P} + 2\text{NADH} + 2\text{H}^+ \rightarrow 2\text{Glycerol-1-phosphate} + 2\text{NAD}^+ \quad (2)$$

The indicator reaction (Eqn. 2) produces a detectable spectrophotometric response because of the oxidation of NADH to NAD^+. When NADH and the enzymes needed are abundant, the indicator reaction is not rate-limiting and the measured NADH concentration indicates the rate of the PFK-catalyzed reaction (Eqn. 1).

5.2.4.2 *Kinetic model structure development*

When reaction (2) is not limiting, the concentrations of ATP and NADH vary proportionally; i.e.,

$$\frac{d[ATP]}{dt} = \frac{1}{2}\frac{d[NADH]}{dt} = -v \quad (3)$$

where v represents the reaction velocity of both reactions; [ATP] and [NADH] are the concentrations of ATP and NADH, respectively; and t is time.

The reaction catalyzed by PFK (Eqn. 1) does not obey the classical Michaelis-Menten kinetics because of substrate inhibition even at constant pH. PFK is an allosteric enzyme which is characterized by the existence of both catalytic and allosteric sites (Li et al., 1999; Schöneberg et al., 2013; Zheng and Kemp 1994). While ATP is a substrate for the reaction, it also inhibits PFK activity; in other words, ATP affects reaction velocity in two ways: as a substrate, which binds to the catalytic site, and as an inhibitor, which binds to the allosteric inhibitory site of PFK. For convenience, we refer to the effect of substrate on reaction velocity without enzyme inhibition as the "substrate effect" and the reduction in reaction velocity by an inhibitor from the uninhibited case as the "inhibitor effect". In addition, the PFK-catalyzed reaction is highly sensitive to hydrogen ions.

Because the affinity of the catalytic site to ATP is much greater than that of the inhibitory site (as shown later in Subsection 3.2.3), we simplify the reactions by assuming that the binding of substrate molecules is sequential; i.e., the substrate binds to the catalytic site before binding to the inhibitory site. The reactions accounting for the effects of substrate inhibition and hydrogen ions on PFK are then as represented in Figure 5.1.

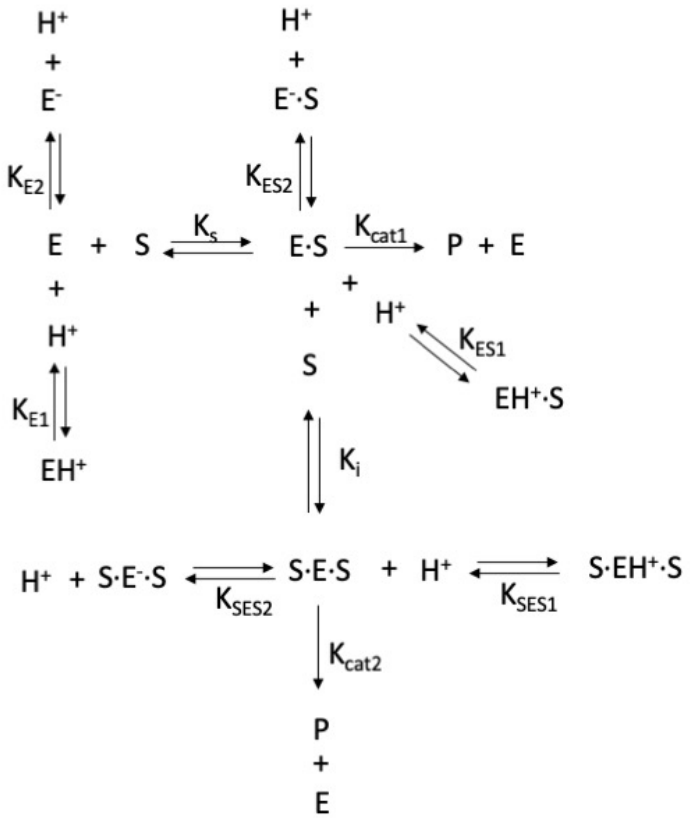

Figure 5.1 - Reactions accounting for the effects of substrate inhibition and hydrogen ions on PFK. E, S and P denote enzyme, substrate, and product, which are PFK, ATP, and F-1,6-P, respectively; E·S and S·E·S are enzyme-substrate complexes formed through substrate binding to the catalytic site and to both the catalytic site and inhibitory site of the enzyme. K_{E1}, K_{E2}, K_{ES1}, K_{ES2}, K_{SES1}, K_{SES2} are the association and dissociation constants between H^+ and E, E·S or S·E·S, respectively; K_s and K_i are the dissociation constants for S and E and that for E·S and E, respectively; K_{cat1} and K_{cat2} are the catalytic rates of product generation from the E·S and S·E·S complexes, respectively.

Based on steady-state and rapid equilibrium assumptions, a reaction velocity equation can be derived from the reactions presented in Figure 1 as shown below:

$$v = K_{cat1}[E \cdot S] + K_{cat2}[S \cdot E \cdot S] = \frac{\left(\frac{v_{max}^{E \cdot S}}{f_2} + \frac{v_{max}^{S \cdot E \cdot S}[S] f_3}{f_2 K_i \quad f_2}\right)}{\left(\frac{K_s f_1}{[S] f_2} + 1 + \frac{[S] f_3}{K_i f_2}\right)} \quad (4)$$

with

$$f_1 = \frac{[H^+]}{K_{E1}} + 1 + \frac{K_{E2}}{[H^+]} \quad (5)$$

$$f_2 = \frac{[H^+]}{K_{ES1}} + 1 + \frac{K_{ES2}}{[H^+]} \quad (6)$$

$$f_3 = \frac{[H^+]}{K_{SES1}} + 1 + \frac{K_{SES2}}{[H^+]} \quad (7)$$

where [S], [H^+], [E·S] and [S·E·S] are the concentrations of ATP, hydrogen ions, E·S and S·E·S complexes, respectively; $v_{max}^{E\cdot S}$ and $v_{max}^{S\cdot E\cdot S}$ are the maximum velocities for the catalyzed reactions of E·S and S·E·S, respectively.

Eqns. (3-7) form a kinetic model structure with adjustable parameters and are used to analyze the kinetic characteristics of the enzymatic reactions in the PFK assay.

5.2.5 *Parameter estimation and model validation*

The model parameters in Eqns. (3-7) were adjusted by using the Levenberg-Marquardt algorithm to achieve optimal fit to experimental measurements (Marquardt, 1963). The least-squares optimization algorithm was implemented in MATLAB (Version 2018, Mathworks, Natick, MA, USA).

The relative standard error of predictions (RESP) and the coefficient of determination (R^2) were calculated to assess the degree of agreement between model predictions and experimental observations. The RESP was calculated as:

$$RESP = \frac{1}{n}\sqrt{\frac{\sum_{i=1}^{N}(x_i^* - x_i)^2}{\sum_{i=1}^{N} x_i^{*2}}}$$

where x_i^* and x_i are the i^{th} measurement and predicted data points, respectively; N is the number of data points in an experimental run; and n is the number of runs.

5.3 Results and Discussion

5.3.1 *Conventional initial-velocity method*

The initial reaction velocity at a given initial ATP concentration and pH was obtained as the slope of the initial linear part of [F-1,6-P] as a function of time and is plotted against pH in Figure 5.2. As noted previously, the velocity of substrate (ATP or F6P) consumption or product (F-1,6-P) generation is proportional in magnitude to (double) the consumption rate of the measured NADH indicator. A trendline is fitted to the data in Figure 5.2 to show the general pattern of variations.

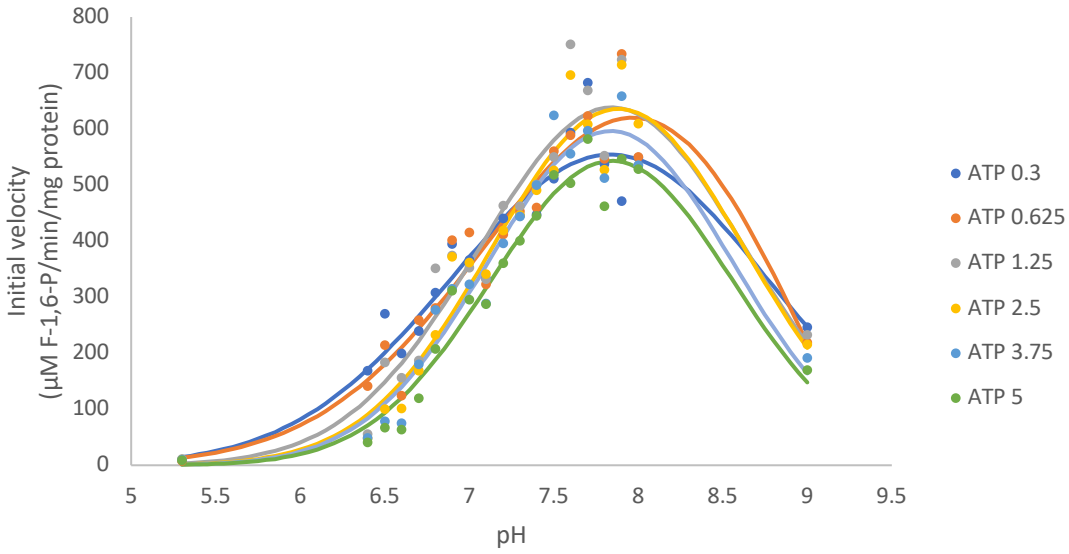

Figure 5.2 - Scatterplot of measured initial velocities along with fitted trendlines for initial ATP concentrations of 0.3, 0.625, 1.25, 2.5, 3.75, and 5 mM at varied pH levels.

Several observations may be made from Figure 5.2. Changes in pH considerably influence the PFK activity indicated by the measured initial velocity. The variations follow roughly skewed bell-shaped curves at various initial ATP concentrations. The pH

that initiates the reaction shifts to the alkaline side as ATP concentration increases. The reaction does not proceed when assayed at low pH in the presence of high ATP concentrations. Increasing the initial ATP concentration has a marked influence on the initial reaction velocity and this effect is more pronounced around pH 8, about which the initial reaction velocities peak. From the measurements, the peak velocity increased as ATP concentration increased from 0.3 mM to 1.25 mM but then decreased as the ATP concentration further increased from 1.25 mM to 5 mM, indicating a complexity of the ATP effects on the initial velocity.

It has been reported that the degree of inhibition of a reaction can be expressed by the ratio of the velocity in the presence of an inhibitor to that in the absence of the inhibitor (Chou and Talalay 1977). In the absence of the inhibitor, the dependence of reaction velocity on the substrate concentration can be described by the Michaelis-Menten rate equation $v = \frac{v_{max}[S]}{K_m+[S]}$, where v_{max} is the maximum reaction velocity, K_m is the Michaelis-Menten constant, and [S] is the substrate concentration. However, the parameter values (v_{max} and K_m) cannot be determined unless there is a way, experimental or theoretical, to separate or isolate the substrate effect from the inhibitor effect. To suppress the substrate effect for observation of the inhibitor effect, the enzymatic reaction may be assumed to follow the first-order kinetics, and thus the initial reaction velocity would be proportional to the substrate concentration. As a result, the initial velocity may be divided by the initial ATP concentration as an approximate way to suppress the substrate effect. Figure 5.3 shows the initial velocities divided by the initial ATP concentrations plotted against pH at various initial ATP concentrations with trendlines.

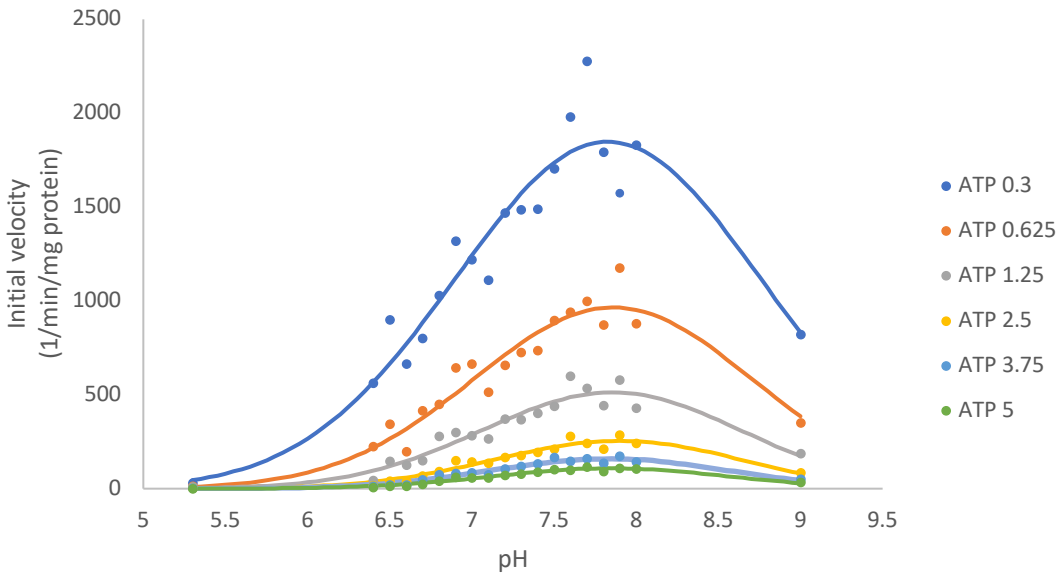

Figure 5.3 - Measured initial velocities divided by initial ATP concentrations vs. pH with trendlines for varied ATP concentrations (0.3, 0.625, 1.25, 2.5, 3.75, and 5 mM).

As shown in Figure 5.3, division by the initial ATP concentration as an approximate way to suppress the substrate effect substantially changed the initial velocity curves. At a given pH, the initial reaction velocity, as an indicator of PFK activity, decreases as ATP concentration increases from 0.3 mM to 5 mM, suggesting that the degree of PFK inhibition is enhanced by increasing ATP concentration. Moreover, based on the trendlines, the peak velocity (indicating the optimum pH for PFK activity) appears to shift slightly to the acidic side as ATP concentration increases.

While the conventional initial-velocity method is a convenient way to observe or estimate enzyme activity, it involves several difficulties and inaccuracies as discussed below. First, the initial substrate/inhibitor (ATP) concentration is used as the concentration in effect, but the substrate is constantly being consumed at different rates. Therefore, when a measurement is made, the substrate concentration does not only differ

from the initial value used for an experiment but also differs by a different amount across experiments because reaction velocity varies. As a result, the inhibitor concentration in effect is uncertain. Second, it is difficult to measure the initial velocity consistently across experiments. Even if the first measurement could be made at precisely the same time after initiation of the reactions, which is a challenge practically, the reactions are at different stages because velocity differs. As shown in Figure 5.3, the scatter in the measured initial velocity increased as ATP concentration decreased because measurement inconsistencies were greater when the reaction velocity was higher. Third, unless there is a way to nullify the substrate or the inhibitor effect, the two effects cannot be separated in the measured initial velocities. While division by the initial substrate (ATP) concentration may help suppress the substrate effect, the assumption of substrate effect following simple first-order kinetics is inconsistent with the purpose of the experiments, which is to analyze the enzyme behavior in an enzymatic reaction. Therefore, a kinetic model can be used to advantage to avoid these difficulties.

5.3.2 *Kinetic modeling method*

5.3.2.1 *Parameter estimation and model validation*

Comparisons between model predictions and experimental measurements for an example pH are shown in Figure 5.4 and the optimized parameters for the kinetic model are listed in Table 5.1.

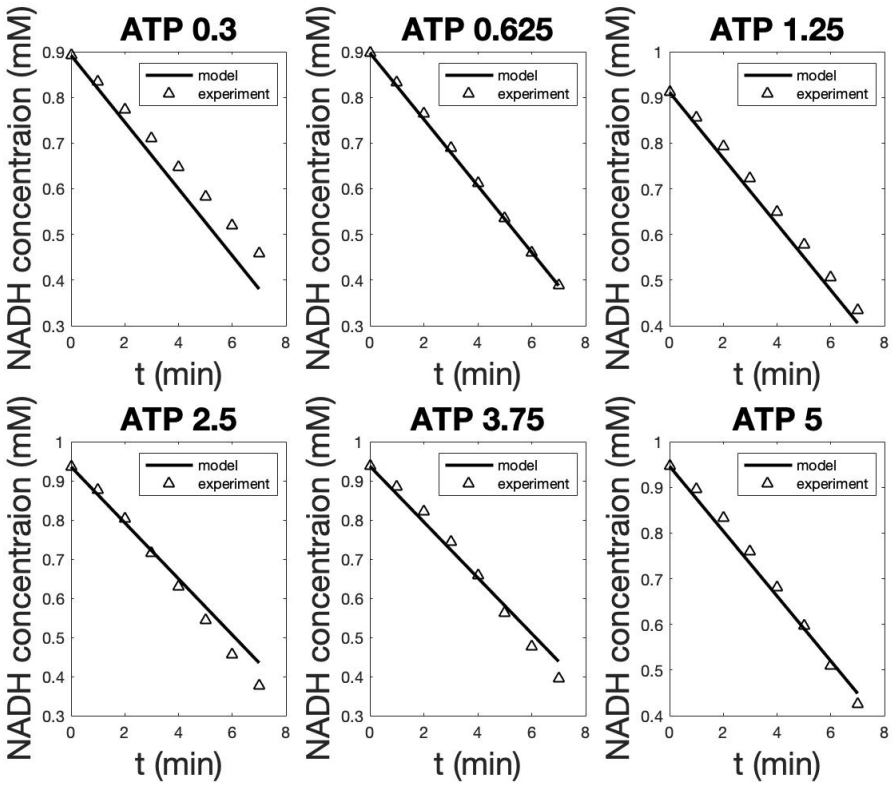

Figure 5.4 - Example plots comparing model predictions against experimental observations for pH 7. Symbols represent experimental data while the solid lines represent the model predictions. NADH was the measured output of the assay and thus used as the modeled output, but F-1,6-P or ATP concentration can be easily calculated from that of NADH.

Table 5.1 Model parameter values used for model predictions shown in Figure 5.4.

Parameter (unit)	Value
$v_{max}^{E\cdot S}$ (μmol F-1,6-P min^{-1} mg^{-1} protein)	347.95
$v_{max}^{S\cdot E\cdot S}$ (μmol F-1,6-P min^{-1} mg^{-1} protein)	77.1
K_s (mmol L^{-1})	0.6753
K_i (mmol L^{-1})	2.5444
K_{E1} (mmol L^{-1})	$10^{-7.45}$
K_{E2} (mmol L^{-1})	$10^{-8.08}$
K_{ES1} (mmol L^{-1})	$10^{-7.08}$
K_{ES2} (mmol L^{-1})	$10^{-9.85}$
K_{SES1} (mmol L^{-1})	$10^{-9.53}$
K_{SES2} (mmol L^{-1})	$10^{-7.02}$

The degree of agreement between model predictions and measurements was assessed in terms of the relative standard error of prediction (RESP) and the determination coefficient (R^2) value, which were 0.1025 ± 0.0131 and 0.9398 ± 0.0907, respectively, over all experiment runs, indicating that the model structure could closely represent the kinetic variations in experimental measurements.

Because the model describes the variables as functions of time, a time-variant rather than an assumed constant ATP concentration is in effect as an inhibitor. Moreover, the model does not need to rely on the time point of reaction initiation as time zero and the initial concentrations as initial conditions. Because it is practically challenging to start a reaction and make the first measurement at precisely the same times for all experiments, the time of reaction initiation is an unreliable time origin. Fortunately, the

first measurement can be used as the initial condition to reduce this uncertainty. Because the rates of substrate consumption and NADH consumption are related through Eqn. (3), the first substrate concentration can be determined as:

$$[S]_1 = [S]_0 - \frac{1}{2}([NADH]_0 - [NADH]_1) \quad (8)$$

where $[S]_1$ is the first measured substrate (ATP or F6P) concentration to be used as the initial condition; $[S]_0$ and $[NADH]_0$ are the substrate and the NADH concentrations, respectively, used to start the reaction; and $[NADH]_1$ is the first measured NADH concentration.

As a result of using the first measurement as the initial condition, the plots in Figure 5.4 start from varied initial points that are different from the concentration (1 mM) used to start the reactions.

The same could be done in the initial-velocity method. After such a correction, however, the inhibitor (ATP) concentrations deviate by varied amounts from the designed values (0.3, 0.625 etc.), making data analysis and presentation more difficult. More significantly, the correction does not address the fact that ATP concentration changes continuously and any single constant value used is not the true concentration in effect.

5.3.2.2 *Kinetic modeling method to analyze the effects of ATP and pH on PFK activity*

The reaction velocities in the presence of inhibition were calculated by using Eqn. (4) and the parameter values listed in Table 5.1 and plotted against pH at various ATP concentrations in Figure 5.5(a). As shown in Figure 5.5(a), a change in pH substantially influences the PFK activity and thus the reaction velocity, and a set of bell-like curves are obtained at various ATP concentrations. The optimum pH for PFK activity

(corresponding to the peak reaction velocity) is shifted to the alkaline side with increasing ATP concentration. The effect of ATP on PFK activity is more obvious over the pH range from 8 to 10. Moreover, increasing the ATP concentration has a marked influence on the maximum PFK activity. The maximum PFK activity initially increases as ATP concentration increases from 0.3 mM to 1.25 mM and then decreases as the ATP concentration further increases from 1.25 mM to 5 mM. This trend of the maximum PFK activity as a function of ATP concentration is consistent with the result obtained by using the conventional initial-velocity method as shown in Figure 5.2.

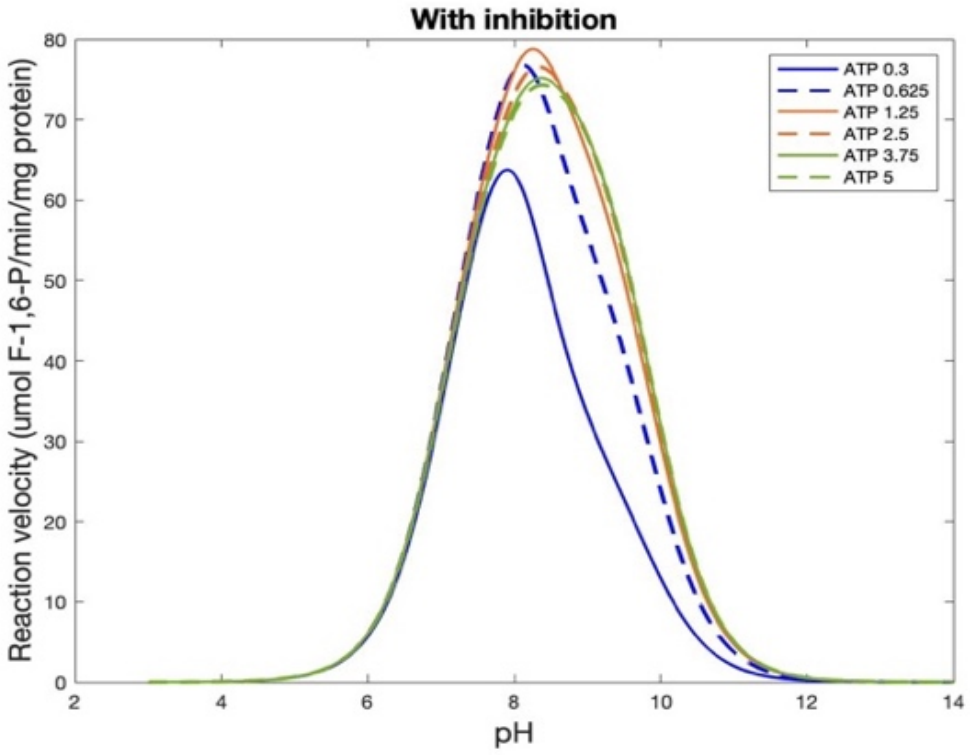

(a)

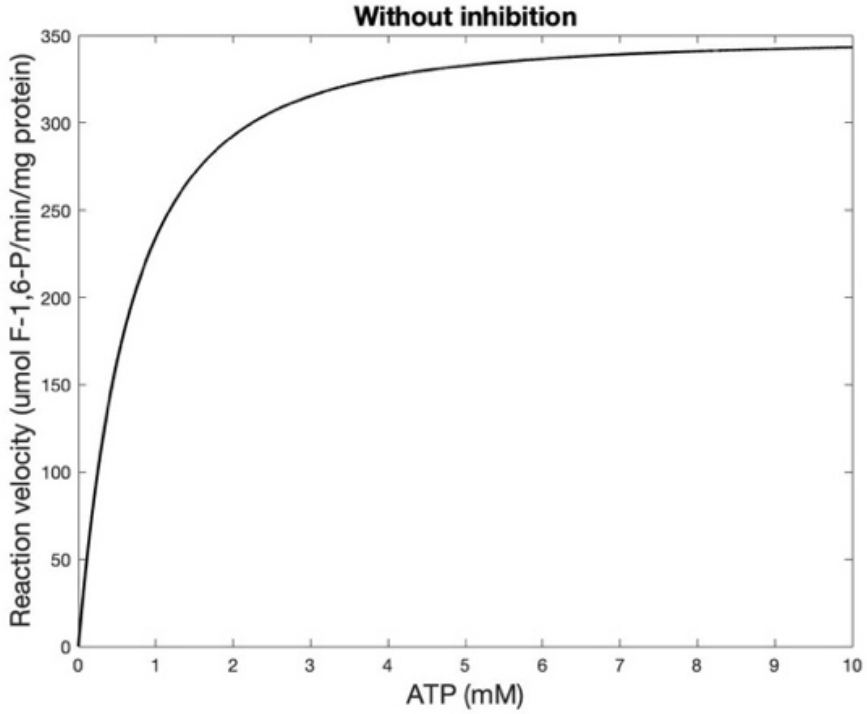

(b)

Figure 5.5 - Reaction velocities in the presence (a) and absence (b) of substrate inhibition

To obtain the reaction velocities in the absence of inhibition, f_1, f_2, and f_3 in Eqn. (4) can be set to 1 to eliminate the pH effect and $v_{max}^{S\cdot E\cdot S}$ substituted with $v_{max}^{E\cdot S}$ to eliminate the substrate inhibitor effect to give,

$$v_{mm} = \frac{\left(v_{max}^{E\cdot S} + \frac{v_{max}^{E\cdot S}[S]}{K_i}\right)}{\left(\frac{K_S}{[S]} + 1 + \frac{[S]}{K_i}\right)} \tag{9}$$

Eqn. (9) represents the substrate effect on reaction velocity without inhibition and is plotted against ATP concentration in Figure 5.5(b). The plot is analogous to the Michaelis-Menten saturation curve, which exhibits a hyperbolic increase with substrate increase. At low ATP concentrations (lower than 1 mM), the velocity increases almost

linearly with the substrate concentration, while at high substrate concentrations (greater than 7 mM), the velocity exhibits saturation near 350 μmol F-1,6-P min^{-1} mg^{-1} protein.

The degree of reaction velocity reduction or PFK activity inhibition may be shown as the ratio of the velocity in the presence of inhibition to that in the absence of the inhibition and the ratio curves are plotted against pH at various ATP concentrations in Figure 5.6.

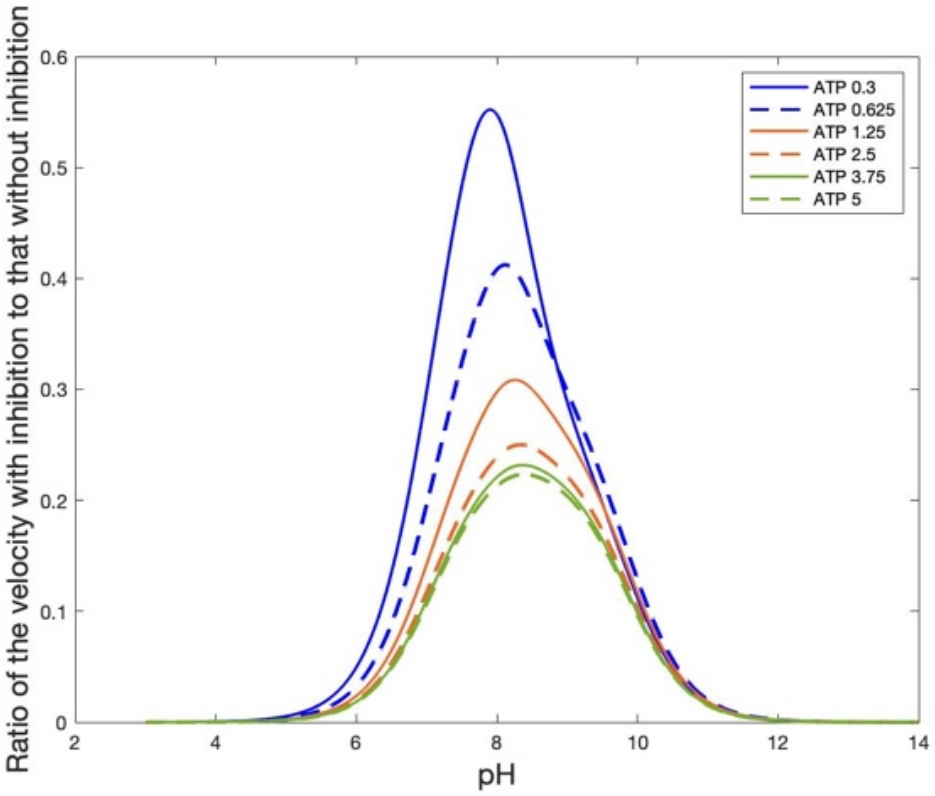

(a)

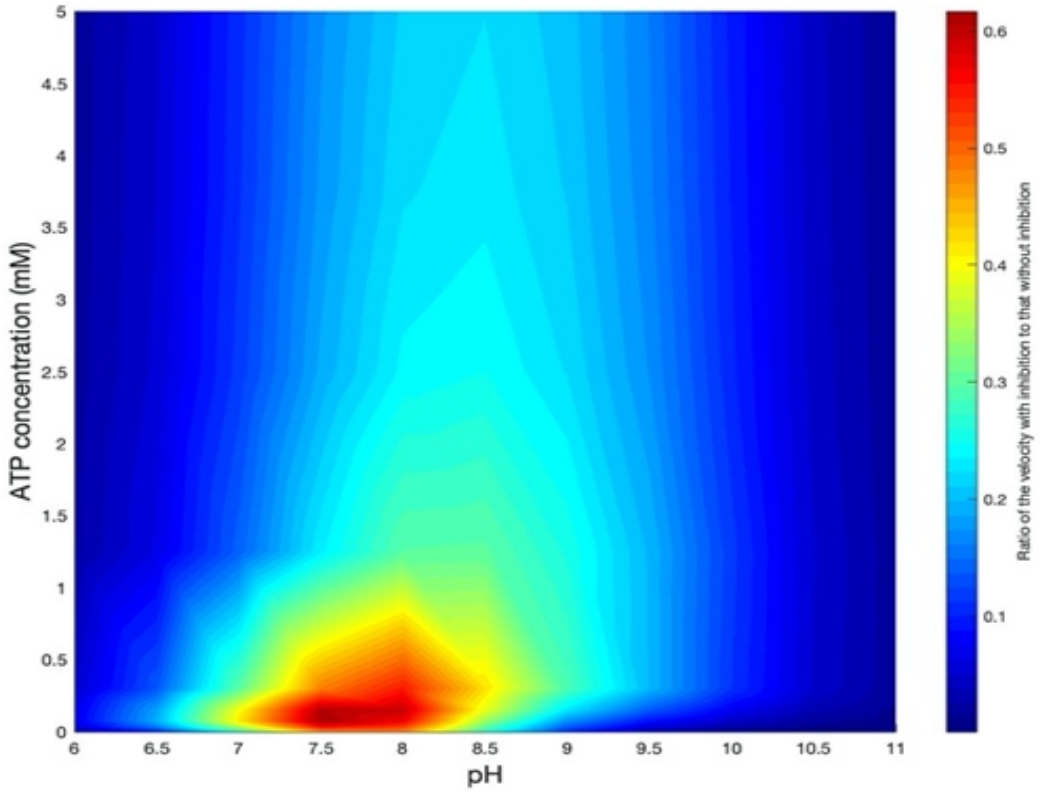

(b)

Figure 5.6 - A family of curves (a) and contour plot (b) of PFK activity shown by the reaction velocity with inhibition as a percentage of reaction velocity without inhibition against pH at various ATP concentrations.

As shown in Figure 5.6, the optimum pH for PFK activity (peak velocity) is shifted to the alkaline side with increasing ATP concentrations. Furthermore, increasing the ATP concentration had a marked influence on the PFK activity, and the effect of ATP on PFK activity is pronounced over the pH range from 7 to 9. As can be seen in Figure 5.6, at a given pH, PFK activity continually decreases as ATP concentration increases from 0.3 mM to 5 mM, suggesting that the degree of inhibition of PFK is enhanced by increasing ATP concentration. This is in agreement with the result obtained by using the

conventional initial-velocity method as shown in Figure 5.3. However, in contrast to the conventional initial-velocity method, which gives only a qualitative picture, the kinetic modeling method is useful in obtaining the degree of inhibition based on reaction velocity. As shown in Figure 5.6, for example, at the pH optimum, about 55% of PFK activity is inhibited at ATP concentration of 0.3 mM, while approximately 80% of PFK activity is inhibited when ATP concentration is 5 mM.

5.3.2.3 *Further analysis of PFK activity based on the model*

As shown in Table 5.1, the parameter K_i, which represents the dissociation constant of a substrate molecule binding to the inhibitory site to form S·E·S, is approximately 4-fold of K_s, which denotes the dissociation constant of a substrate molecule binding to the catalytic site to form E·S. This indicates that the affinity of the substrate binding to the catalytic site is about four times that to the inhibitory site. $v_{max}^{E\cdot S}$ is approximately five times $v_{max}^{S\cdot E\cdot S}$, suggesting that when a substrate binds to the inhibitory site of the enzyme to form S·E·S, the catalytic activity of the enzyme is reduced by a factor of 5.

During the reactions, the enzyme is present in three forms: (1) Unsaturated or free form (E), which makes no direct contribution to product generation, (2) In complex E·S, which is not substrate-inhibited and produces product at one rate, and (3) In complex S·E·S, which is substrate-inhibited and produces a product as a lower rate. The overall observed velocity (v) of the reaction catalyzed by PFK thus depends on the proportions of these three enzyme populations. [E·S], [S·E·S] and [E] as proportions of the total enzyme concentration $[E_T]$ = [E]+[E·S]+[S·E·S] can be calculated as $\frac{[E\cdot S]}{[E_T]} =$

$\frac{1}{\left(\frac{K_S f_1}{[S] f_2}+1+\frac{[S] f_3}{K_i f_2}\right)}$, $\frac{[\mathrm{S{\cdot}E{\cdot}S}]}{[\mathrm{E_T}]} = \frac{[\mathrm{E{\cdot}S}][\mathrm{ATP}]}{K_i(\frac{f_2}{f_3})}$, and $\frac{[E]}{[\mathrm{E_T}]} = \frac{(\frac{f_1}{f_2})[\mathrm{E{\cdot}S}]K_S}{[\mathrm{ATP}]}$, respectively, and are plotted against ATP concentration in Figure 5.7.

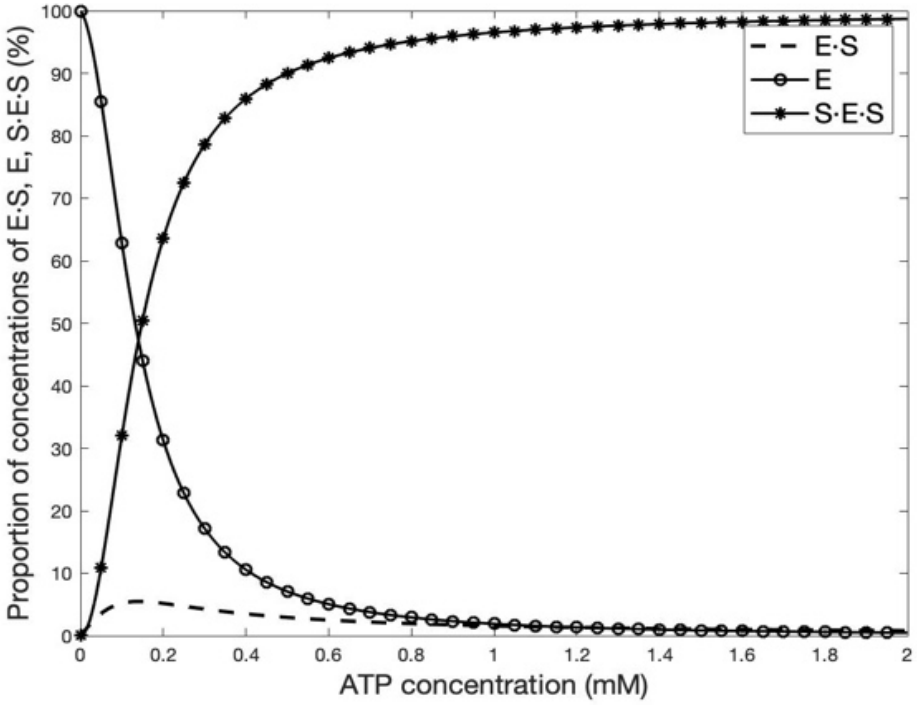

Figure 5.7 - Proportions of [E·S], [S·E·S] and [E] against ATP concentration

As shown in Figure 5.7, the fraction of [E·S] initially increases with [ATP] and reaches a maximum of 5% at an ATP concentration of 0.12 mM and then drops as the ATP concentration increases. At the same time, [S·E·S] increases in a sigmoid pattern and its fraction reaches 90% near a concentration of 0.6 mM of ATP. This shows that when [ATP] is elevated, the inhibited form (S·E·S) quickly becomes the dominant form. While the affinity of ATP to the catalytic site of PFK is higher than that to the inhibitory site, the velocity of product generation via the S·E·S pathway (i.e., consumption of

S·E·S) is much slower than that via the E·S pathway as shown below, leading to accumulation of the inhibited form when ATP concentration increases.

The velocities of product generation by the E·S and S·E·S pathways can be computed as

$v_{ES} = \frac{\left(\frac{v_{max}^{E\cdot S}}{f_2}\right)}{\left(\frac{K_s f_1}{[S]f_2}+1+\frac{[S]f_3}{K_i f_2}\right)}$ and $v_{SES} = \frac{\left(\frac{v_{max}^{S\cdot E\cdot S}[S]f_3}{f_2 K_i \quad f_2}\right)}{\left(\frac{K_s f_1}{[S]f_2}+1+\frac{[S]f_3}{K_i f_2}\right)}$ and are plotted against ATP concentration in Figure 5.8(a). In addition, the percent contributions of E·S and S·E·S pathways to product generation ($\frac{v_{ES}}{v_{ES}+v_{SES}}$ and $\frac{v_{SES}}{v_{ES}+v_{SES}}$) are plotted against ATP concentration in Figure 5.8(b).

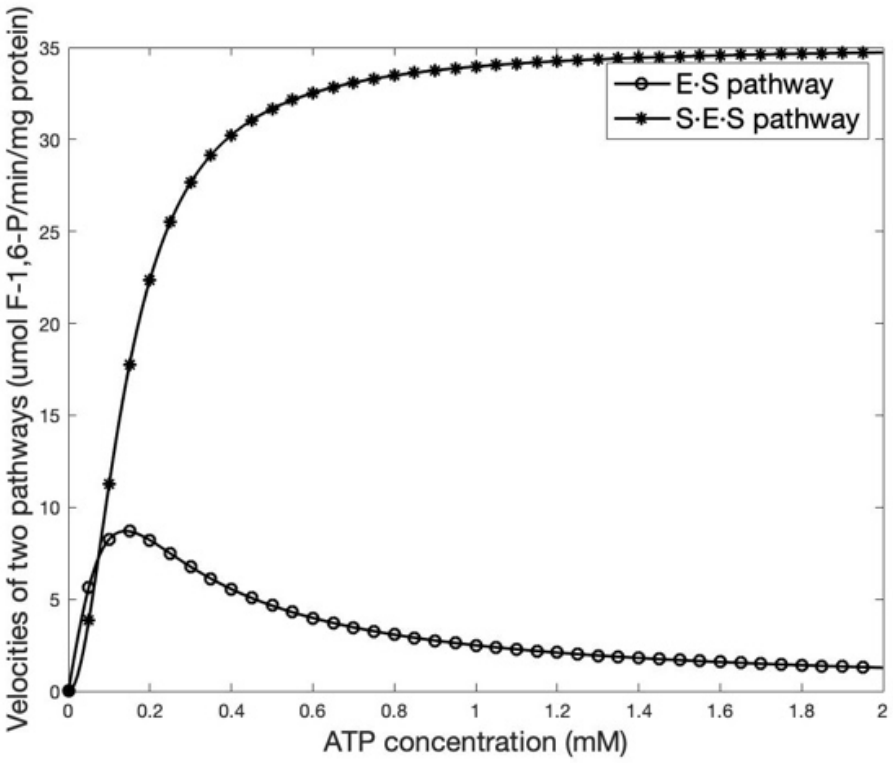

(a)

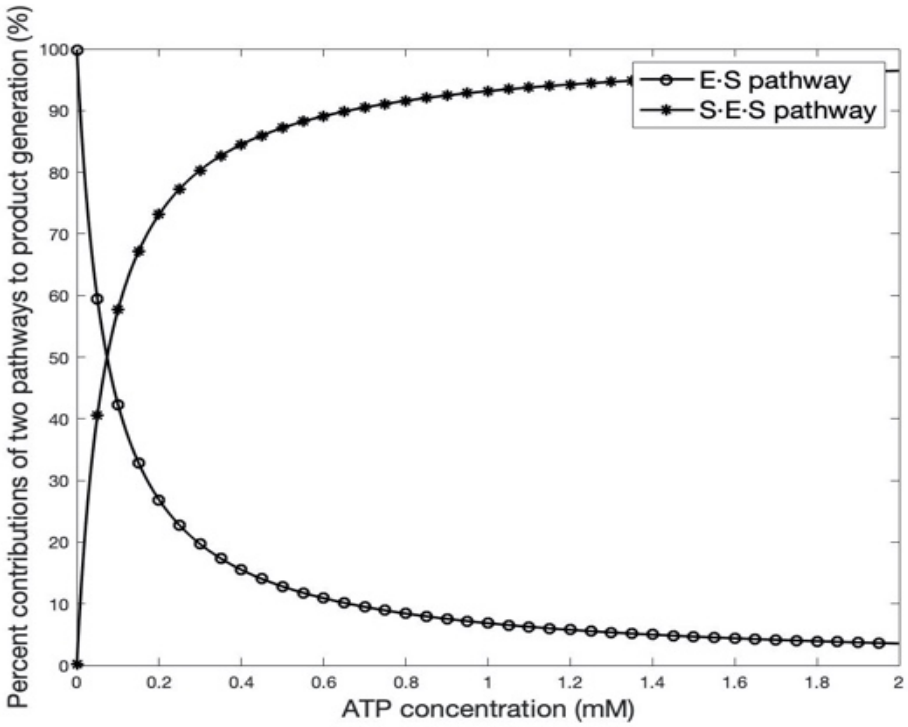

(b)

Figure 5.8 - Velocities (a) and percent contributions (b) of E·S and S·E·S pathways to product generation

As can be seen in Figure 5.8(a), the velocity of product generation through the E·S pathway initially goes up and reaches a maximum of 8 μmol F-1,6-P min^{-1} per mg of protein at approximately 0.15 mM of ATP concentration and then decreases as the ATP concentration increases, while the velocity of product generation through the S·E·S pathway increases rapidly in a sigmoid way and reaches a maximum of 35 μmol F-1,6-P/min per mg of protein near a concentration of 1.2 mM of ATP.

Figure 5.8(b) shows that the E·S pathway is likely the dominant pathway to generate product when ATP concentration is lower than 0.12 mM, while afterwards, the

S·E·S pathway prevails, resulting in slower overall velocity because the S·E·S pathway is much slower in product generation.

The conventional initial-velocity method is simple and commonly used, and the initial velocity is widely accepted as an indicator of enzyme activity in most enzymatic assays. However, the former is not an effective means of quantifying enzyme activity under substrate inhibition because of the difficulties discussed earlier, the most significant which is that the substrate effect and inhibitor effect cannot be separated in the measured initial velocity. In this context, we proposed that for the observation of the inhibitor effect, the initial velocity may be divided by the initial substrate concentration to suppress the substrate effect based on the assumption of first-order kinetics. Although the assumption is not realistic, the division can suppress the substrate effect to allow better observation of the inhibitor effect.

The kinetic modeling method reveals enzyme activity by using a kinetic model representing the underlying enzymatic reactions. The primary advantage of the method is that it allows for quantitative separation of the substrate effect and inhibitor effect so that the latter can be quantified and modeled. The model parameter values can provide insights into different aspects of the underlying reactions such as affinity between reactants, and the model can be used to analyze the relative contributions of different reaction pathways and different forms of an enzyme, as illustrated herein. In addition, the method does not require accurate timing of the initial measurement. Therefore, this modeling method is more general and flexible.

The initial-velocity method showed quantitatively similar trends and effects of ATP and pH as the modeling method, indicating a level of agreement between the two

methods. The former is simple and can be used to gain a general picture of enzyme activity as affected by pH and a substrate inhibitor. It can also be used to determine the optimal and range of pH over which an enzyme functions. However, for a more detailed analysis and quantification of enzyme activity, the modeling approach should be the method of choice.

5.4 Conclusions

We present a new method by kinetic modeling to estimate PFK activity and quantify the inhibitory effects of ATP and pH on PFK. In contrast to the conventional initial-velocity method, which gives a qualitative picture of the inhibition of PFK activity under varied conditions, the proposed model can separate the substrate effect from the inhibitor effect and thus quantify the inhibitor effect. The use of a kinetic model to evaluate enzyme activity and quantify the degree of inhibition can be extended to other enzymes as long as the underlying reaction mechanisms are known. Kinetic analyses of PFK based on the proposed model indicated that the affinity of the substrate binding to the catalytic sites is 4-fold of that the inhibitory site. Increasing ATP concentration leads to a reduced overall reaction velocity as a result of increasing proportion of enzyme complexes with ATP bound to the inhibitory site.

Acknowledgment

This project was supported by the National Institute of Food and Agriculture, U.S. Department of Agriculture, under award number 2017-67017-26470.

CHAPTER 6

SUMMARY AND RECOMMENDATIONS

6.1 Summary

The overall goal of this research was to model and analyze energy metabolism in postmortem muscles with three specific objectives.

Specific Objective 1: Develop a kinetic model of energy metabolism and analyze pH variations in postmortem muscles based on measurements from an *in vitro* glycolytic system.

Results: A proposed kinetic model structure with optimized parameters closely described observed variations in metabolites and pH under varied conditions and the estimated parameter values consistently reflected what is known or can be expected, indicating a desirable level of model complexity. Simulation and analysis of pH variations based on the model provided insights into the rate and extent of pH decline in postmortem muscles. Postmortem pH is influenced by the rates of ATP hydrolysis and glycolysis, half-inhibition H^+ concentration for phosphofructokinase activity, and to a much lesser extent, pH buffering capacity. All other reactions have negligible effects and phosphofructokinase activity has the strongest influence.

Specific Objective 2: Analyze contributions of energy pathways to ATP production and pH variations in postmortem muscles based on *in vivo* measurements.

Results: A kinetic model was developed to describe variations in metabolites (ATP, ADP, AMP, IMP, glycogen, lactate, and muscle oxygenation) and pH in postmortem muscles and was validated with data measured from normal and electrically stimulated beef samples. Analysis of ATP production and pH variations based on the model showed the relative contributions of different pathways. ATP is produced primarily by creatine kinase- and myokinase-mediated reactions, and anaerobic glycolysis. Aerobic respiration lasts up to 9 hours postmortem but contributes less than 1% of the total ATP production. Similarly, pH decline in postmortem muscles is mainly due to ATP hydrolysis and glycolysis (-0.52 and -0.6 after 24 hours). Aerobic respiration, on the other hand, leads to a pH increase but the amount is negligible (0.0043 after 24 hours). Analysis of the effects of various factors on pH variations showed that electrical stimulation affects pH primarily through ATP hydrolysis and anaerobic glycolysis. The initial muscle oxygen saturation and phosphocreatine stores showed minor impacts on pH.

Specific Objective 3: Analyze phosphofructokinase (PFK) activity as affected by pH and ATP concentration.

Results: A new method by kinetic modeling was presented to estimate PFK activity and quantify the inhibitory effects of ATP and pH on PFK. In contrast to the conventional initial-velocity method, which gives a qualitative picture of the inhibition of PFK activity under varied conditions, the proposed model can separate the substrate effect from the inhibitor effect and thus quantify the inhibitor effect. The use of a kinetic model to evaluate enzyme activity and quantify the degree of inhibition can be extended to other enzymes as long as the underlying reaction mechanisms are known. Kinetic

analyses of PFK based on the proposed model indicated that the affinity of the substrate binding to the catalytic sites is 4-fold of that to the inhibitory site. Increasing ATP concentration leads to a reduced overall reaction velocity as a result of increasing proportion of enzyme complexes with ATP bound to the inhibitory site.

6.2 Recommendations

The PFK activity model developed in Specific Objective 3 could be incorporated into the *in vivo* kinetic model developed in Specific Objective 2. The parameters of the combined model would be adjusted by using the Levenberg-Marquardt algorithm to achieve optimal model fit to the experimental data from beef *Longissimus lumborum*. After parameter optimization, the model could be used to simulate and analyze the kinetic behaviors of the glycolytic processes in postmortem muscles. Since a more accurate PFK model has been developed in Specific Objective 3, incorporating it into the *in vivo* model would make the combined model closer to reality, allowing for a more specific and more complete analysis of pH variations. We could determine which reactions or initial conditions have the greatest impact on pH in postmortem muscles through simulations. This would provide insights into the fundamental mechanisms of postmortem muscle glycolytic processes, which are important to meat quality.

REFERENCES

Allison, C. P., R. O. Bates, A. M. Booren, R. C. Johnson and M. E. Doumit (2003). "Pork quality variation is not explained by glycolytic enzyme capacity." Meat Sci **63**(1): 17-22.

Arkinstall, M. J., C. R. Bruce, S. A. Clark, C. A. Rickards, L. M. Burke and J. A. Hawley (2004). "Regulation of fuel metabolism by preexercise muscle glycogen content and exercise intensity." J Appl Physiol (1985) **97**(6): 2275-2283.

Ashmore, C. R., L. Doerr, G. Foster and F. Carroll (1971). "Respiration of mitochondria isolated from dark-cutting beef." J Anim Sci **33**(3): 574-577.

Baker, A. J., R. Brandes, T. M. Schendel, S. D. Trocha, R. G. Miller and M. W. Weiner (1994). "Energy use by contractile and noncontractile processes in skeletal muscle estimated by ^{31}P-NMR." Am J Physiol Cell Physiol **266**(35): C825-831.

Birbrair, A., T. Zhang, Z. M. Wang, M. L. Messi, G. N. Enikolopov, A. Mintz and O. Delbono (2013). "Role of pericytes in skeletal muscle regeneration and fat accumulation." Stem Cells Dev **22**(16): 2298-2314.

Bisswanger, H. (2014). "Enzyme assays." Perspect Sci **1**(1–6): 41–55. https://doi.org/10.1016/j.pisc.2014.02.005

Bock, P. E. and C. Frieden (1976). "Phosphofructokinase. I. Mechanism of the pH-dependent inactivation and reactivation of the rabbit muscle enzyme." J Biol Chem **251**(18): 5630-5636.

Bosca, L., J. J. Aragon and S. A. Sols(1985). "Modulation of muscle phosphofructokinase at physiological concentration of enzyme." J Biol Chem **260**(4): 2100–2107. https://doi.org/10.1016/s0021-9258(18)89522-9

Bowker, B. C., C. Botrel, D. R. Swartz, A. L. Grant and D. E. Gerrard (2004). "Influence of myosin heavy chain isoform expression and postmortem metabolism on the ATPase activity of muscle fibers." Meat Sci **68**(4): 587-594.

Bowker, B. C., A. L. Grant, J. C. Forrest and D. E. Gerrard (2000). "Muscle metabolism and PSE pork 1." J Anim Sci **79**(E-Suppl_1): 1-8.

Bruce, H. L., J. R. Scott and J. M. Thompson (2001). "Application of an exponential model to early postmortem bovine muscle pH decline." Meat Sci **58**(1): 39-44.

Chal, J., M. Oginuma, Z. Al Tanoury, B. Gobert, O. Sumara, A. Hick, F. Bousson, Y. Zidouni, C. Mursch, P. Moncuquet, O. Tassy, S. Vincent, A. Miyanari, A. Bera, J. M. Garnier, G. Guevara, M. Hestin, L. Kennedy, S. Hayashi, B. Drayton, T. Cherrier, B. Gayraud-Morel, E. Gussoni, F. Relaix, S. Tajbakhsh and O. Pourquié (2015). "Differentiation of pluripotent stem cells to muscle fiber to model Duchenne muscular dystrophy." Nat Biotechnol **33**(9): 962-969.

Chalovich, J. M. (2002). "Regulation of striated muscle contraction: a discussion." J Muscle Res Cell Motil **23**(4): 353-361.

Chasiotis, D. (1988). "Role of cyclic AMP and inorganic phosphate in the regulation of muscle glycogenolysis during exercise." Med Sci Sports Exerc **20**(6): 545-550.

Cheetham, M. E., L. H. Boobis, S. Brooks and C. Williams (1986). "Human muscle metabolism during sprint running." J Appl Physiol (1985) **61**(1): 54-60.

Chou, T. C. and P. Talalay (1977). "A simple generalized equation for the analysis of multiple inhibitions of Michaelis-Menten kinetic systems." J Biol Chem **252**(18): 6438–6442. https://doi.org/10.1016/s0021-9258(17)39978-7

Conley, K. E., W. F. Kemper and G. J. Crowther (2001). "Limits to sustainable muscle performance: interaction between glycolysis and oxidative phosphorylation." J Exp Biol **204**(Pt 18): 3189-3194.

Delbono, O., K. S. O'Rourke and W. H. Ettinger (1995). "Excitation-calcium release uncoupling in aged single human skeletal muscle fibers." J Membr Biol **148**(3): 211-222.

Dennis, S. C., W. Gevers and L. H. Opie (1991). "Protons in ischemia: where do they come from; where do they go to?" J Mol Cell Cardiol **23**(9): 1077-1086.

DiCarlo, S. E., E. Sipe, J. P. Layshock and S. Varyani (1998). "Experiment demonstrating skeletal muscle biomechanics." Am J Physiol **275**(6 Pt 2): S59-71.

Dobson, G. P., E. Yamamoto and P. W. Hochachka (1986). "Phosphofructokinase control in muscle: nature and reversal of pH-dependent ATP inhibition." Am J Physiol **250**(1 Pt 2): R71-76.

Dubinsky, W. P. (1987). "Resolution and reconstitution of the factors controlling chloride permeability in the trachea." Prog Clin Biol Res **254**: 167-180.

Eicher, J. J., J. L. Snoep and J. M. Rohwer (2012). Determining enzyme kinetics for systems biology with nuclear magnetic resonance spectroscopy. Metabolites **2**(4): 818–843. https://doi.org/10.3390/metabo2040818

El Rammouz, R., C. Berri, E. Le Bihan-Duval, R. Babilé and X. Fernandez (2004). "Breed differences in the biochemical determinism of ultimate pH in breast muscles of broiler chickens--a key role of AMP deaminase?" Poult Sci **83**(8): 1445-1451.

England, E. M., S. K. Matarneh, T. L. Scheffler, C. Wachet and D. E. Gerrard (2014). "pH inactivation of phosphofructokinase arrests postmortem glycolysis." Meat Sci **98**(4): 850-857.

England, E. M., S. K. Matarneh, T. L. Scheffler, C. Wachet and D. E. Gerrard (2015). "Altered AMP deaminase activity may extend postmortem glycolysis." Meat Sci **102**: 8-14.

England, E. M., S. K. Matarneh, R. M. Mitacek, A. Abraham, R. Ramanathan, J. C. Wicks, H. Shi, T. L. Scheffler, E. M. Oliver, E. T. Helm and D. E. Gerrard (2018). "Presence of oxygen and mitochondria in skeletal muscle early postmortem." Meat Sci **139**: 97-106.

Foster, D. L. and R. H. Fillingame (1979). "Energy-transducing H+-ATPase of Escherichia coli. Purification, reconstitution, and subunit composition." J Biol Chem **254**(17): 8230-8236.

Gevers, W. (1977). "Generation of protons by metabolic processes in heart cells." J Mol Cell Cardiol **9**(11): 867-874.

Gibbs, C. L. and C. J. Barclay (1998). "Efficiency of skeletal and cardiac muscle." Adv Exp Med Biol **453**: 527-535; discussion 535-526.

Gibson, F. (1983). "Biochemical and genetic studies on the assembly and function of the F1-F0 adenosine triphosphatase of Escherichia coli." Biochem Soc Trans **11**(3): 229-240.

Gomes, A. V., J. D. Potter and D. Szczesna-Cordary (2002). "The role of troponins in muscle contraction." IUBMB Life **54**(6): 323-333.

Goodman, M. N. and J. M. Lowenstein (1977). "The purine nucleotide cycle. Studies of ammonia production by skeletal muscle in situ and in perfused preparations." J Biol Chem **252**(14): 5054-5060.

Hamm, R. (1977). "Postmortem breakdown of ATP and glycogen in ground muscle: A review." Meat Sci **1**(1): 15-39.

Hammelman, J. E., B. C. Bowker, A. L. Grant, J. C. Forrest, A. P. Schinckel and D. E. Gerrard (2003). "Early postmortem electrical stimulation simulates PSE pork development." Meat Sci **63**(1): 69-77.

Hancock, C. R., E. Janssen and R. L. Terjung (2005). "Skeletal muscle contractile performance and ADP accumulation in adenylate kinase-deficient mice." Am J Physiol Cell Physiol **288**(6): C1287-1297.

Hargreaves, M. and E. A. Richter (1988). "Regulation of skeletal muscle glycogenolysis during exercise." Can J Sport Sci **13**(4): 197-203.

Henckel, P., A. Karlsson, M. T. Jensen, N. Oksbjerg and J. S. Petersen (2002). "Metabolic conditions in Porcine longissimus muscle immediately pre-slaughter and its influence on peri- and post mortem energy metabolism." Meat Sci **62**(2): 145-155.

Hill, G. A. and C. W. Robinson (1975). "Substrate inhibition kinetics: Phenol degradation by Pseudomonas putida." Biotechnol Bioeng **17**(11): 1599–1615. https://doi.org/10.1002/bit.260171105

Hochachka, P. W. and G. B. McClelland (1997). "Cellular metabolic homeostasis during large-scale change in ATP turnover rates in muscles." J Exp Biol **200**(Pt 2): 381-386.

Hopkins, D. L., B. W. Holman and R. J. van de Ven (2015). "Modelling lamb carcase pH and temperature decline parameters: relationship to shear force and abattoir variation." Meat Sci **100**: 85-90.

Hwang, I. H., C. E. Devine and D. L. Hopkins (2003). "The biochemical and physical effects of electrical stimulation on beef and sheep meat tenderness." Meat Sci **65**(2): 677-691.

Hwang, I. H. and J. M. Thompson (2001a). "The effect of time and type of electrical stimulation on the calpain system and meat tenderness in beef longissimus dorsi muscle." Meat Sci **58**(2): 135-144.

Hwang, I. H. and J. M. Thompson (2001b). "The interaction between pH and temperature decline early postmortem on the calpain system and objective tenderness in electrically stimulated beef longissimus dorsi muscle." Meat Sci **58**(2): 167-174.

Immonen, K., R. G. Kauffman, D. M. Schaefer and E. Puolanne (2000). "Glycogen concentrations in bovine longissimus dorsi muscle." Meat Sci **54**(2): 163-167.

Josell, A., A. C. Enfält, G. von Seth, G. Lindahl, I. Hedebro-Velander, L. Andersson and K. Lundström (2003). "The influence of RN genotype, including the new V199I allele, on the eating quality of pork loin." Meat Sci **65**(4): 1341-1351.

Kokkonen, P., A. Beier, S. Mazurenko, J. Damborsky, D. Bednar and Z. Prokop (2021). “Substrate inhibition by the blockage of product release and its control by tunnel engineering.” RSC Chem Biol **2**(2): 645–655. https://doi.org/10.1039/d0cb00171f

Kuffi, K. D., S. Lescouhier, B. M. Nicolai, S. De Smet, A. Geeraerd and P. Verboven (2018). "Modelling postmortem evolution of pH in beef M." J Food Sci Technol **55**(1): 233-243.

Kushmerick, M. J. (1997). "Multiple equilibria of cations with metabolites in muscle bioenergetics." Am J Physiol **272**(Kushmerick): C1739-1747.

Lehmann, G., E. Segal, K. K. Muradian and V. E. Fraifeld (2008). "Do mitochondrial DNA and metabolic rate complement each other in determination of the mammalian maximum longevity?" Rejuvenation Res **11**(2): 409-417.

Lin, Y. Lu, P.Tang, C.Mei, Q.Sanding, G.Rodrigues, A.D. (2001). “Substrate inhibition kinetics for cytochrome P450-catalyzed reaction.” Drug Metab Dispos **29**: 368-374.

Li, Y., D. Rivera, W. Ru, D. Gunasekera and R. G. Kemp (1999). “Identification of allosteric sites in rabbit phosphofructo-1-kinase.” Biochemistry **38**(49): 16407–16412. https://doi.org/10.1021/bi9917611

Lomiwes, D., M. M. Farouk, G. Wu and O. A. Young (2014). "The development of meat tenderness is likely to be compartmentalised by ultimate pH." Meat Sci **96**(1): 646-651.

Lowenstein, J. M. (1972). "Ammonia production in muscle and other tissues: the purine nucleotide cycle." Physiol Rev **52**(2): 382-414.

Lundström, K., A. Andersson and I. Hansson (1996). "Effect of the RN gene on technological and sensory meat quality in crossbred pigs with Hampshire as terminal sire." Meat Sci **42**(2): 145-153.

Luo, Y., J. P. Davis, S. B. Tikunova, L. B. Smillie and J. A. Rall (2003). "Myofibrillar determinants of rate of relaxation in skinned skeletal muscle fibers." Adv Exp Med Biol **538**: 573-581; discussion 581-572.

Marquardt, D.W. (1963). “An algorithm for least-squares estimation of nonlinear parameters.” J Soc Ind Appl Math **11**: 431-441.

Matarneh, S. K., M. Beline, E. S. S. de Luz, H. Shi and D. E. Gerrard (2018). "Mitochondrial F1-ATPase extends glycolysis and pH decline in an in vitro model." Meat Sci **137**: 85-91.

Matarneh, S. K., E. M. England, T. L. Scheffler, E. M. Oliver and D. E. Gerrard (2015). "Net lactate accumulation and low buffering capacity explain low ultimate pH in the longissimus lumborum of AMPKγ3 R200Q mutant pigs." Meat Sci **110**: 189-195.

Matarneh, S. K., E. M. England, T. L. Scheffler, C. N. Yen, J. C. Wicks, H. Shi and D. E. Gerrard (2017). "A mitochondrial protein increases glycolytic flux." Meat Sci **133**: 119-125.

Matarneh, S. K., C. N. Yen, J. M. Elgin, M. Beline, S. da Luz E Silva, J. C. Wicks, E. M. England, R. A. Dalloul, M. E. Persia, I. I. Omara, H. Shi and D. E. Gerrard (2018). "Phosphofructokinase and mitochondria partially explain the high ultimate pH of broiler pectoralis major muscle." Poult Sci **97**(5): 1808-1817.

McGeehin, B., J. J. Sheridan and F. Butler (2001). "Factors affecting the pH decline in lamb after slaughter." Meat Sci **58**(1): 79-84.

Meinke, M. H. and R. D. Edstrom (1991). "Muscle glycogenolysis. Regulation of the cyclic interconversion of phosphorylase a and phosphorylase b." J Biol Chem **266**(4): 2259-2266.

Monin, G., A. Mejenes-Quijano, A. Talmant and P. Sellier (1987). "Influence of breed and muscle metabolic type on muscle glycolytic potential and meat pH in pigs." Meat Sci **20**(2): 149-158.

Monin, G., P. Sellier, L. Ollivier, R. Goutepongea and J. P. Girard (1981). "Carcass characteristics and meat quality of halothane negative and halothane positive pietrain pigs." Meat Sci **5**(6): 413-423.

Mookerjee, S. A., A. A. Gerencser, D. G. Nicholls and M. D. Brand (2017). "Quantifying intracellular rates of glycolytic and oxidative ATP production and consumption using extracellular flux measurements." J Bio Chem **292**(17): 7189-7207.

Mortimer, S. I., J. H. van der Werf, R. H. Jacob, D. L. Hopkins, L. Pannier, K. L. Pearce, G. E. Gardner, R. D. Warner, G. H. Geesink, J. E. Edwards, E. N. Ponnampalam, A. J. Ball, A. R. Gilmour and D. W. Pethick (2014). "Genetic parameters for meat quality traits of Australian lamb meat." Meat Sci **96**(2 Pt B): 1016-1024.

Page, J. K., D. M. Wulf and T. R. Schwotzer (2001). "A survey of beef muscle color and pH." J Anim Sci **79**(3): 678-687.

Puolanne, E. and R. Kivikari (2000). "Determination of the buffering capacity of postrigor meat." Meat Sci **56**(1): 7-13.

Pösö, A. R. and E. Puolanne (2005). "Carbohydrate metabolism in meat animals." Meat Sci **70**(3): 423-434.

Ramos, P. M., C. Li, M. A. Elzo, S. E. Wohlgemuth and T. L. Scheffler (2020). “Mitochondrial oxygen consumption in early postmortem permeabilized skeletal muscle fibers is influenced by cattle breed.” J Anim Sci **98**(3).

Rathgeber, B., J. Boles and P. Shand (1999). "Rapid post mortem pH decline and delayed chilling reduce quality of Turkey breast meat." Poultry Sci **78**: 477-484.

Reed, M. C., A. Lieb and H. F. Nijhout (2010). “The biological significance of substrate inhibition: A mechanism with diverse functions.” BioEssays **32**(5): 422–429. https://doi.org/10.1002/bies.200900167

Rhoads, D. G. and J. M. Lowenstein (1968). “Initial velocity and equilibrium kinetics of myokinase.” J Biol Chem **243**(14): 3963-3972.

Rios, A. C. and C. Marcelle (2009). “Head muscles: aliens who came in from the cold?” Dev Cell **16**(6): 779-780.

Robergs, R. A., F. Ghiasvand and D. Parker (2004). “Biochemistry of exercise-induced metabolic acidosis.” Am J Physiol Regul Integr Comp Physiol **287**(3): R502-516.

Savell, J. W., S. L. Mueller and B. E. Baird (2005). “The chilling of carcasses.” Meat Sci **70**(3): 449-459.

Scheffler, T. L. and D. E. Gerrard (2007). "Mechanisms controlling pork quality development: The biochemistry controlling postmortem energy metabolism." Meat Sci **77**(1): 7-16.

Scheffler, T. L., S. K. Matarneh, E. M. England and D. E. Gerrard (2015). "Mitochondria influence postmortem metabolism and pH in an in vitro model." Meat Sci **110**: 118-125.

Schöneberg, T., M. Kloos, A. Brüser, J. Kirchberger and N. Sträter (2013). “Structure and allosteric regulation of eukaryotic 6-phosphofructokinases.” Biol Chem **394**(8): 977–993. https://doi.org/10.1515/hsz-2013-0130

Schwägele, F., C. Haschke, K. O. Honikel and G. Krauss (1996a). "Enzymological investigations on the causes for the PSE-syndrome, I. Comparative studies on pyruvate kinase from PSE- and normal pig muscles." Meat Sci **44**(1-2): 27-40.

Schwägele, F., C. Haschke, G. Krauss and K. O. Honikel (1996b). "Comparative studies of pyruvate kinase from PSE and normal pig muscles." Z Lebensm Unters Forsch **203**(1): 14-20.

Scopes, R. K. (1973). "Studies with a reconstituted muscle glycolytic system. The rate and extent of creatine phosphorylation by anaerobic glycolysis." Biochem J **134**(1): 197-208.

Scopes, R. K. (1974a). "Studies with a reconstituted muscle glycolytic system. The anaerobic glycolytic response to simulated tetanic contraction." Biochem J **138**(1): 119-123.

Scopes, R. K. (1974b). "Studies with a reconstituted muscle glycolytic system. The rate and extent of glycolysis in simulated post-mortem conditions." Biochem J **142**(1): 79-86.

Scott, I. D. and D. G. Nicholls (1980). "Energy transduction in intact synaptosomes. Influence of plasma-membrane depolarization on the respiration and membrane potential of internal mitochondria determined in situ." Biochem J **186**(1): 21-33.

Sharma, B. (2011a). "Kinetic characterisation of phosphofructokinase purified from Setaria cervi: A bovine filarial parasite." Enzyme Res **2011**(1). https://doi.org/10.4061/2011/939472

Sharma, B. (2011b). "Modulation of phosphofructokinase (PFK) from Setaria cervi, a bovine filarial parasite, by different effectors and its interaction with some antifilarials." Parasites Vectors **2011**(4): 227. http://www.parasitesandvectors.com/content/4/1/227

Shearer, J., I. Marchand, M. A. Tarnopolsky, D. J. Dyck and T. E. Graham (2001). "Pro- and macroglycogenolysis during repeated exercise: roles of glycogen content and phosphorylase activation." J Appl Physiol (1985) **90**(3): 880-888.

Shou, M., Y. Lin, P. Lu, C. Tang, Q. Mei, D. Cui, W. Tang, J. S. Ngui, C. C. Lin, R. Singh, B. K. Wong, J. A. Yergey, J. H. Lin, P. G. Pearson, T. A. Baillie, A. D. Rodrigues and T. H. Rushmore (2000). "Enzyme Kinetics of Cytochrome P450-Mediated Reactions." Curr Drug Metab **2**.

Sola-Penna, M., D. da Silva, W. S. Coelho, M. M. Marinho-Carvalho and P. Zancan (2010). "Regulation of mammalian muscle type 6-phosphofructo-1-kinase and its implication for the control of the metabolism." IUBMB Life **62**(11). https://doi.org/10.1002/iub.393

Sorinmade, S. O., H. R. Cross, K. Ono and W. P. Wergin (1982). "Mechanisms of ultrastructural changes in electrically stimulated beef Longissimus muscle." Meat Sci **6**(1): 71-77.

St-Pierre, J., M. D. Brand and R. G. Boutilier (2000). "Mitochondria as ATP consumers: cellular treason in anoxia." Proc Natl Acad Sci U S A **97**(15): 8670-8674.

Stanley, W. C. and R. J. Connett (1991). "Regulation of muscle carbohydrate metabolism during exercise." FASEB J **5**(8): 2155-2159.

Stepanov, V., P. Mateo, B. Gillet, J. C. Beloeil, P. Lechene and J. A. Hoerter (1997). "Kinetics of creatine kinase in an experimental model of low phosphocreatine and ATP in the normoxic heart." Am J Physiol **273**(4): C1397-1408.

Stokes, I. and M. Gardner-Morse (2002). "The role of muscles and effects of load on growth." Stud Health Technol Inform **91**: 314-317.

Tang, J., C. Faustman, T. A. Hoagland, R. A. Mancini, M. Seyfert and M. C. Hunt (2005). "Postmortem oxygen consumption by mitochondria and its effects on myoglobin form and stability." J Agric Food Chem **53**(4): 1223-1230.

Tanner, L. B., A. G. Goglia, M. H. Wei, T. Sehgal, L. R. Parsons, J. O. Park, E. White, J. E. Toettcher and J. D. Rabinowitz (2018). "Four Key Steps Control Glycolytic Flux in Mammalian Cells." Cell Syst **7**(1). https://doi.org/10.1016/j.cels.2018.06.003

Thompson, J. M., D. Perry, B. Daly, G. E. Gardner, D. J. Johnston and D. W. Pethick (2006). "Genetic and environmental effects on the muscle structure response post-mortem." Meat Sci **74**(1): 59-65.

Ui, M. (Ui). "A role of phosphofructokinase in pH-dependent regulation of glycolysis." Biochim Biophys Acta **124**(2): 310-322.

Vandenberghe, K., E. A. Richter and P. Hespel (1999). "Regulation of glycogen breakdown by glycogen level in contracting rat muscle." Acta Physiol Scand **165**(3): 307-314.

van de Ven, R. J., K. L. Pearce and D. L. Hopkins (2013). "Modelling the decline of pH in muscles of lamb carcases." Meat Sci **93**(1): 79-84.

van de Ven, R. J., K. L. Pearce and D. L. Hopkins (2014). "Post-mortem modelling of pH and temperature in related lamb carcases." Meat Sci **96**(2 Pt B): 1034-1039.

Vetharaniam, I., R. A. Thomson, C. E. Devine and C. C. Daly (2010). "Modelling muscle energy-metabolism in anaerobic muscle." Meat Sci **85**(1): 134-148.

Viljoen, H. F., H. L. de Kock and E. C. Webb (2002). "Consumer acceptability of dark, firm and dry (DFD) and normal pH beef steaks." Meat Sci **61**(2): 181-185.

Wang, C., S. K. Matarneh, D. Gerrard and J. Tan (2021). “Modelling of energy metabolism and analysis of pH variations in postmortem muscle.” Meat Sci **182**.

Wang, C., S. K. Matarneh, D. Gerrard and J. Tan (2022). “Contributions of energy pathways to ATP production and pH variations in postmortem muscles.” Meat Sci **189**. https://doi.org/10.1016/j.meatsci.2022.108828

Wang, X., X. Zhang, D. Wu, Z. Huang, T. Hou, C. Jian, P. Yu, F. Lu, R. Zhang, T. Sun, J. Li, W. Qi, Y. Wang, F. Gao and H. Cheng (2017). “Mitochondrial flashes regulate ATP homeostasis in the heart.” eLife **6**: e23908.

Warner, R. D., R. H. Jacob, K. Rosenvold, S. Rochfort, C. Trenerry, T. Plozza and M. B. McDonagh (2015). "Altered post-mortem metabolism identified in very fast chilled lamb M. longissimus thoracis et lumborum using metabolomic analysis." Meat Sci **108**: 155-164.

Warriss, P. D., E. A. Bevis and P. J. Ekins (1989). "The relationships between glycogen stores and muscle ultimate pH in commercially slaughtered pigs." Br Vet J **145**(4): 378-383.

Webb, B. A., F. Forouhar, F. E. Szu, J. Seetharaman, L. Tong and D. L. Barber (2015). “Structures of human phosphofructokinase-1 and atomic basis of cancer-associated mutations.” Nature **523**(7558): 111–114. https://doi.org/10.1038/nature14405

Wei, L., F. Mousawi, D. Li, S. Roger, J. Li, X. Yang and L. H. Jiang (2019). “Adenosine triphosphate release and P2 receptor signaling in PiEzO1 channel-dependent mechanoregulation.” Front Pharmacol **10**: 1304.

Welsh, D.G. and M. I. Lindinger (1993). “Energy metabolism and adenine nucleotide degradation in twitch-stimulated rat hindlimb during ischemia-reperfusion.” Am J Physiol **264**(4 Pt1): E655-661

Wu, B. (2011). “Substrate inhibition kinetics in drug metabolism reactions.” Drug Metab Rev **43**(4): 440–456. https://doi.org/10.3109/03602532.2011.615320

Xing, T., F. Gao, R. K. Tume, G. Zhou and X. Xu (2019). “Stress Effects on Meat Quality: A Mechanistic Perspective.” Comp Rev Food Sci and Food Safety **18**(2): 380-401.

Yano, D. and T. Suzuki (2018). “Kinetic Analyses of the Substrate Inhibition of Paramecium Arginine Kinase.” Protein J **37**(6): 581–588. https://doi.org/10.1007/s10930-018-9798-2

Zammit, P. S., T. A. Partridge and Z. Yablonka-Reuveni (2006). "The skeletal muscle satellite cell: the stem cell that came in from the cold." J Histochem Cytochem **54**(11): 1177-1191.

Zeng, Z., C. Li and P. Ertbjerg (2017). "Relationship between proteolysis and water-holding of myofibrils." Meat Sci **131**: 48-55.

Zhang, H., O. Varmalova, F. M. Vargas, C. N. Falany and T. S. Leyh (1998). "Sulfuryl Transfer: The Catalytic Mechanism of Human Estrogen Sulfotransferase." J Biol Chem **273**(18). http://www.jbc.org/

Zheng, R. and R. G. Kemp (1994). "Identification of Interactions That Stabilize the Transition State in Escherichia coli Phosphofiucto-1-kinase." J Biol Chem **269**(28).

Zhu, X., M. Ruusunen, M. Gusella, M. Ylä-Ajos, X. Xu, G. Zhou and E. Puolanne (2013). "High early post-mortem temperature induces activation of AMP-activated protein kinase and development of pale, soft and exudative characteristics in turkey muscles." Meat Sci **93**(3): 600-606.

VITA

Chengcheng Wang was born on December 2, 1985 in Xiangyang, Hubei province, China. In September 2005, she entered Yantai University in Shandong Province, China and received a Bachelor of Science in Biotechnology from Yantai University in May 2009. In September 2009, she entered Sun Yat-sen University in Guangdong Province, China and received a Master of Science in Genetics from Sun Yat-sen University in June 2012. In June 2018, she was admitted by the Department of Biomedical, Biological and Chemical Engineering, University of Missouri-Columbia, as a Ph. D. candidate. She has been studying energy metabolism in postmortem muscle under the advisement of Dr. Jinglu Tan.